ANGULAR CORRELATIONS NEAR THE FERMI ENERGY

By

Daniel Fox

A DISSERTATION

Submitted to

Michigan State University

in partial fulfillment of the requirements

for the degree of

DOCTOR OF PHILOSOPHY

Department of Physics and Astronomy

1987

ABSTRACT

ANGULAR CORRELATIONS NEAR THE FERMI ENERGY

By

Daniel Fox

Angular correlations between light particles have been studied to
e the extent to which a thermally equilibrated system is formed in
y ion collisions near the Fermi energy. The results of two
iments are reported.

Light particle correlations have been measured at energies (35-50
nucleon) near the fermi energy. Light particle spectra and large
correlations were measured for 40 and 50 MeV/nucleon C+C, Ag and
The single particle inclusive energy spectra are well fit by a three
g source parameterization. The correlations were done with tag
tors at θ=25° and 45° with ϕ=0°, 90° and 180°. Coincident particles
detected at θ=15°-150°. The decay of particle unstable states was
to contribute noticeably to the same side in-plane correlations.
wo-particle correlations were found to be dominated by momentum
rvation effects.

ight particle correlations at small relative momentum were measured
and 35 MeV/nucleon N+Ag and single particle inclusive spectra were
ed for 35 MeV/nucleon N+Ag at θ=35°, 45°, 60° and 80°. Source
were extracted from the two-particle correlation functions and were
to be consistent with previous measurements using two-particle
ations and the coalescence model. The populations of particle
le states were extracted and used together with the measured single
le inclusive spectra and previously measured Y and neutron emitting

es to determine the temperature of the emitting system using the
tum statistical model. The temperature extracted from the relative
lations of states, using the quantum statistical model, was found to
$.8^{+2.8}_{-2.4}$ MeV which is substantially lower than the 14 MeV temperature
acted from the slopes of the kinetic energy spectra.

ACKNOWLEDGMENTS

I would like to thank my advisor Gary Westfall for his help and
ance over the last three years which has helped to make this work
ble. I would also like to thank Dan Cebra, Jeff Karn, Cam Parks,
Pradhan, Bob Tickle, Skip VanderMolen, Hans van der Plicht and Ken
for their help during the experiments. I would also like to thank
her fellow graduate students, past and present, for their help,
t and friendship over the last four years. Finally I would like to
the staff of the National Superconductiong Cyclotron Laboratory for
ing the facilities and beam time without which this work could not
een completed.

TABLE OF CONTENTS

LIST OF TABLES

LIST OF FIGURES

ent mass indicating a common origin for the observed particles.
cles detected in coincidence with intermediate rapidity fragments
rojectile like fragments were also found to come the same source [Ha
Particles in coincidence with projectile like fragments very close
e beam mass were found, however, to have a slower source velocity by
30%, but the source temperature was found to be the same as the
rature extracted from the singles spectra.

While single particle inclusive kinetic energy spectra of light and
mediate mass fragments have suggested emission of all particles from
ame thermally equilibrated intermediate velocity source some
nce of non-thermal processes has been observed. At relativistic
ies quasi-elastic p-p scattering has been seen [Na 79, Ta 80, Ta
Other two-paritcle correlations have suggested that momentum
rvation plays a key role in intermediate energy reactions [Ly 82, Ts
r 85, Ch 86b]. More recently experiments have sought to measure the
rature of the intermediate source by measuring the relative
ations of various nuclear states [Mo 84, Mo 85, Mo 86, Xu 86, Jn
Ch 87, Po 86b, Bi 87b]. The temperatures extracted from the
ations of nuclear states has been shown to be considerably lower
the temperatures extracted from the kinetic energy spectra.

Large Angle Correlations

Two-particle large-angle correlations have been used to study the
t to which thermalization occurs at relativistic [Na 79, Ta 80, Ta
nd at intermediate [Ly 82, Ts 84, Kr 85, Ch 86b] energies. The
experiments [Na 79, Ta 80, Ta 81] measured the ratio of in-plane to
f-plane correlations. Tag detectors were placed at $(\theta,\Phi)=(40°,\pm 90°$

40°,180°). Coincidences were measured between these tag detectors spectrometer at Φ=0° that covered angles from Θ=10° to 50°. The of the number of in-plane (Φ_{tag}=180°) to out-of-plane (Θ_{tag}=±90°) ations was measured. For a completely thermalized system this should be one. For 800 MeV/nucleon C+C an enhancement of about 70% served in the ratio of in-plane to out-of-plane correlations at s and energies corresponding to quasi-elastic p-p scattering. For a smaller enhancement of about 30% was observed. For C+Pb the of in-plane to out-of-plane correlations was found to be about 0.9 endent of angle. This was interpreted to be due to shadowing by the .

In a similar experiment [Kr 85a, Kr 85b] the ratio of in-plane to f-plane correlations was measured at 85 MeV/nucleon for C+C, Al, Cu +Au [Kr 85a, Kr 85b]. As at 800 MeV/nucleon the C+C system showed hancement in the ratio of in-plane to out-of-plane correlations. enhancement was attributed not to quasi-elastic scattering but r to emission from a recoiling thermal source. In addition the cement was found to increase with increasing mass of the detected cle pair.

At lower energies momentum conservation has been shown to be an tant factor in two particle large angle correlations for light ms while heavy systems have been described using a rotating ideal Ly 82, Ts 84, Ch 86b]. Azimuthal correlations of light particles in V/nucleon O+Au reactions have been shown to have a strong preference emission in the same plane [Ts 84]. The data were well described by culation in which the particles were assumed to be emitted from a ting moving source. For lighter systems (O+C) both in-plane and

Chapter I

Introduction

The extent to which thermalization occurs in intermediate and ativistic energy heavy ion nuclear physics has been the focus of many eriments in the last decade. At relativistic energies single particle clusive spectra of light particles were found to be thermal in earence, leading to the introduction of the fireball model [We 76, Go . The basic idea behind the fireball model is that the region of rlap between the projectile and target forms a hot source moving at a ocity slightly less than half the beam velocity. The source expands tting particles with Maxwell-Boltzmann type energy distributions. In ition the spectra of light nuclei (d,t,^{3}He,^{4}He) were found to be well cribed by the coalescence model [Gu 76, Go 77]. In the coalescence el composite fragments are formed when nucleons are emitted close ether in phase space.

At intermediate energies, $20<E_{beam}<200$ MeV/nucleon, single particle lusive spectra were measured for light and intermediate mass particles found again to be well described by a Maxwell-Boltzmann type energy tribution [We 82, Ja 83, We 84]. Additional evidence for a thermal rce was found in the behavior of the d/p and ^{4}He/p ratios [We 82, ch were found to be in general agreement with calculations using the eball model [We 76, Go 77]. The intermediate mass particles were wn to come from the same source as the light nuclei [Ja 83]. Also the lescence model, which had previously been applied at relativistic rgies [Gu 76, Go 77] and at lower energies [Aw 82] to light nuclei, applied to both light and intermediate mass fragments [Ja 85]. The racted coalescence and source radii showed little variation with

muthal correlations are dominated by momentum conservation effects ch lead to a strong enhancement of planar emission on opposite sides the beam [Ch 86b].

In recent results for 60 MeV/nucleon Ar+Au reactions the two ticle correlations were found to be much more isotropic [Ar 85]. The relation functions for two proton correlations vary by only about 10% a function of Θ and Φ compared to variations of 50% for 25 MeV/nucleon u [Ts 84, Ch 86b]. Even two alpha correlations showed much less ular dependence at 60 MeV/nucleon, varying by 50% as a function of le compared to a factor of five variation for two triton correlations 25 MeV/nucleon. One interesting feature in the 60 MeV/nucleon data is t the azimuthal correlations have their minimum at Φ=45° and not Φ=90° is seen at 25 MeV/nucleon. The more isotropic behavior at 60 /nucleon is most likely due to the larger size of the emitting source ch makes it easier to balance the momentum of the emitted particle.

Nuclear Temperature Measurements

A few years ago Morrissey et al. [Mo 84, Mo 85] tested the idea of rmal equilibrium by measuring the populations of excited states of ht nuclei that decay by Y-ray emission. For a thermalized system the io of the populations of the excited state to the population of the und state is given by

$$\frac{j_{ex}+1}{j_{gs}+1} e^{-E_{ex}/kT}, \qquad (I-1)$$

re j_{gs} and j_{ex} are the spins of the ground and excited states, spectively, E_{ex} is the excitation energy of the excited state, and kT the temperature. Morrissey et al. measured the populations of the -lying, Y-ray emitting states of ^{6}Li, ^{7}Li, ^{8}Li and ^{7}Be emitted from reaction 35 MeV/nucleon $^{14}N+Ag$. The kinetic energy spectra of the , ^{7}Li, ^{8}Li and ^{7}Be ground states indicated a temperature of about 10 . The populations of the Y-ray emitting states, however, were found correspond to a source temperature of less than 1 MeV.

Morrissey et al. checked their method of measuring the nuclear perature by studying the system $^{14}N+^{12}C$ at low bombarding energies .5-350 MeV) [Mo 86]. The Y-ray emitting states of ^{7}Be and ^{10}B emitted n the ^{26}Al compound nucleus were measured. The temperatures extracted n the excited state populations were found to be constant down to ut 112 MeV at which point the temperature began to decrease. Between 5 and 112 MeV the measured temperature agreed with the expected perature from the compound nucleus when the rotational energy of the ound nucleus is taken into account.

Two possible explanations for the surprisingly low temperatures acted from the Y-ray emitting states have been proposed. In one lanation nuclei emitted in particle bound excited states experience l state interactions with neutrons resulting in their deexcitation 84]. As a result the number of observed excited nuclei is siderably less than those originally emitted and hence a lower erature is extracted. The second explanation is based on the quantum istical model [St 63, Ha 86, Ha 87]. In this model the temperature sured by the populations of Y-ray emitting states is lower than the

e temperature of the emitting states because of the sequential decay
heavier particle unbound states. Sequential decay primarily feeds the
und states, thus lowering the measured temperature [Ha 87]. Using the
ntum statistical model Xu et al. [Xu 86] showed that the populations
Y-ray emitting states from the reaction S+Ag at 22.3 MeV/nucleon was
sistent with a temperature of T>4 MeV. Without using the quantum
tistical model the extracted temperature was between 0.5 and 2.4 MeV
ending on wich excited state was used to extract the temperature.

The method of Morrissey et al. has more recently been extended to
ticle unstable states of light nuclei [Ch 86a, Ch 87, Po 85a, Po 85c,
86b]. The use of particle unstable states has the advantage of
owing the measurement of higher temperatures than most of the Y-ray
tting states due to the higher excitation energies of most of the
ticle unstable states compared to those of the Y-ray emitting states.
the system 35 MeV/nucleon N+Au [Ch 86a] temperatures of between 3 and
eV were extracted from the particle unstable states of ^{6}Li neglecting
effects of feeding from higher lying states. The higher temperatures
e obtained for higher total energy of the emitted ^{6}Li parent nuclei.
peratures extracted for states in ^{5}Li and ^{6}Li in coincidence with
sion fragments were found to be about 5 MeV [Ch 87] independent of the
ding angle of the two fission fragments. For 60 MeV/nucleon Ar+Au [Po
] a temperature of about 5.5 MeV was obtained using the quantum
tistical model to fit the populations of a large number of states. In
Ar+Au experiment a large array of plastic scintillator was used to
vide multiplicity information. Although the two particle correlations
ied considerably as a function of multiplicity, the extracted

perature showed no significant variation as a function of multiplicity 87].

More recent experiments have examined particle unstable states that ay by neutron emission. The system 35 MeV/nucleon N+Ag was studied king at neutron emitting states in ^{7}Li, ^{8}Li, ^{10}Be and ^{12}B [Bl 87a, Bl]. These states were found to yield higher temperatures than the Y- states of the same system. The temperature extracted from the $^{*}_{7.456}$ state, when corrected for feeding of the ground state, was found 2.8±0.3 MeV.

The use of particle unstable states to measure nuclear temperatures not without problems. The effects of feeding from higher states is ll important and may change the apparent temperature by a factor of or more. Even some of the particle unbound states, such as $^{8}Be^{*}_{3.04}$, be heavily fed [Ha 87]. In addition the extraction of the ulations of the excited states may be complicated by final state eractions of randomly emitted particles.

Contents and Organization of the Thesis

In order to probe the extent to which a thermally equilibrated rce is created in heavy ion reactions around the Fermi energy we have formed two experiments. In the first experiment single particle lusive kinetic energy spectra and two-particle large angle relations of light nuclei were studied for 40 and 50 MeV/nucleon C uced reactions on C, Ag and Au targets. The measured single particle lusive energy spectra are fit using a three moving source fit. A

entum conservation model is used to determine the extent to which rgy and momentum conservation effects the measured two-particle relations.

In the second experiment the populations of particle unstable states e measured for 25 and 35 MeV/nucleon N induced reactions on a Ag get using two-particle correlations at small relative momentum. The ulations of particle unstable states are extracted from the two- ticle correlations. The quantum statistical model is used to extract source temperature for 35 MeV/nucleon N+Ag from the populations of particle bound and unbound states measured in the present work oined with the data of Morrissey and Bloch for the Y and neutron tting states. In addition information about the space-time extent of emitting system is extracted from the two-particle correlation ctions.

The rest of this thesis is arranged as follows. The experimental ups are described in Chapter II. The detector calibrations, reaction s correction, and efficiency calculation for a multi-wire proportional nter used in the unstable resonance experiment are discussed in pter III. The results of the large angle correlation and unstable onance experiments are presented and discussed in Chapters IV and V pectively. Chapter VI contains a summary of the results and clusions.

Chapter II

Experimental Setup

Both experiments described in this dissertation were performed in 1.5 meter scattering chamber at the National Superconducting otron Lab (NSCL) at Michigan State using beams from the K500 otron. The chamber and electronics setups will be discussed in this ter. The detector calibrations are described in Chapter III.

Unstable Resonance Experiment.

Two types of detectors were used in the unstable resonance riment. The energy of the observed light particles (p,d,t,^{3}He,^{4}He) measured using sixteen fast-slow plastic phoswich telescopes. tion information was obtained by the use of a three plane multi-wire ortional counter (MWPC). The phoswiches will be discussed first.

Particle identification and energy measurement was achieved using an of sixteen fast-slow phoswich telescopes. Each telescope consisted 1.6 mm thick fast plastic (BC-412) ΔE detector optically coupled to mm long slow plastic (BC-444) E detector. The properties of the tic scintillators are given in Table II-1. The signals from each scope were read using a single Amperex 2202 ten stage omultiplier. The photomultiplier has a maximum response for light wavelength λ=425±30 nm which is the same as the wavelength of mum emission of the plastics given in Table II-1. In order to get ΔE and E from the single signal the signal was split using a 50Ω ter and sent to two different charge integrating ADCs. Figure II-1 what the signals from the ΔE and E detectors look like. The pure

Table II-1

Plastic Scintillator Properties

	Fast Plastic (BC-412)	Slow Plastic (BC-444)
Rise Time (ns)	1.0	19.5
Decay Time (ns)	3.3	179.7
Pulse Width (FWHM ns)	4.2	171.9
Wavelength Of Maximum Emission (nm)	434	428
Light Output, % Anthracene	60	41

(From Bicron Corporation data sheets [Bi 85].)

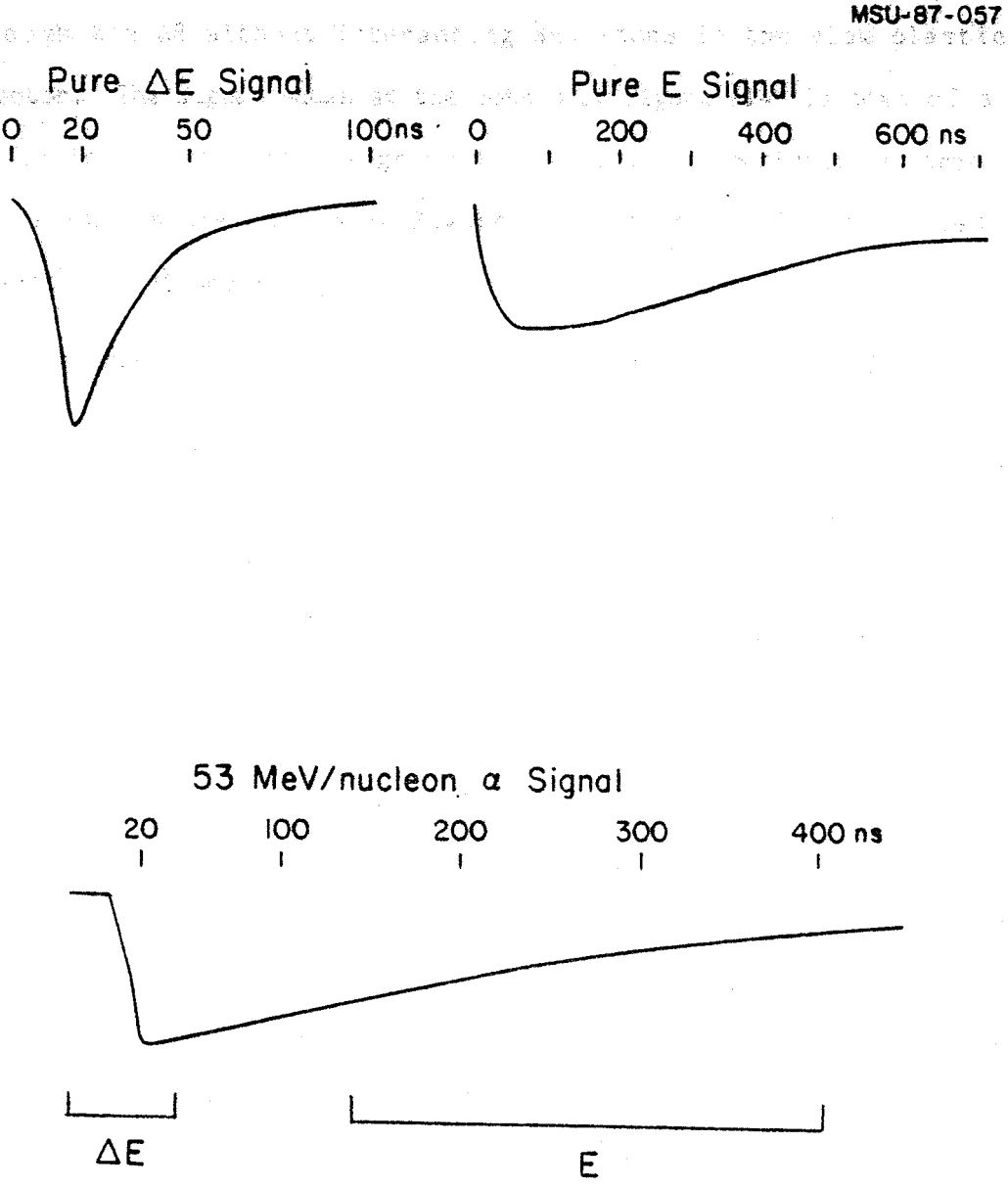

Figure II-1 Phoswich signals and ADC gates.

ignal comes from a very low energy particle which stops in the fast tic ΔE. The pure E signal comes from a neutron or gamma which passes ough the ΔE without interacting and stops in the slow plastic E ctor. The signal shown at the bottom of Figure II-1 is that of a 53 nucleon α from the large angle correlation experiment calibration. shown in the bottom of Figure II-1 are the ADC gates used to rate the ΔE and E signals.

The lower and upper energy cuts of the phoswiches for p,d,t,^{3}He and are given in Table II-2. The energy resolution of the phoswiches was ured as part of the calibration of the phoswiches for the large angle elation experiment. For a 106 MeV deuteron, which loses 2 MeV in the etector and 104 MeV in the E detector, the resolution was determined e 39% in the ΔE and 2.8% in the E. Resolution of the proton band the neutrons and gammas is usually lost around 100 MeV. Due to lems with the photomultiplier bases the resolution of the helium opes was poor in the unstable resonance experiment. In this riment the gains on the phoswiches were set such that the high gy cuts ranged from 75 to 140 MeV for Z=1 and from 135 to 250 MeV for

In addition a previously unknown delay of about 25 ns in the ADCs lted in most of the phoswiches having higher low energy cuts than e listed in Table II-2, for Z=1 particles the low energy cuts ranged 15 to 25 MeV and for Z=2 from 45 to 65 MeV.

The phoswiches were designed to fit, when stacked as shown in Figure , behind the MWPC and to be placed as far from the target as possible s to provide the greatest possible angular resolution. In this riment the phoswiches had an opening angle of 5.7° each and the re array had a solid angle of 165 msr.

Table II-2

Phoswich Low And High Energy Cuts

Particle	Low Energy Cut (MeV)	High Energy Cut (MeV)
p	11.9	135
d	16.1	182
t	19.2	218
^{3}He	41.7	478
^{4}He	47.4	541

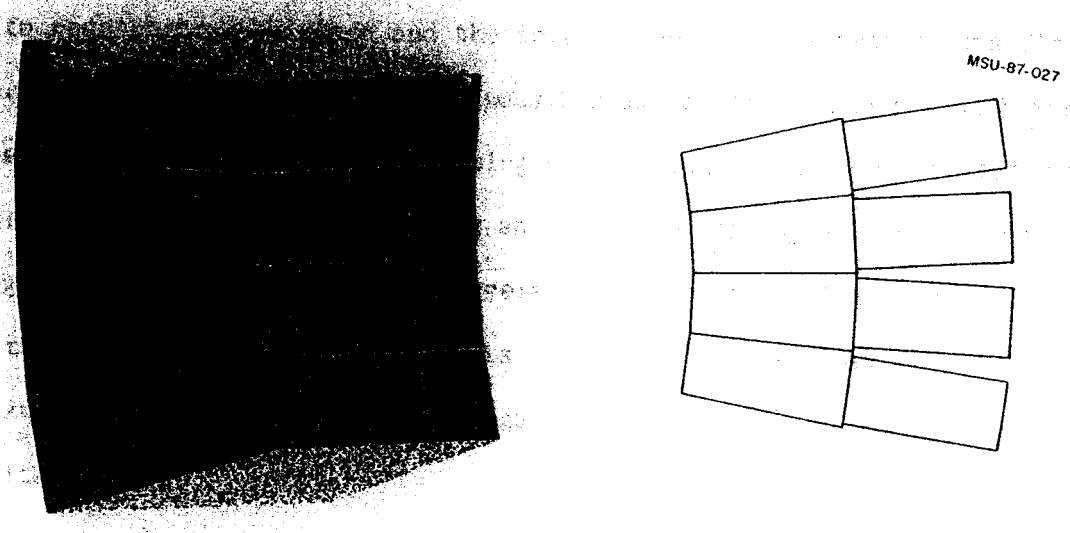

Figure II-2 Phoswich array used in the unstable resonance experiment.

To improve further the angular resolution of the array a multi-wire proportional counter (MWPC) [Ha 84] was placed in front of the phoswiches. The MWPC contained three wire planes, two at right angles with respect to each other and the third at 45° with respect to the first two planes in order to resolve possible ambiguities in events with more than one particle. The wire spacing of this counter is 2.5 mm, but the wires are paired together giving an effective spacing of 5 mm to provide angular resolution of 0.7°. The relative momentum for two 60 MeV alphas with an opening angle of 0.7° is 5 MeV/c. The MWPC was filled with a mixture of Argon-Ethane (50%/50%) gas at 500 torr and had an operating voltage of V_{cath}=-3000V.

Beams of 25 and 35 MeV/nucleon ^{14}N were used on a target of 1.6 mg/cm^2 Ag. The beam energies were determined by the cyclotron settings. Data were taken with the MWPC at central angles of θ=35°, 45°, 60° and 80° for the 35 MeV/nucleon ^{14}N beam and at θ=45° for the 25 MeV/nucleon beam.

The electronics diagram for the unstable resonance experiment is shown in Figure II-3. Use of the new LeCroy FERA modules (Fast Encoding And Readout ADCs) enabled us to do some preliminary gating before writing an event to tape [Va 85]. Using software gates, we were able to eliminate from each event particles that stopped in the ΔE detector, for which particle identification was not possible. In addition only those events in which two or more of the detectors had valid particles were written to tape.

The data acquisition for both experiments was controlled by a VAX-750 connected to two MC68010 CPUs residing on a VME bus [Va 85]. The first MC68010 acquires data from the CAMAC crate containing the ADCs and

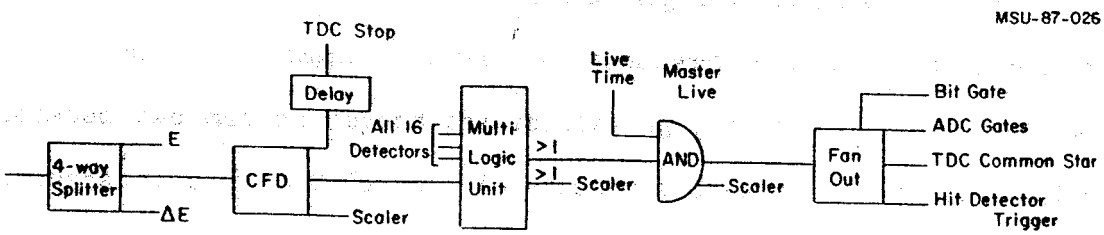

Figure II-3 Electronics diagram for the unstable resonance experiment.

IDCS until its 8 Kbyte buffer is full. Control of the CAMAC crate is then passed to the second CPU while the first CPU transfers its buffer to the VAX. Scalers are read every 10 seconds and sent to the VAX by an LSI-11/23 which resides in a second CAMAC crate along with the scalar modules. The LSI also controls the starting and stopping of runs.

In both experiments the beam was monitored in a shielded faraday cup located two meters beyond the scattering chamber. The current was integrated by a BIC Current Integrator and was recorded using a CAMAC scaler module. In order to avoid previous problems [Ha 84] with the current integrator double firing, the current integrator's output was run through a variable width gate generator with the width adjusted until the multiple firing was no longer observed. The average intensity of the beam was 2 particle namps.

B. Singles Measurement For The Unstable Resonance Experiment.

The singles energy spectra for the ground states of the He, Li, and Be isotopes studied in the unstable resonance experiment were measured in a separate experiment using a single two element Si stack. The stack consisted of a 400 μm ΔE detector and a 5 mm E detector. Data were taken at the same angles, θ=35°, 45°, 60° and 80°, that were measured in the unstable resonance measurement. The energy range measured for each isotope is given in Table II-3. In order to reduce the contamination of the ^{7}Li cross section from decaying ^{8}Be nuclei [Bl 86] the Si stack was positioned so as to have a solid angle of 1.54 msr. The fraction of ^{8}Be that identify as ^{7}Li as a function of energy is shown in Figure II-4.

Telescope Energy Ranges For Unstable Resonance Singles Measurement

Particle	Low Energy Cut (MeV)	High Energy Cut (MeV)
^{3}He	26	111
^{4}He	29	126
^{6}He	35	151
^{6}Li	54	237
^{7}Li	59	254
^{7}Be	80	350
^{9}Be	92	392
^{10}Be	95	411

Table II-3

Telescope Energy Ranges For Unstable Resonance Singles Measurement

Particle	Low Energy Cut (MeV)	High Energy Cut (MeV)
^{3}He	26	111
^{4}He	29	126
^{6}He	35	151
^{6}Li	54	237
^{7}Li	59	254
^{7}Be	80	350
^{9}Be	92	392
^{10}Be	95	411

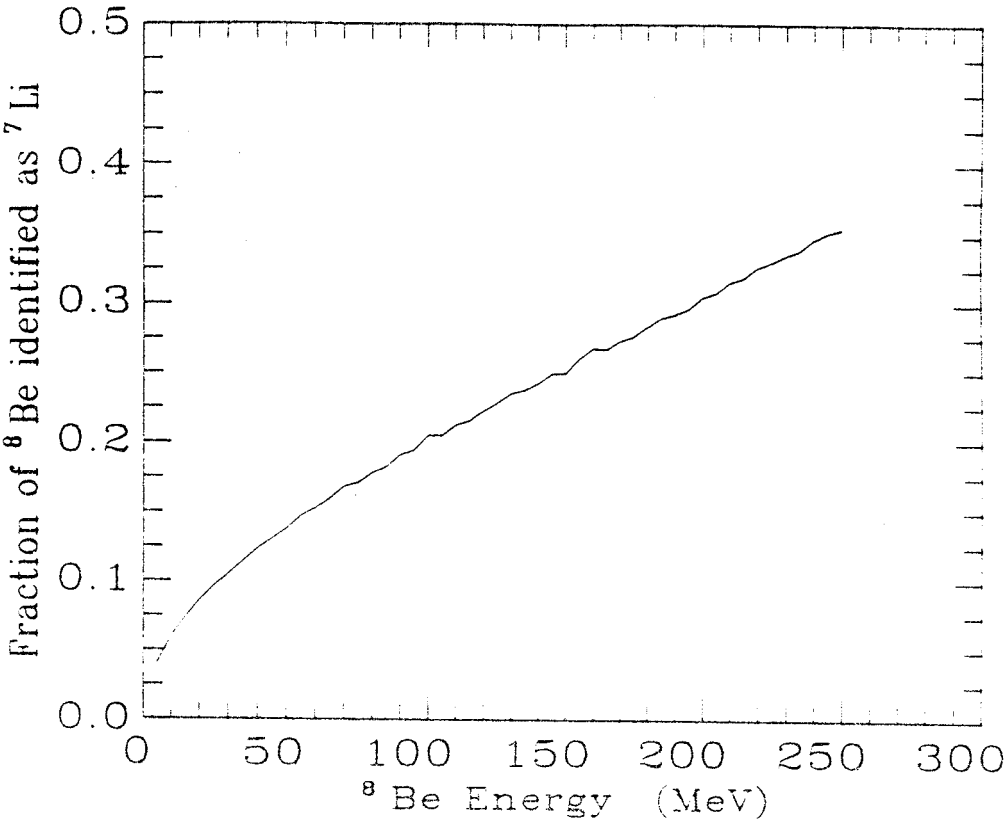

Figure II-4 Fraction of ^{8}Be nuclei that identify as ^{7}Li.

Even for this small solid angle the fraction of ^{8}Be that were identified as ^{7}Li is between 10 and 35% depending on the energy of the decaying ^{8}Be.

C. Large Angle Correlation Experiment.

The experimental setup for the large angle correlation experiment is shown in Figure II-5 and the positions and solid angles of the detectors are given in Table II-4. All thirteen telescopes used in this experiment were fast-slow plastic phoswiches of the type used in the unstable resonance experiment. Two pairs of telescopes were used as tag counters and nine telescopes were used as array counters. One pair of tag telescopes was placed at $\theta=45°$ with $\Phi=180°$ and 90°. The second pair of tag telescopes was placed at $\theta=25°$ with the same azimuthal angles as the first pair. The tag telescopes at $\Phi=180°$ are known as in-plane tag telescopes and the pair at $\Phi=90°$ are called the out-of-plane tag telescopes. The nine array telescopes were placed at angles ranging from $\theta=15°$ to $\theta=150°$ with $\Phi=0°$. Copper collimators were placed in front of all thirteen telescopes. The collimators were thick enough to stop 160 MeV protons. During the experiment the array detector at $\theta=35°$ did not function properly and is not included in the analysis.

The electronics for the large angle correlation experiment are shown in Figure II-6. Three types of events were taken, singles, coincidences involving at least one tag telescope and one array telescope, and coincidences involving any two telescopes. Singles were taken only during separate singles runs. Low coincidence rates (250-1000 coincidences/second) allowed the taking of all coincidences and not just of coincidences involving a tag telescope and an array telescope.

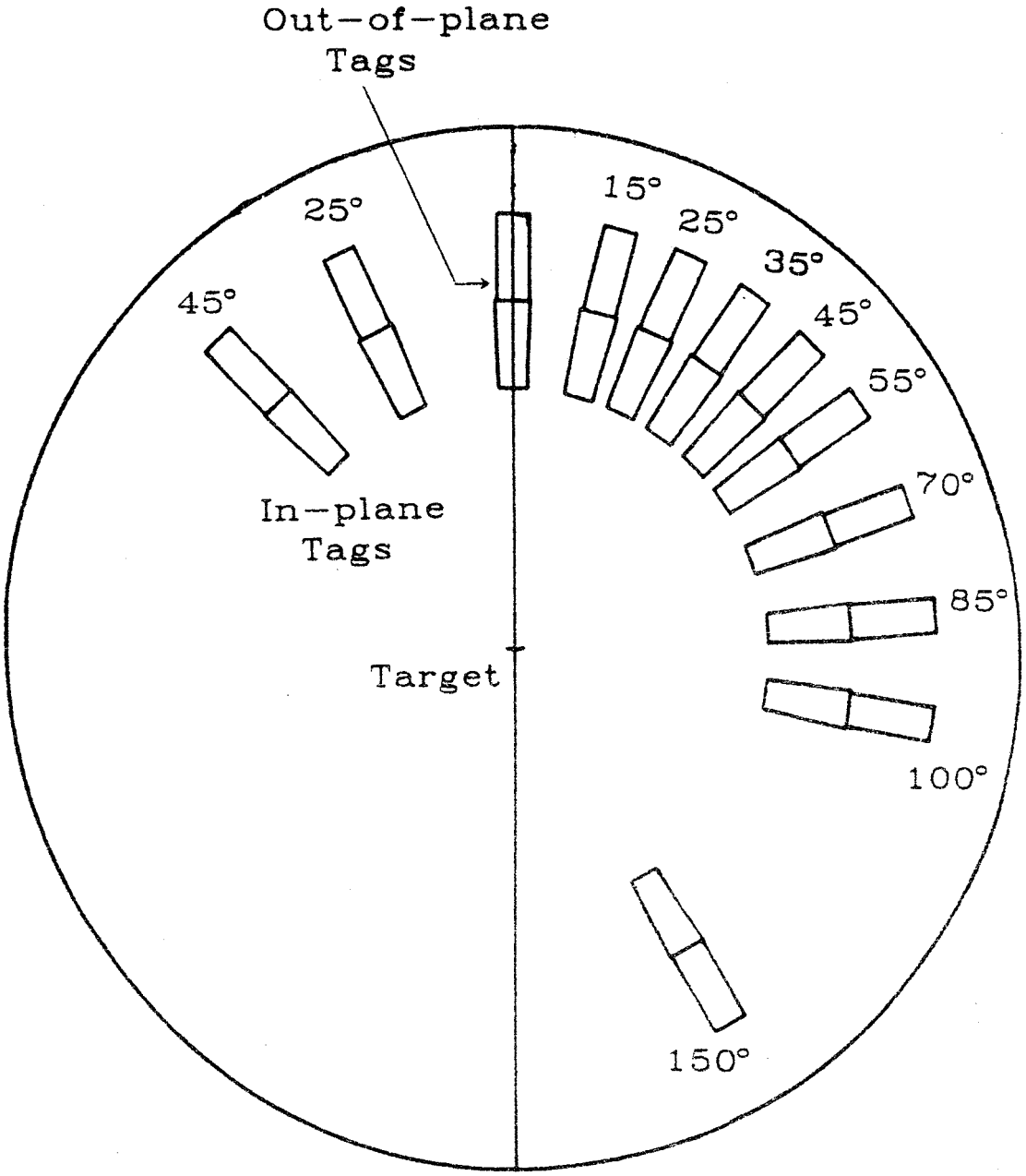

Figure II-5 Chamber setup for the large angle correlation experiment.

Table II-4

Telescope Positions And Solid Angles For

The Large Angle Correlation Experiment

Telescope	θ (Deg.)	Φ (Deg.)	Solid Angle (msr)
In-Plane Tag 1	25	180	1.22
In-Plane Tag 2	45	180	2.41
Out-Of-Plane Tag 1	25	90	1.22
Out-Of-Plane Tag 2	45	90	2.41
Array Telescope 1	15	0	1.02
Array Telescope 2	25	0	1.22
Array Telescope 3	35	0	1.02
Array Telescope 4	45	0	2.41
Array Telescope 5	55	0	1.02
Array Telescope 6	70	0	2.41
Array Telescope 7	85	0	2.41
Array Telescope 8	100	0	2.41
Array Telescope 9	150	0	2.41

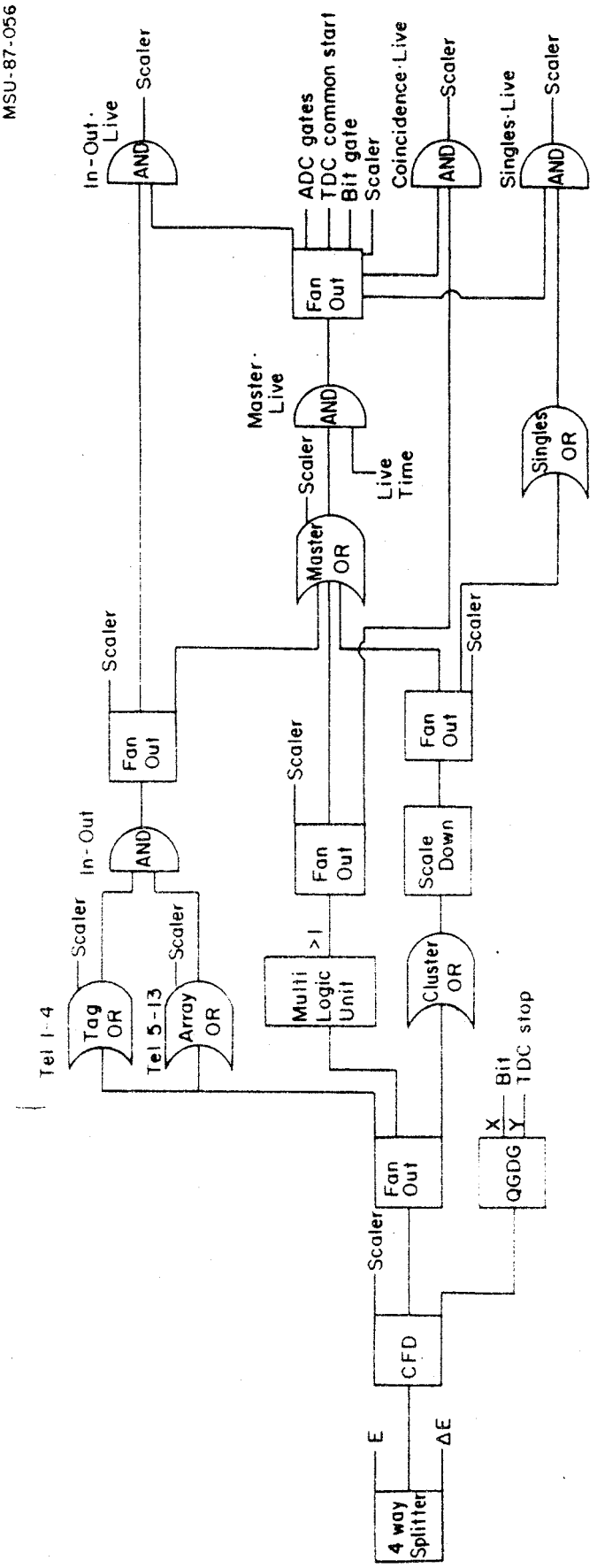

Figure II-6 Electronics diagram for the large angle correlation experiment.

The targets used in the experiment were a 26 mg/cm^2 graphite target, 4.0 mg/cm^2 Ag, and 5.5 mg/cm^2 Au. Beams of 40 and 50 MeV/nucleon ^{12}C were used. The 40 MeV/nucleon beam was used on all four targets while the 50 MeV/nucleon beam was used only on the graphite target. The beam energies were determined from the cyclotron settings. The average beam intensity on the graphite target was 0.5 particle namps, on the other targets the average intensity was 3 particle namps.

Chapter III

Data Analysis And Reduction

In both experiments the data were written to tape in event by event mode for offline analysis at a later time. In the offline analysis two dimensional ΔE-E plots were used to set gates around the different particles. These gates were used in sorting the data into singles and coincident spectra. In this chapter the energy calibrations of the detectors will be discussed, as well as reaction loss corrections for the plastic scintillators and the efficiency of the MWPC used in the unstable resonance experiment.

A. Phoswich Energy Calibrations.

1. Unstable Resonance Experiment.

The phoswich telescopes used in the unstable resonance experiment were calibrated using beams of 25 MeV/nucleon deuterons and alphas on targets of CD_2 and Ag. The phoswich array was placed at central angles ranging from θ=0° to 75°. Calibration points were obtained from elastic and inelastic scattering.

As part of the calibrations, corrections had to be made for two different problems. The first correction was required because the ΔE gate unavoidably samples part of the E signal causing the spectra to curl up at large energy as shown in Figure III-1. In this experiment the problem was compounded by a then unknown delay in the FERA gates mentioned in Chapter II. To correct for these problems the ΔE value used to calculate the energy of a particle was taken to be the difference

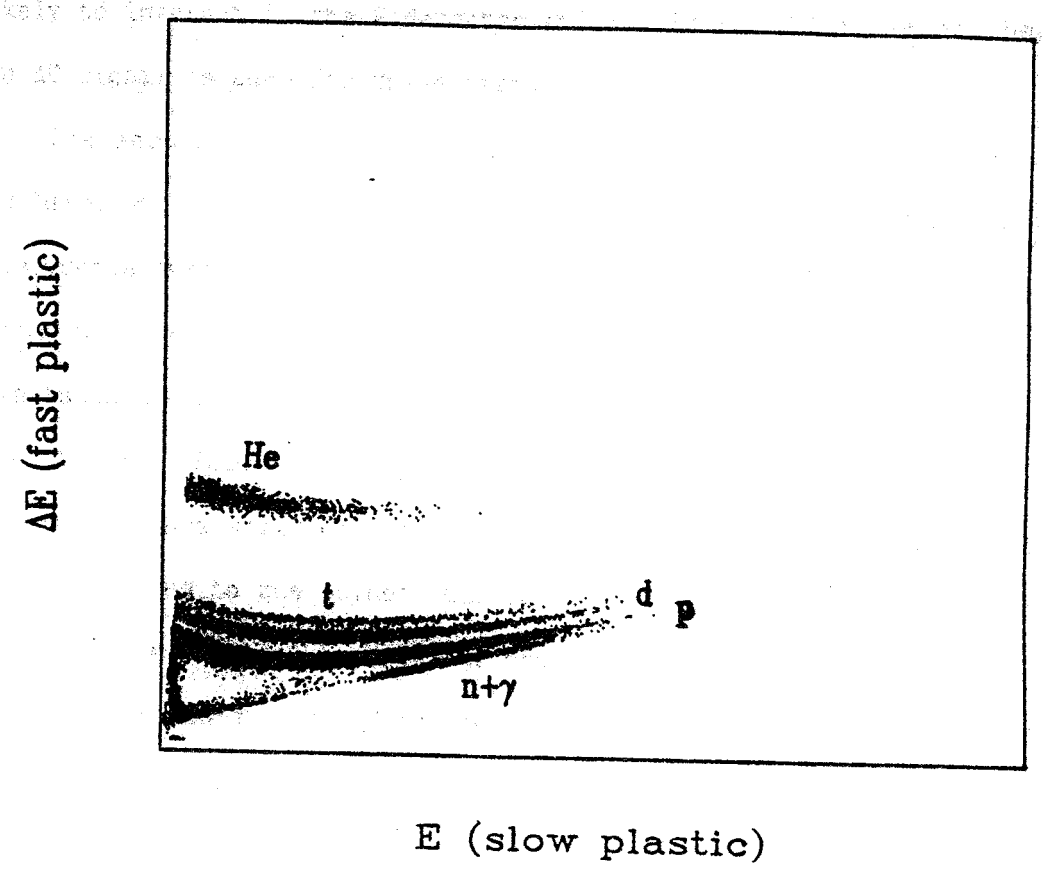

Figure III-1 ΔE-E spectra from the unstable resonance experiment.

between the ADC value and the center of the neutron and gamma line at the same E value. This is done because the neutrons and gammas are most likely to interact in the E detector and not in the ΔE detector, hence the ΔE signal is zero for these events.

The second problem that had to be corrected for was a small difference in timing, and hence in the gates, between singles and coincidence events that was discovered during the experiment. After about 36 hours of operation the MWPC failed. In order to calibrate the data taken up to that point a full set of calibration data was taken at that time. Upon playing back these data it was found that the calibration data which were taken in singles mode had a small shift in timing compared to the coincidence data. To allow us to correct for this timing problem we took two sets of deuteron calibration data at the end of the experiment. The first set was taken in the same singles mode as the first deuteron calibration. The second set was taken in a simulated coincidence mode by putting two wires for each telescope onto the multiplicity logic unit and requiring a two fold coincidence. By comparing the two sets of deuteron calibrations a multiplicative factor was obtained that related the two settings and was used to correct the first set of calibrations which was taken only in a singles mode.

An example of the phoswich calibrations is shown in Figure III-2. The calibration points were found to be linear. The deuteron calibration shown is from the second calibration and was taken in the simulated coincidence mode. The alpha calibration is for the same phoswich but is from the first set of calibrations. The larger positive intercepts are due to the timing problem involving the ADC gates that was discussed in Chapter II.

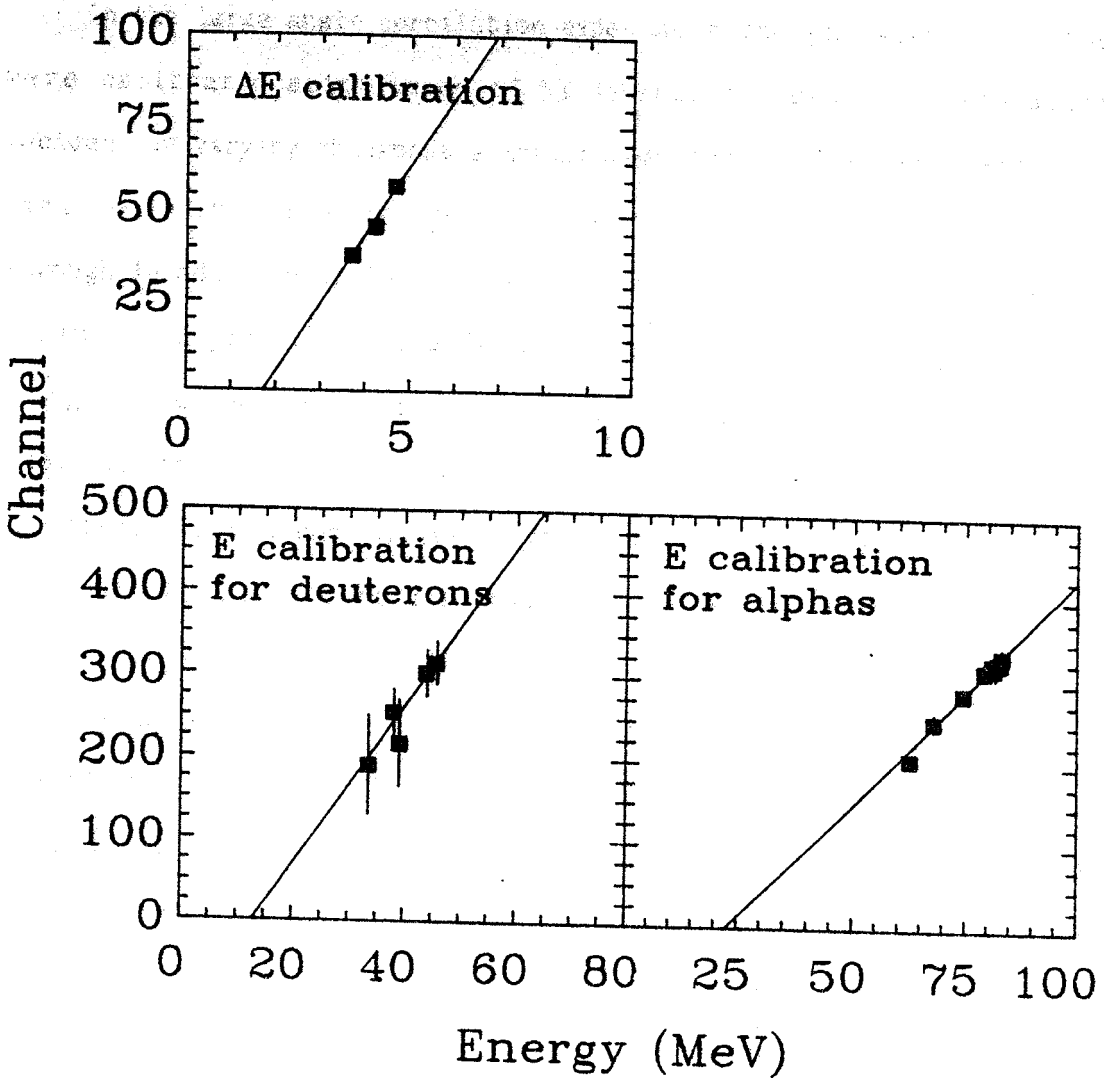

Figure III-2 Example of a phoswich calibration for the unstable resonance experiment.

2. Large Angle Correlation Experiment.

In the large angle correlation experiment the phoswich telescopes were calibrated using beams of 53 MeV/nucleon deuterons and alphas incident on varying thickness aluminum degraders. The degraders had a small hole in the center to allow part of the undegraded beam to pass through in addition to four different thicknesses to provide a series of calibration points ranging from approximately 1/5 of the total beam energy up to the full beam energy in equal steps. Using the degraders enabled us to get calibration points that spanned a wide range of energies. As mentioned in the previous section a correction had to be made to the ΔEs because the fast ΔE gate samples part of the slow E signal.

Examples of the energy calibrations are shown in Figure III-3 for one of the phoswiches. The calibrations were found to be linear with intercepts very close to zero. Because the gains on the phoswiches varied, fewer than the five points the degraders were designed to provide were obtained for all counters. For those that had only one or two points the calibrations were forced to go through zero. The punch-in energies of the light particles were then checked and small adjustments (1-4 MeV) made in the intercepts were made to force agreement with range-energy calculations for the punch-in energies for p, d, t, ^{3}He and ^{4}He.

In the large angle correlation experiment the phoswich gains were set such that we were able to observe fragments with Z=1-6 in the forward detectors. It is well known that the light output of plastic scintillators is nonlinear as a function of Z [Ba 67, Ne 61, Bu 76, Be 76]. We obtained approximate calibrations for particles with Z=3-6 by

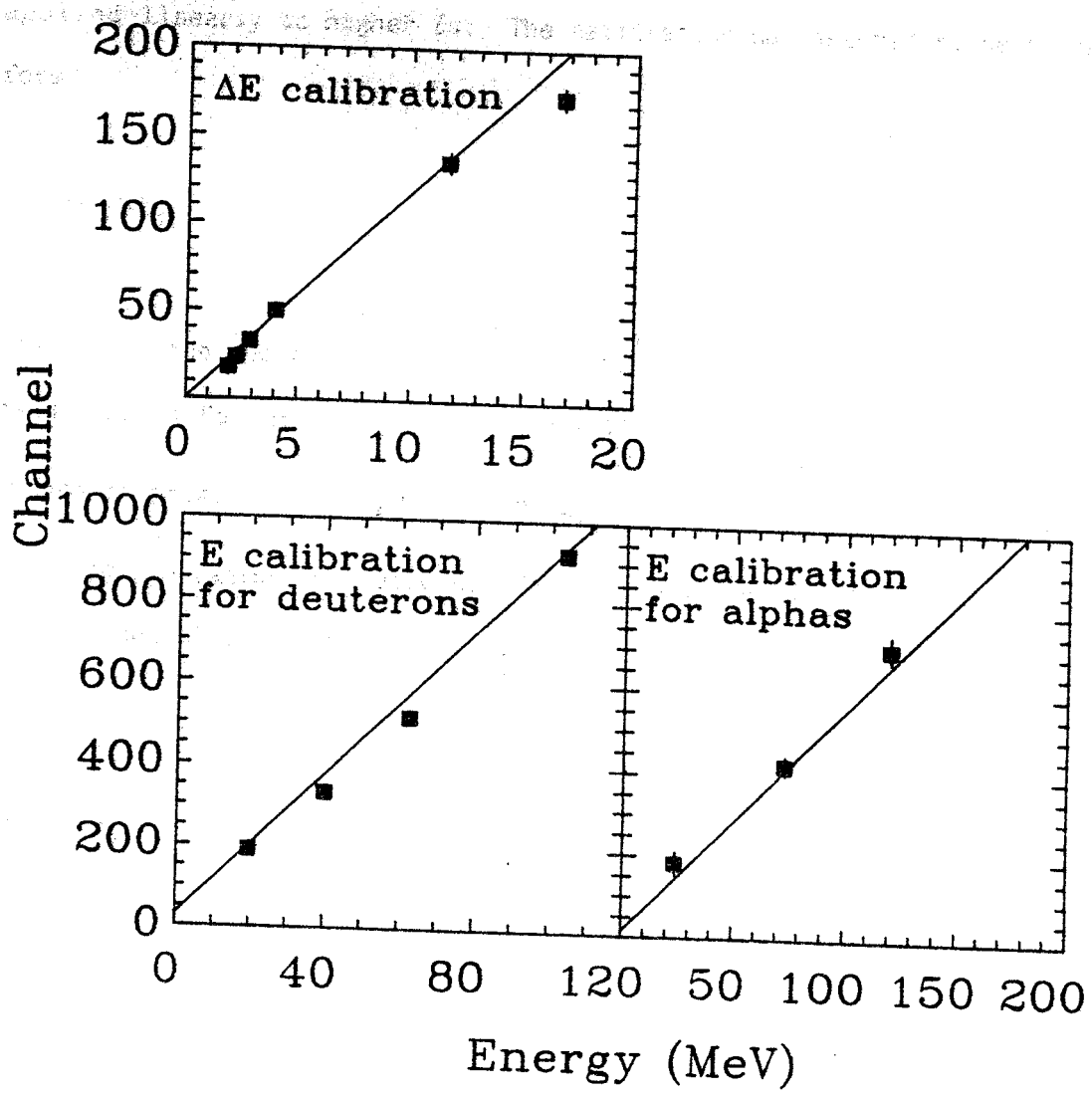

Figure III-3 Example of a phoswich calibration for the large angle correlation experiment.

using the ΔE punch-through points and comparing the measured ΔE signal to the expected ΔE value assuming that the deuteron calibrations could be applied linearly to higher Zs. The calibration was assumed to be of the form

$$E = m\alpha_Z c - b_Z \qquad \text{(III-1)}$$

where E is the energy deposited in the detector, m is the slope of the calibration for deuterons, c is the ADC value, and b_Z is an intercept chosen to provide the proper low energy cut for the given element. α_Z is a correction factor that accounts for the nonlinearity in response of the plastic scintillator and is defined as

$$\alpha_Z = \frac{C_Z E_d}{C_d E_Z} \qquad \text{(III-2)}$$

where C_Z and C_d are the punch through channels for a particle of charge Z, and for a deuteron. E_Z and E_d are the punch through energies for a particle of charge Z, and for a deuteron. The values for α_Z were determined for every telescope for Z>1, when a given Z was seen in more than one telescope the value used in the calibration was the average of all telescopes. The values for α_Z and b_Z are given in Table III-1.

As a check on the accuracy of this method ^{4}He spectra were generated using both this method and the α calibration obtained from the calibration beam. A comparison of the two spectra is shown in Figure

Table III-1

Values of a_Z and b_Z for Z=2-6

Particle	a_Z	b_Z (MeV)
^{4}He	.659	10
Lithium	.502	20
^{7}Be	.466	30
Boron	.372	45
Carbon	.334	65

4. The spectra generated by the α calibration are shown as lines
e the data points are for the spectra generated by the calibration
ined from the punch through points. As is seen in Figure III-4, the
calibrations yield almost identical spectra. Another indication that
punch-through calibration is reasonably good is that moving source
, which are shown in Chapter IV, to the Li and Be spectra yielded
ce velocities similar to those of the light particles. The excellent
ement between the two calibrations means that in future experiments
ill not be necessary to calibrate the phoswiches separately for
erons and alphas as has been done in the past. Instead the
bration need be done for one element and then extended to all other
rved elements using the method outlined above.

Silicon Detector Calibration.

The silicon detectors used in the singles measurement for the
able resonance experiment were calibrated using calibrated pulsers.
calibrations obtained using the pulsers were checked by comparing the
h-in and punch-through energies for the observed isotopes given by
calibrations to those calculated using the code DONNA [Me 81]. The
con detector calibrations are shown in Figure III-5.

Reaction Loss Corrections.

Nucleons traveling through plastic scintillators lose energy not
through interactions with the atomic electrons, but also through
ear reactions in the scintillators. The interaction with the atomic
trons produces the full energy peak in the scintillator. The nuclear

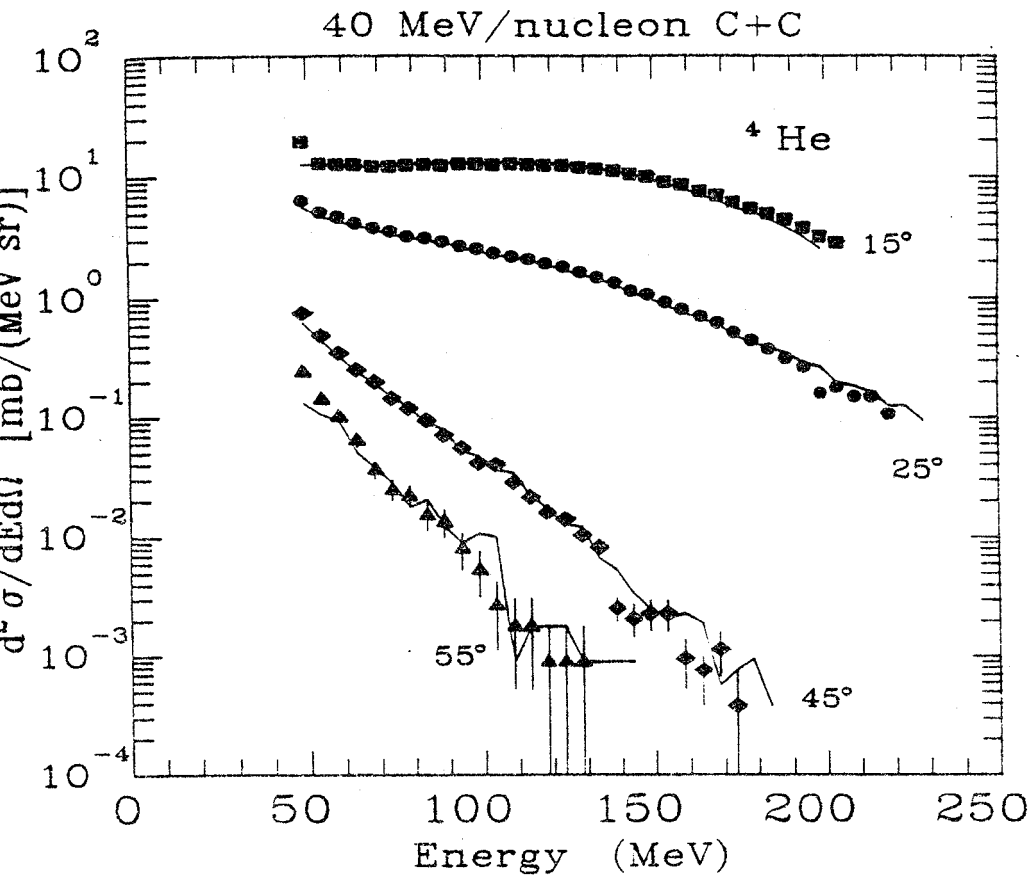

re III-4 Comparison of the two different α calibrations.

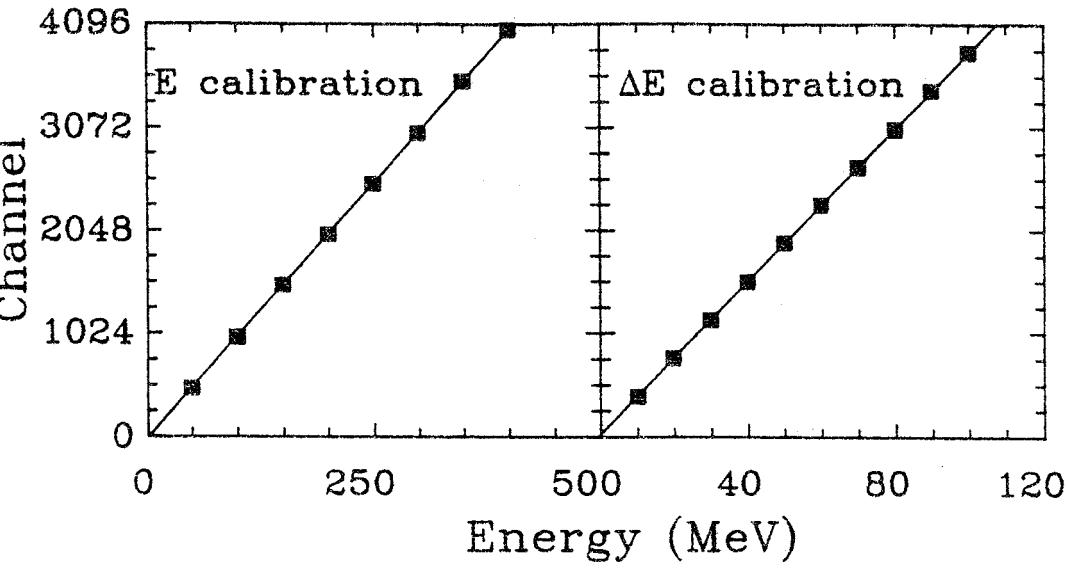

Figure III-5 Silicon detector calibration.

actions, however, produce reaction products such as neutrons, gammas
d alphas, which, because of the nonlinearity of the scintillator,
oduces less light in the scintillator than the original particle would
e produced. The reaction leads to the loss of the particle from the
l energy peak, thus making particle identification impossible using
E plots.

We have used the calculations of Hasselquist [Ha 84] for the
ction loss in plastic scintillator. The calculation is patterned
er that of Measday and Richard-Serre [Me 69]. In the calculation the
ge of the particle is divided up into small steps and the reaction
ss section for each step is calculated. The fraction of particles
t due to interactions is then given by

$$-e^{-\sum_i n_i \sigma_i} \qquad \text{(III-3)}$$

re n_i is the number of atoms/cm^2 in the i^{th} step. The calculated
ction cross section, σ_i is given by

$$N\pi R^2(1-V_c/E)(1+(\kappa/E)^{\lambda}) \qquad \text{(III-4)}$$

re R is the interaction radius given by

$$r_0(A_1^{1/3} + A_2^{1/3}-1) \qquad \text{(III-5)}$$

r_0=1.2 fm. The coulomb potential, V_c, is given by

$=Z_1Z_2e^2/R.$ (III-6)

κ and λ are adjustable parameters determined by fitting to data given Measday [Me 69]. The energy spectra are corrected by dividing by 1-f ich is the fraction of particles that do not interact in the ntillator. For 100 MeV protons 10% of the incident protons are lost to nuclear interactions in the scintillators.

MWPC Efficiency.

As mentioned in Chapter II a multi-wire proportional counter (MWPC) used to obtain more precise position resolution in the unstable sonance experiment. In order to measure the populations of particle table states the efficiency of the MWPC must be calculated. In this tion the procedure used to calculate the overall MWPC efficiency will outlined and all the factors that influence the efficiency will be cussed.

The MWPC efficiency was calculated using a Monte Carlo simulation. each trial the parent nucleus is constrained to hit somewhere on the swich array with its energy and angle determined using the energy and ular distributions for the ground state of the same isotope, or the sest stable isotope for those cases where the ground state is unbound. nucleus is then allowed to decay in it's rest frame, with the two ay products having a relative momentum Δp. The decay products are n transformed into the lab system with a random rotation about the jectory of the parent nucleus. The position in the phoswich array t each decay product hits, if it hits the array, is then found. If

th particles hit the array, and if they hit two different phoswiches, en their energies are compared to the individual energy cuts of the oswiches they hit. Next the wire efficiency as a function of energy r the particles involved is checked. Finally a check is made for the ssibility that the particles scatter out of the scintillator or are st due to a nuclear reaction in the scintillator. The fraction of ials for a given Δp in which both particles survive all of these checks the efficiency for detection at that Δp.

The wires of the MWPC have efficiencies that vary as a function of e particle's energy, mass, and charge. In Figure III-6 the efficiency the MWPC wires for particles that were detected in one of the oswiches behind the MWPC is shown. The lines are simple linear fits to e curves using one or two intersecting lines. For all wires the ficiency for the helium isotopes shows no variation as a function of ergy. The efficiency for the hydrogen isotopes has a strong variation a function of energy and mass. The efficiency of the wires was ermined for each MWPC angle setting and was incorporated into the ficiency calculation using linear fits like the ones shown in Figure -6.

A charged particle passing through a medium will experience many ll elastic scatterings which might scatter the particle out of the ector. In the unstable resonance experiment the phoswiches were ollimated, and hence it was possible for particles to be close enough the edge of the phoswich to be scattered out of the detector. This rection can be especially important for those particle pairs with very ll momentum differences Δp, because their small opening angles greatly rease the probability that one or both of the particles will hit near edge of a phoswich. The scattering angle due to multiple scattering

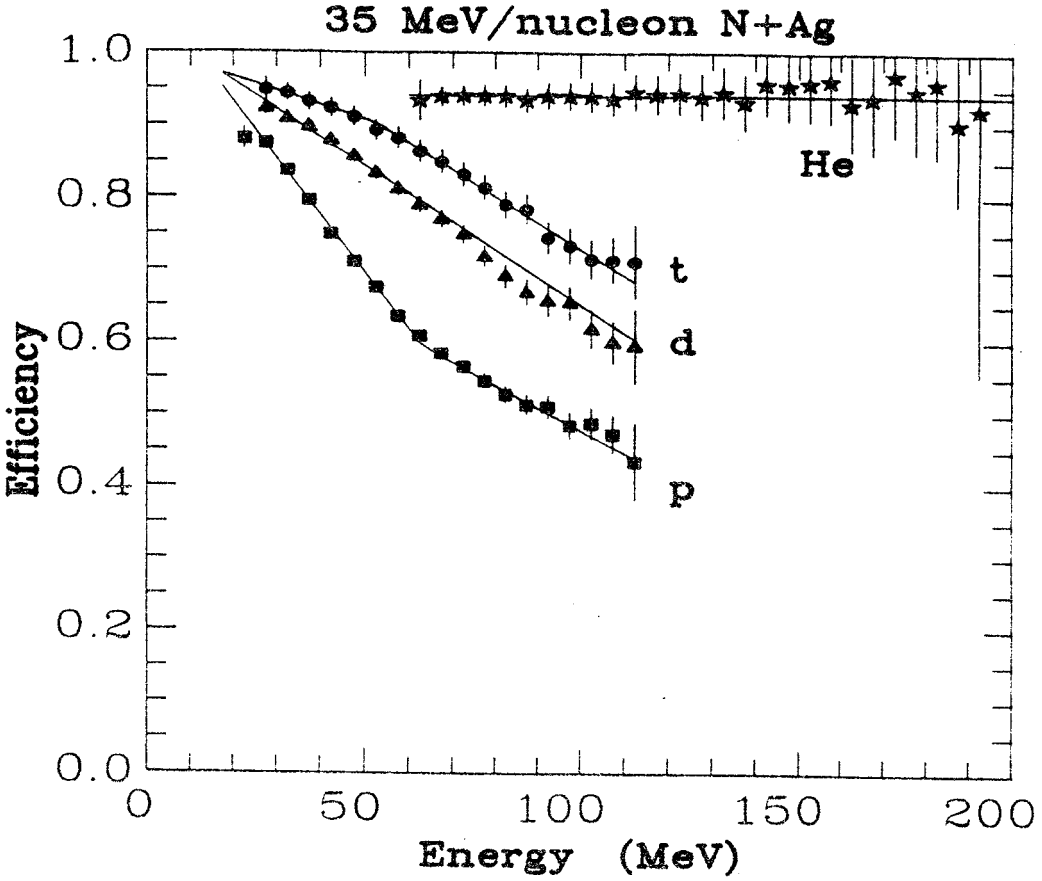

gure III-6 MWPC wire efficiency as a function of mass, charge and energy for the wire in front of one phoswich.

s assumed to have a Gaussian distribution peaked about θ_0 given by [Pa
-]

$$\theta_0 = \frac{14.1}{p\beta} Z_{inc}\sqrt{L/L_R}\,[1+\tfrac{1}{9}\log_{10}(L/L_R)]\,[1+\frac{Am_o}{(t+m_o)A_s}] \text{ (radians)}, \quad \text{(III-7)}$$

ere p, β and Z_{inc} are the momentum, velocity and charge of the incident rticle and L/L_R is the thickness in radiation lengths of the scattering dium. The scatter out calculation was incorporated into the efficiency lculation.

The reaction loss correction discussed in the previous section of is chapter was also used in calculating the efficiency.

The calculated efficiency for the detection of coincident p-t, d-α d α-α pairs are shown in the top part of Figure III-7 for the case when e MWPC array was at 45°. In the bottom part of Figure III-7 the erage opening angles as a function of Δp are shown. The efficiency aks when the average opening angle is about the same as the opening gle of the phoswiches. For smaller values of Δp the chief loss of fficiency comes from both particles hitting the same phoswich. At rger values of Δp the chance of one of the particles hitting outside e array increases, causing the efficiency to decrease.

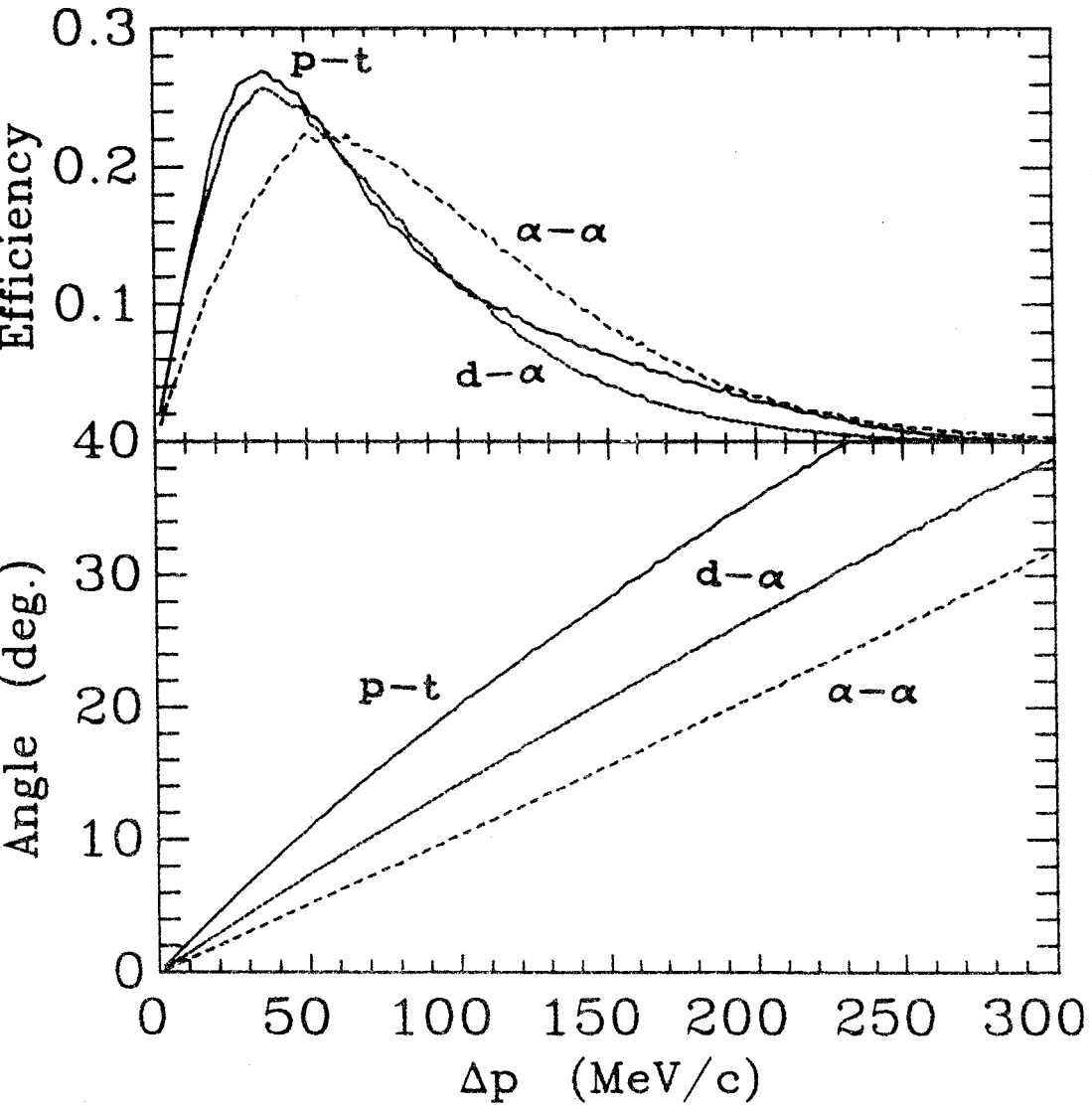

gure III-7 Calculated efficiency for MWPC and phoswich array for p-t, d-α and α-α particle pairs for Θ_{MWPC}=45°.

Chapter IV

Large Angle Correlation Experiment Data And Discussion.

In this chapter the results of the large angle correlation experiment are presented and discussed. The inclusive energy spectra will be discussed first, and then the two-particle correlations will be presented.

A. Inclusive Energy Spectra

1. Light Particle Spectra

The inclusive energy spectra for p, d, t, ^{3}He, and ^{4}He for 40 MeV/nucleon C+C, Ag, Au and 50 MeV/nucleon C+C are shown in Figures IV-1-4, for θ=15°, 25°, 45°, 55°, 70°, 85°, 100°, and 150°. The spectra have been corrected for reaction losses in the phoswiches, and the errors shown are statistical. The spectra are smooth, decreasing monotonically with increasing angle and decaying exponentially at high energies, suggesting a thermal origin for the observed particles. The spectra show signs of emission from a fast projectile-like source at the forward angles, θ=15° and 25°. At low energies there is evidence of emission from a slow target-like source.

2. Moving Source Parameterization.

We have fitted the data with a triple moving source parameterization, which assumes the presence of a projectile-like source, a target-like source, and an intermediate velocity source. All three

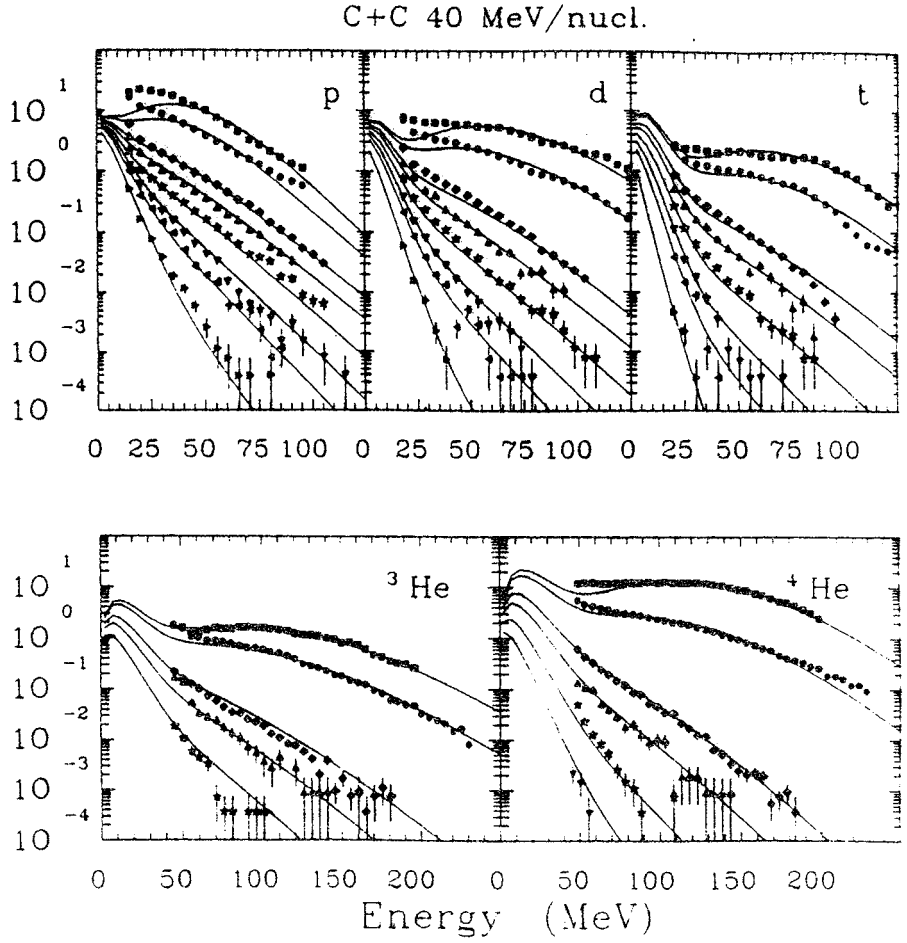

re IV-1 Light particle energy spectra for 40 MeV/nuc. C+C. The lines are the results of moving source fits.

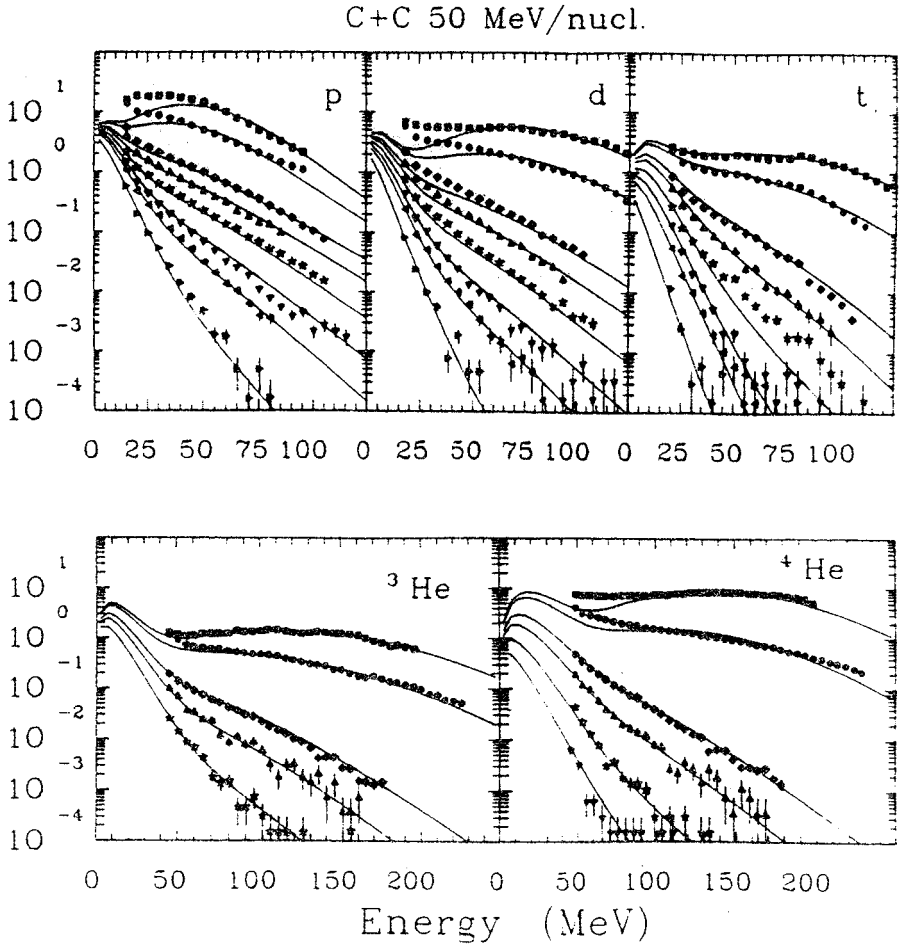

e IV-2 Light particle energy spectra for 50 MeV/nuc. C+C. The lines are the results of moving source fits.

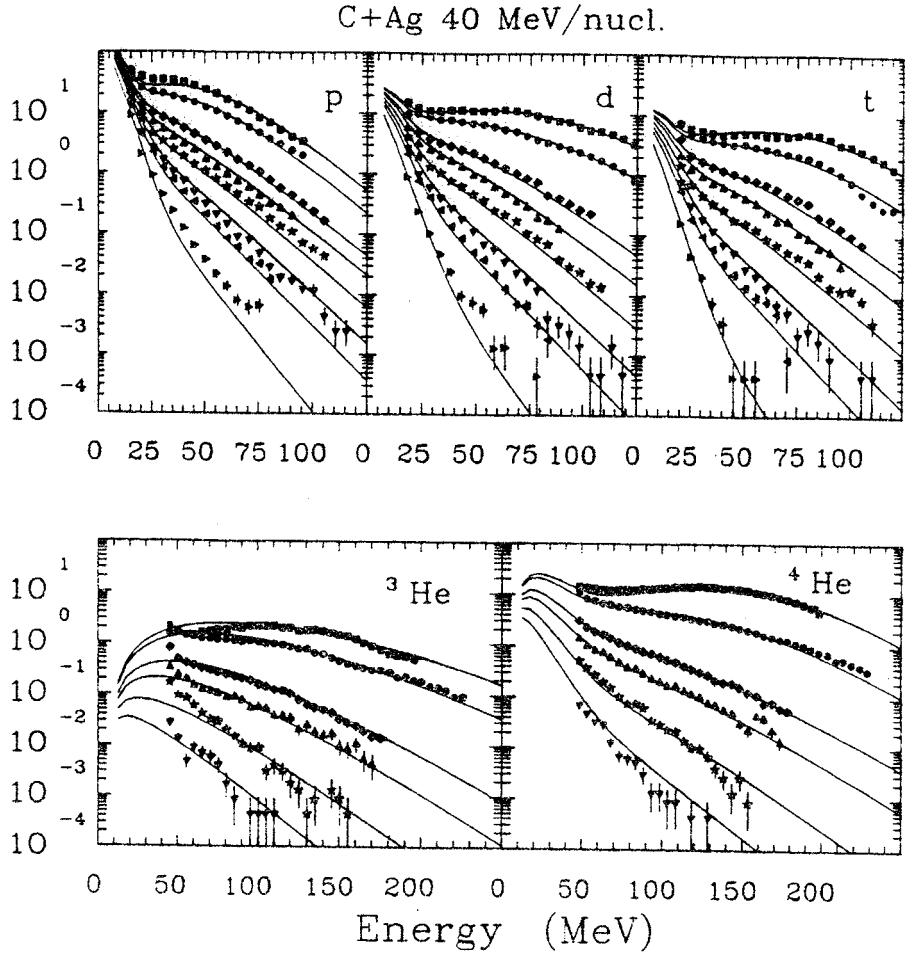

e IV-3 Light particle energy spectra for 40 MeV/nuc. C+Ag. The lines are the results of moving source fits.

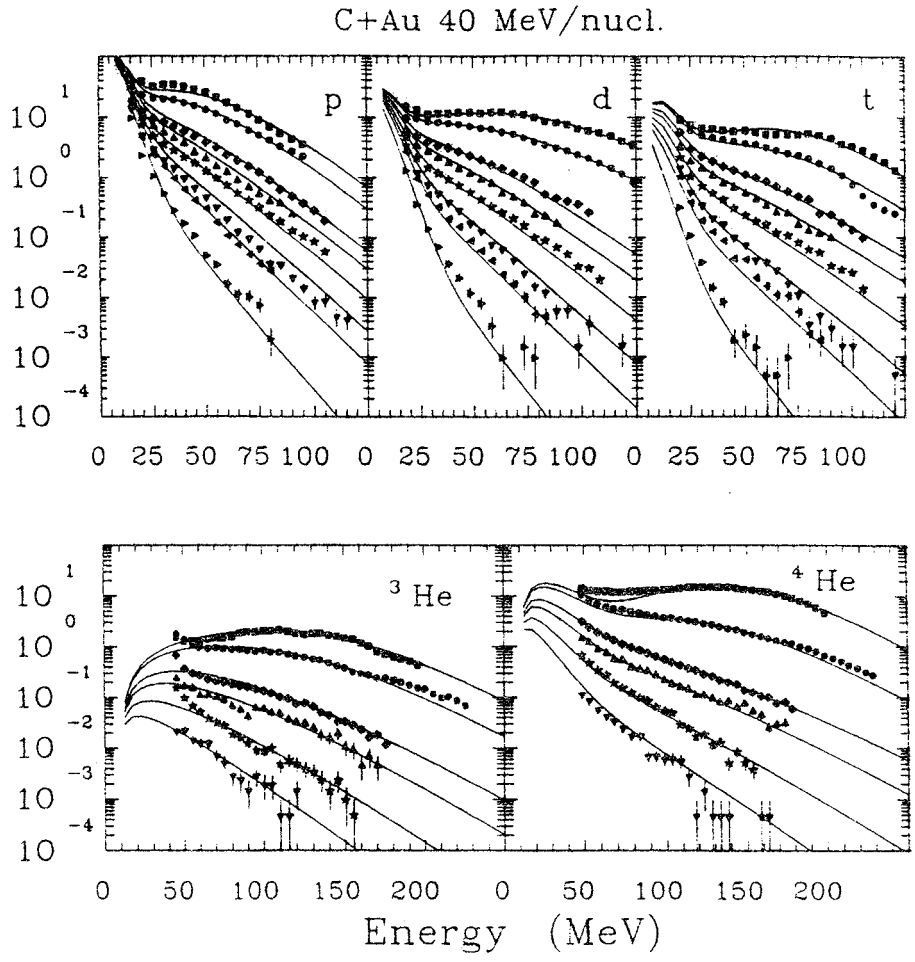

ure IV-4 Light particle energy spectra for 40 MeV/nuc. C+Au. The lines are the results of moving source fits.

rces are assumed to move in the beam direction. While it is true that 40-50 MeV/nucleon the three sources are not well separated, the energy ctra show definite signs of each of the three sources. The energy ctra for each source are assumed to be described by a relativistic well-Boltzmann energy distribution. In the rest frame of each source distribution is given by

$$\frac{d^2\sigma}{dp'd\Omega'} = \frac{\sigma_0}{4\pi m^3} \frac{e^{-E'/\tau}}{2(\tau/m)^2 K_1(m/\tau)+(\tau/m)K_0(m/\tau)} \qquad \text{(IV-1)}$$

re p' and E' are the momentum and total energy of a particle in the rce rest frame, and K_0 and K_1 are modified Bessel functions of the ond kind, and σ_0 and τ are the production cross section and source perature for the given source. The energy spectra in the lab are then en by

$$\frac{}{\Omega} = \frac{pE'd^2\sigma}{p'^2 dp'd\Omega'} \qquad \text{(IV-2)}$$

re

$$= \gamma(E-\beta pcos\theta_{lab}), \qquad \text{(IV-3)}$$

d E are the momentum and total energy of a particle in the lab frame, is the lab angle, and β is the velocity of the source in the lab. each source β, σ_0, and τ are fit using those angles and energies that dominated by the source being fit. The angles and energy ranges fit

each source are listed in Table IV-1. Also listed in Table IV-1 are Coulomb shifts that were applied to the Ag and Au data prior to ing. The fits are shown in Figures IV-1-4 as lines and the extracted meters are listed in Table IV-2. Typical uncertainties are 5-20% for ±0.002-0.007 for β and ±0.2-0.5 MeV for τ. The target-like source not fitted for the ^{3}He spectra for the Ag and Au targets. Due to the of helium spectra backward of θ=85° the target-like source for the um isotopes had to be fit using the low energy part of the spectra at forward angles. In addition the fit for the intermediate source uded the 45° spectra for the helium isotopes. The extracted ameters for the helium isotopes have higher velocities and eratures for the target-like and intermediate sources than do the ogen isotopes. For the projectile-like source the helium isotopes the same velocities as the hydrogen isotopes, but higher eratures. These differences between the extracted parameters might ue to the different angular and energy ranges used in the fits.

The fits are excellent except for some differences at forward angles the carbon target. These differences may be caused by the small size ne sources for the C+C system. The intermediate source size with the est weight (A2πbdb) is twelve nucleons.

3. Heavy Fragment Spectra

The gains on the most forward phoswiches, θ=15°, 25° and 45°, were such that particles between Li and C were also seen. The spectra for e particles are shown in Figures IV-5,6. Both the Li and ^{7}Be ease monotonically with increasing angle. The lines are the results single moving source fit to the Li and ^{7}Be spectra, the extractec

Table IV-1

Energy and Angle Ranges Used for Moving Source Fits and the Coulomb Shifts for Ag and Au Data

ticle	Target		Source					
	Ag	Au	Target-like		Intermediate		Projectile-like	
	V_c	V_c	θ	E	θ	E	θ	E
	(MeV)	(MeV)		(MeV)		(MeV)		(MeV)
	4	5	100-150°	10-50	55-85°	40-125	15-25°	40-125
	4	5	100-150°	10-50	55-85°	50-125	15-25°	40-150
	4	5	85-150°	10-50	55-85°	50- 75	15-25°	50-100
	5	10	45- 70°	40-80	45-70°	80-200	15-25°	80-250
	5	10	45- 85°	40-60	45-55°	100-200	15-25°	80-250

Table IV-2
Moving Source Parameters

Target like source			Intermediate source			Projectile like source		
Cross Section	Velocity	Temp.	Cross Section	Velocity	Temp.	Cross Section	Velocity	Temp.
ticle σ_0 (mb)	β	τ (MeV)	σ_0 (mb)	β	τ (MeV)	σ_0 (mb)	β	τ (MeV)
			40 MeV/nucleon C+C					
620	0.016	4.6	472	0.146	11.4	311	0.259	4.9
470	0.027	4.3	138	0.124	11.1	215	0.234	5.5
460	0.037	3.8	56	0.124	10.3	74	0.201	5.7
280	0.064	5.5	62	0.152	11.8	95	0.251	9.6
970	0.071	5.3	260	0.149	9.7	757	0.240	7.0
			50 MeV/nucleon C+C					
600	0.022	5.3	460	0.174	14.0	361	0.288	5.2
380	0.026	4.8	158	0.145	13.0	239	0.267	6.6
205	0.047	5.5	99	0.153	8.8	51	0.237	5.5
350	0.053	6.2	60	0.184	12.7	90	0.291	9.9
470	0.080	6.8	111	0.165	11.7	652	0.271	7.9
			40 MeV/nucleon C+Ag					
8200	0.015	3.5	1910	0.129	11.9	760	0.257	6.1
1800	0.019	4.2	920	0.123	11.9	411	0.251	7.8
800	0.020	4.2	420	0.113	11.7	157	0.210	6.2
			241	0.179	15.4	66	0.278	11.4
1640	0.063	7.0	808	0.163	16.0	737	0.255	7.0
			40 MeV/nucleon C+Au					
8700	0.012	3.6	2450	0.123	12.2	670	0.263	6.7
2000	0.015	3.8	1020	0.118	12.2	414	0.256	7.5
1100	0.031	4.3	480	0.115	13.3	154	0.208	5.3
			162	0.168	17.1	88	0.267	8.7
1250	0.069	7.7	569	0.154	18.4	866	0.253	6.6

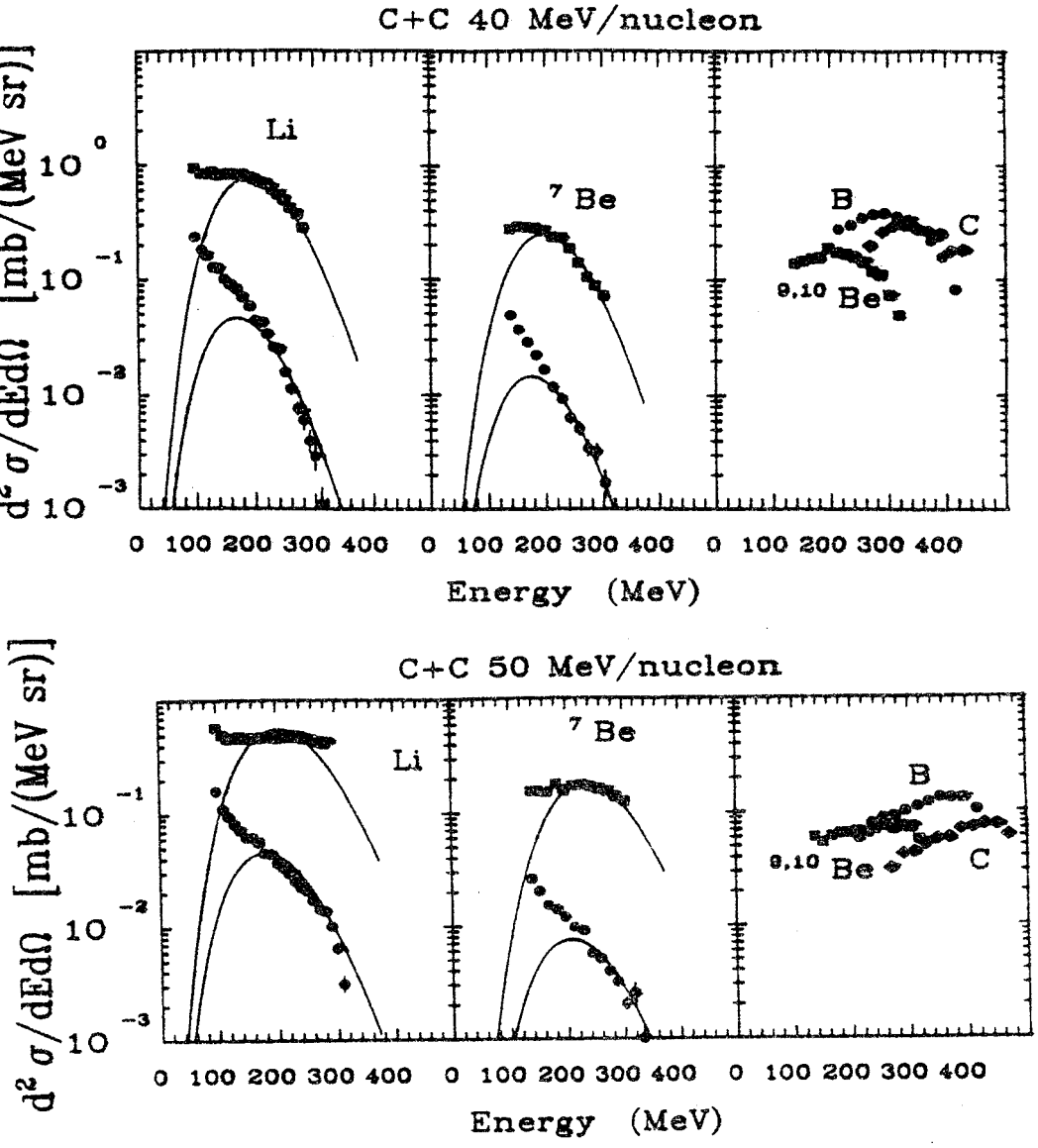

ure IV-5 Heavy fragment energy spectra for 40 MeV/nuc. C+C (top) and 50 MeV/nuc. C+C (bottom). The lines are the results of moving source fits.

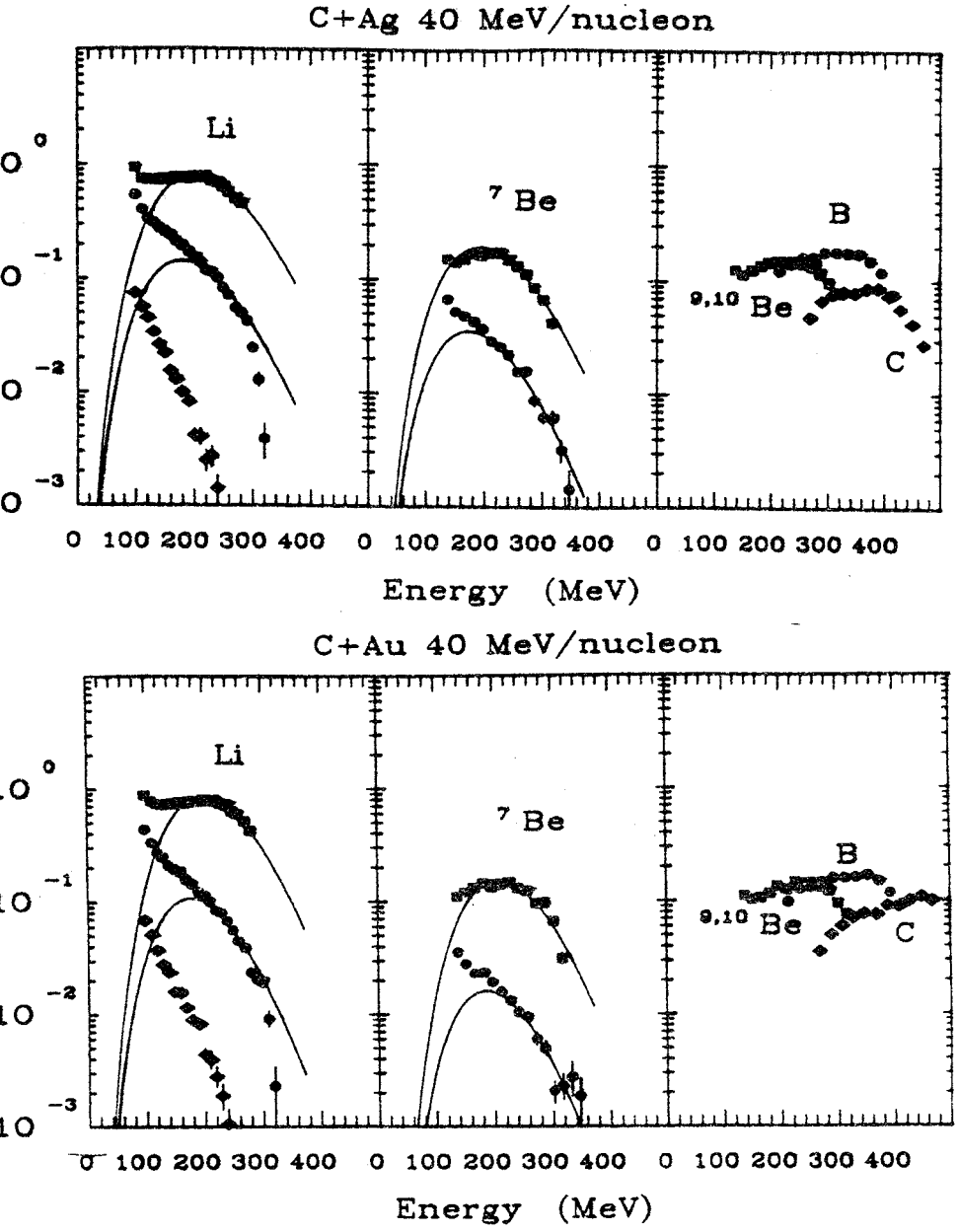

IV-6 Heavy fragment energy spectra for 40 MeV/nuc. C+Ag (top) and C+Au (bottom). The lines are the results of moving source fits.

ource parameters are listed in Table IV-3 along with the Coulomb shifts hat were applied prior to fitting the data. The fits were carried out or E>200 MeV. The fits indicate that the particles are coming from the rojectile-like source. The extracted parameters for Li and ^{7}Be are imilar to those of the projectile-like source for the helium isotopes isted in Table IV-2. The ^{9,10}Be, B and C spectra are shown only for 5°. The ^{9,10}Be, B and C spectra are peaked at energies near the beam nergy indicating that they are coming from the projectile.

. Two-Particle In-Plane Correlations.

1. Two-Particle Correlations, 45° Tag

The two-particle correlations are shown in Figures IV-7-11 for p-p, -d, d-d, d-^{4}He, and ^{4}He-^{4}He. The correlations are shown in terms of the wo-particle correlation cross section, σ_{12}, divided by the singles cross ections, σ_1 and σ_2. In each case one of the particles is detected at =-45° and the second particle is detected between Θ=-170° and +170°. A egative angle for the second particle means the two particles were bserved on the same side of the beam, while a positive angle indicates ission on opposite sides of the beam. For the nonidentical particle ases (p-d, d-^{4}He), the case for which the heavier particle was detected Θ=-45° is shown. The correlations have been integrated over the ergy ranges given in Table IV-4.

In general the correlations for the C+C systems show a broad maximum positive angles which indicates a preference for emission of particles opposite sides of the beam. The magnitude of the peak increases as e mass of the observed particles increase and is slightly larger at 50

Table IV-3

Moving Source Parameters For Li and ^{7}Be

Particle	V_c (MeV)	Cross Section σ_0 (mb)	Velocity β	Temperature τ (MeV)
		40 MeV/nucleon C+C		
Li	0	75±2	0.249±0.001	8.10±0.12
^{7}Be	0	25±1	0.244±0.002	8.18±0.14
		50 MeV/nucleon C+C		
Li	0	59±6	0.283±0.001	10.45±0.16
^{7}Be	0	23±1	0.280±0.002	8.81±0.19
		40 MeV/nucleon C+Ag		
Li	12	82±2	0.244±0.002	12.86±0.20
^{7}Be	16	19±1	0.229±0.001	12.20±0.21
		40 MeV/nucleon C+Au		
Li	15	80±2	0.243±0.002	10.55±0.15
^{7}Be	20	15±1	0.238±0.003	9.85±0.29

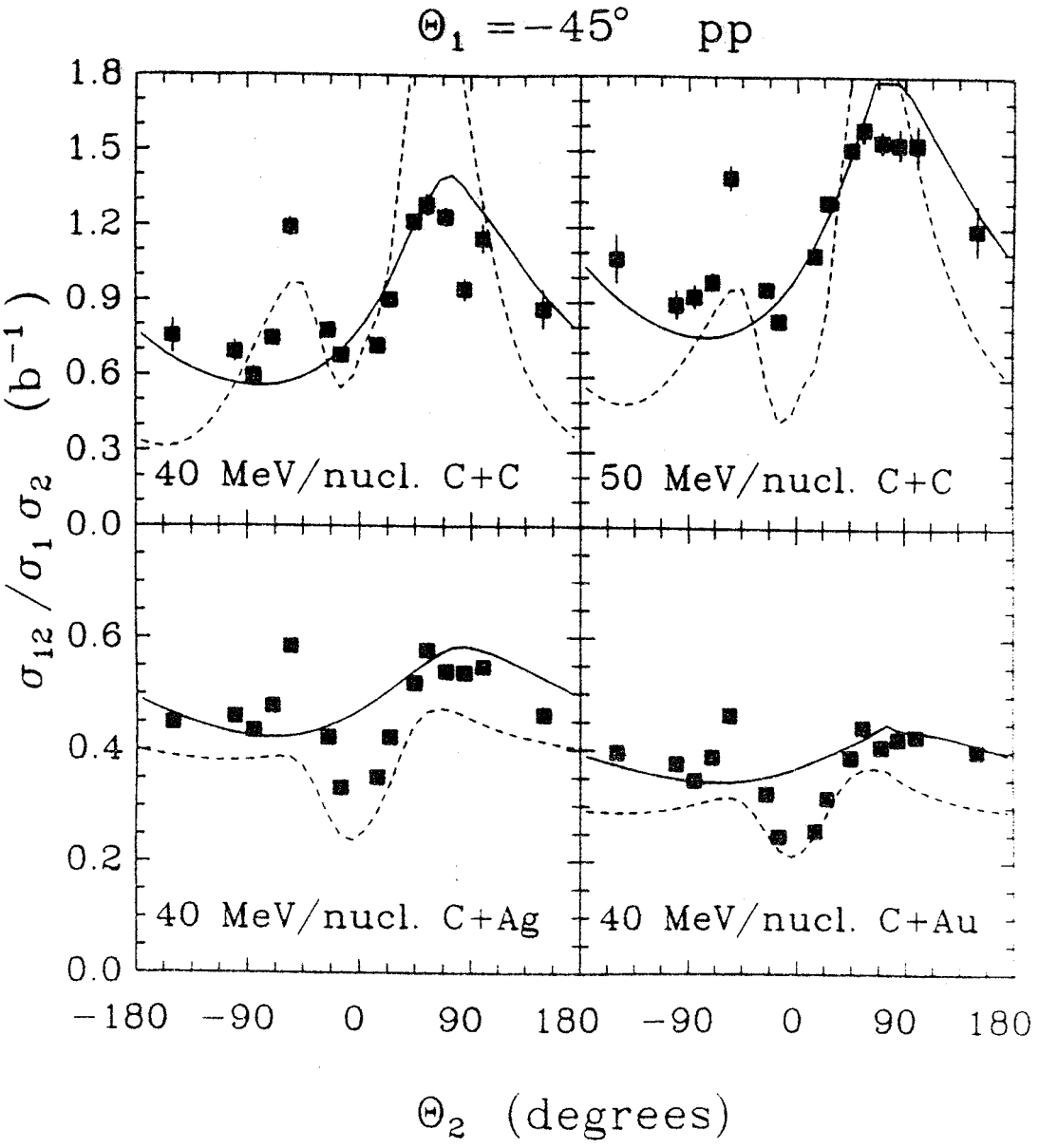

gure IV-7 Two-proton correlation function for which one proton is detected at Θ=-45°. The lines are described in the text.

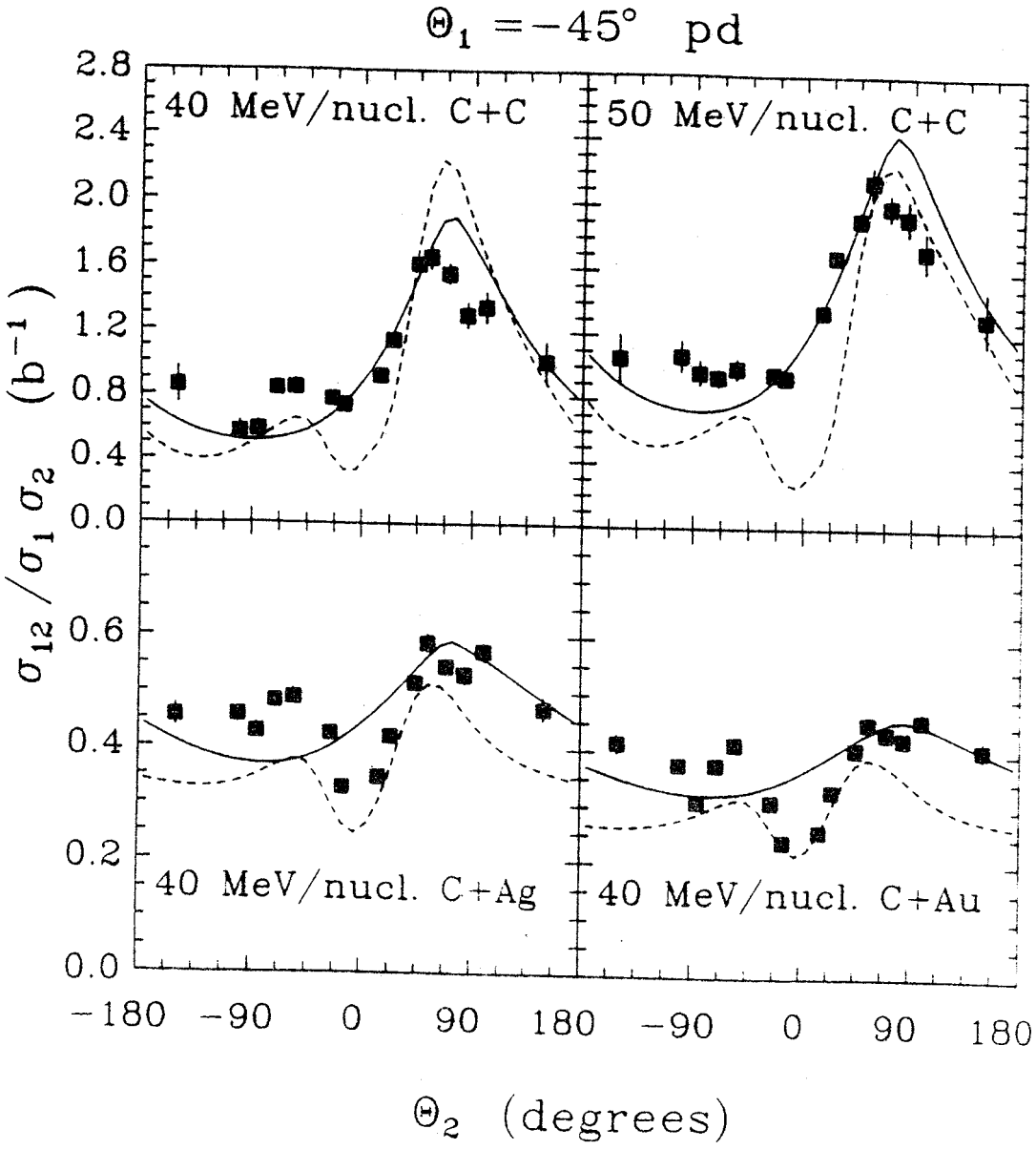

ure IV-8 Proton-deuteron correlation function for which the deuteron is detected at Θ=-45°. The lines are described in the text.

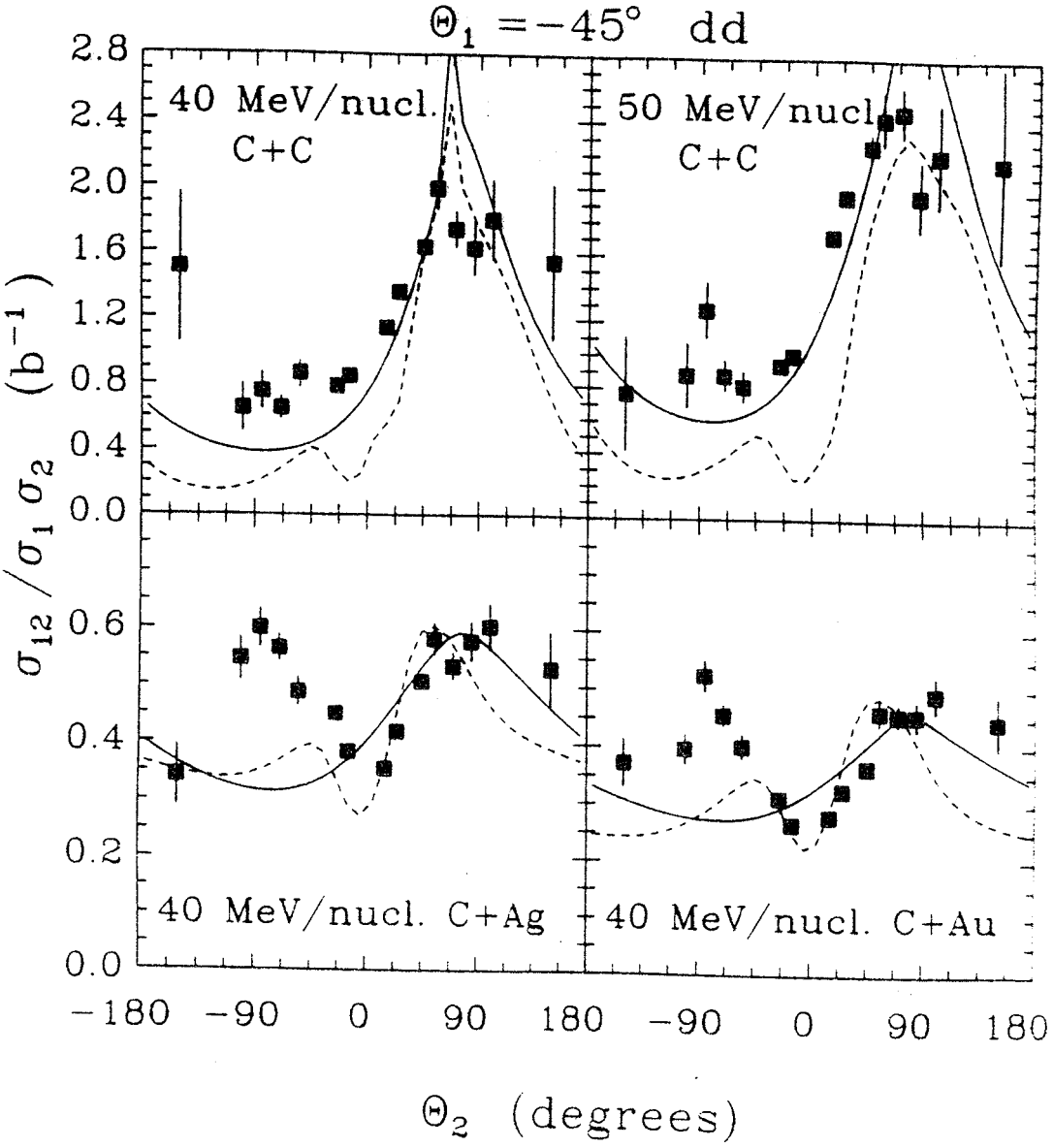

gure IV-9 Two-deuteron correlation function for which one deuteron is detected at Θ=-45°. The lines are described in the text.

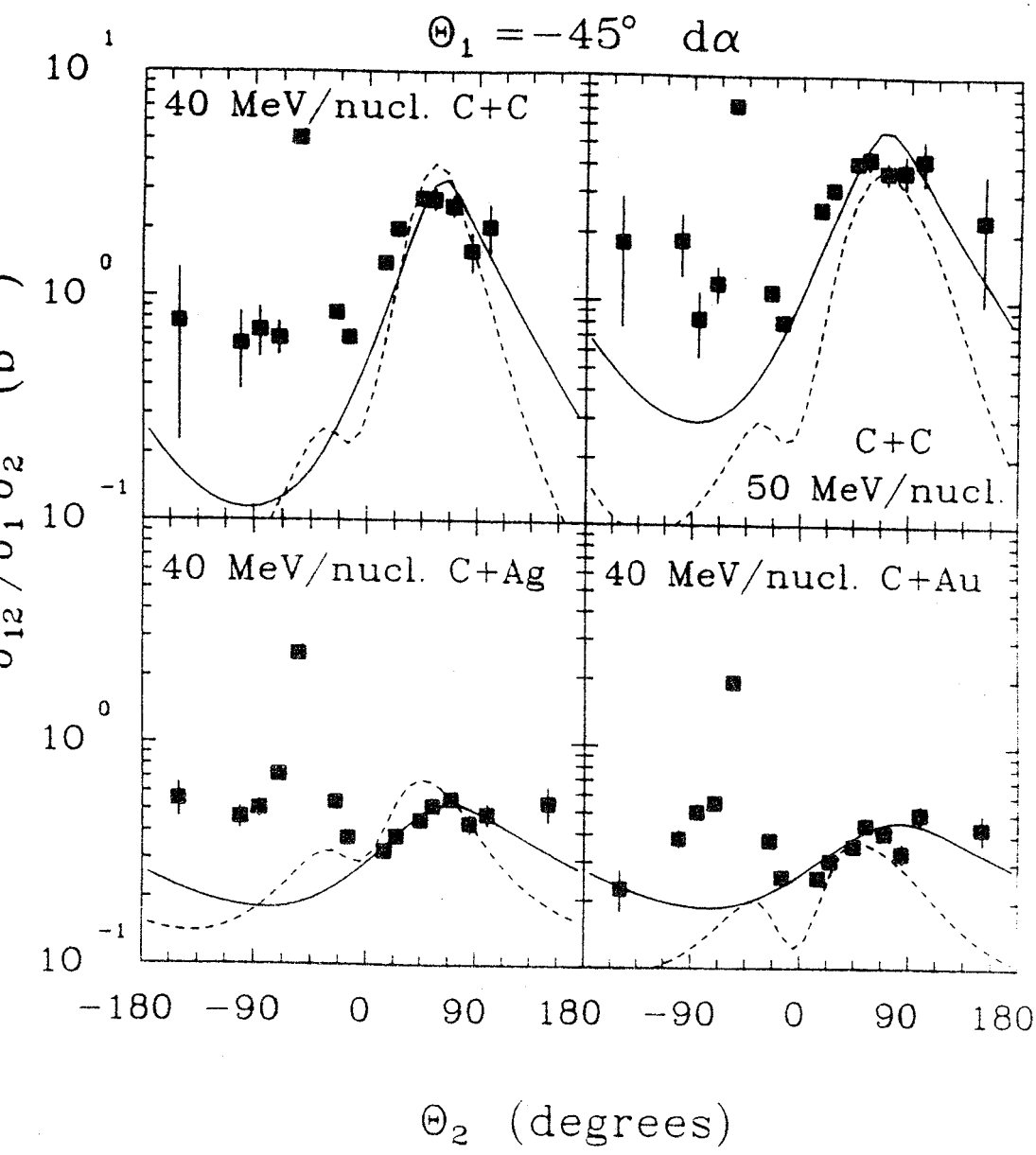

ure IV-10 Deuteron-alpha correlation function for which the alpha is detected at Θ=-45°. The lines are described in the text.

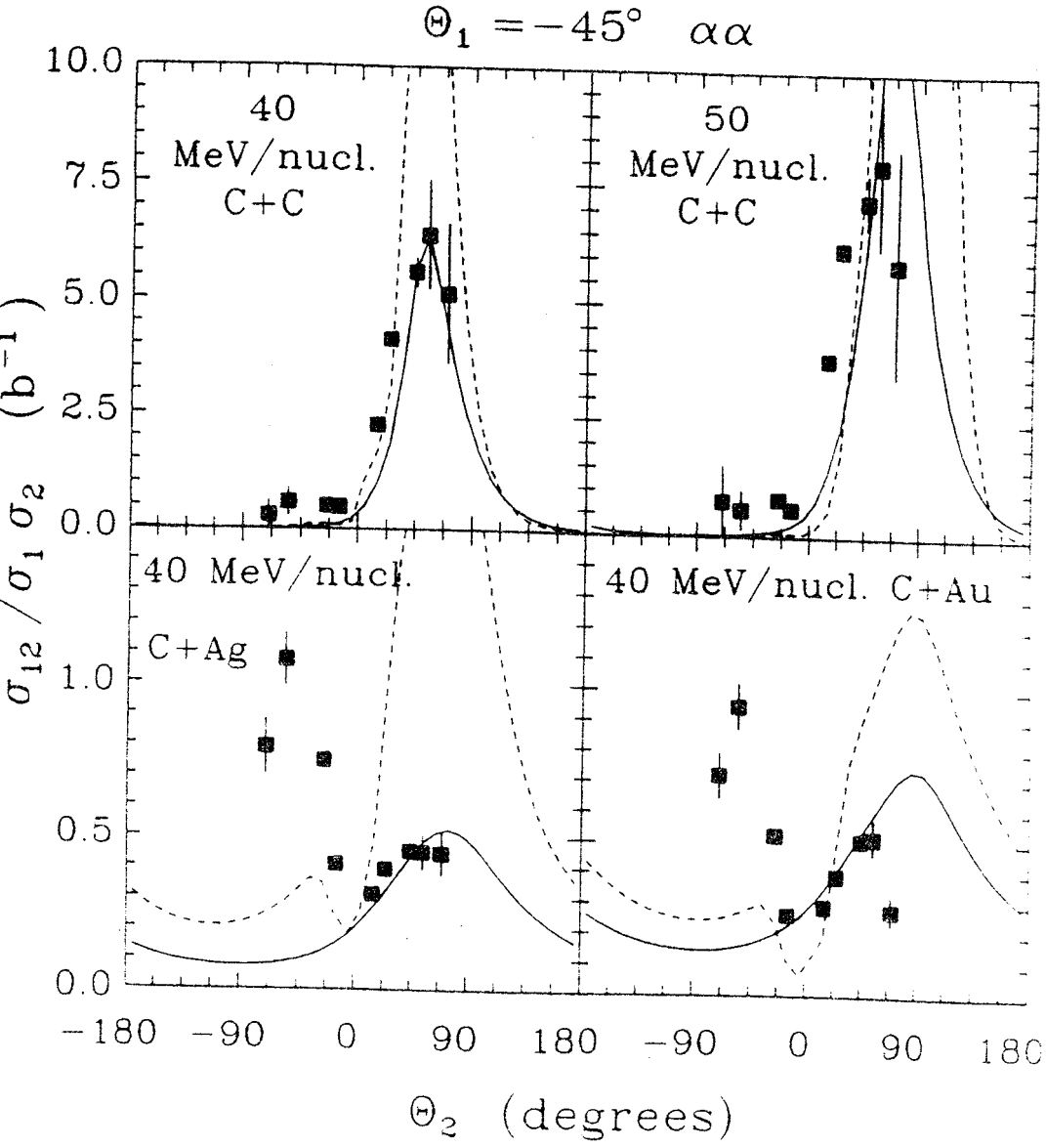

re IV-11 Alpha-alpha correlation function for which one alpha is detected at Θ=-45°. The lines are described in the text.

Table IV-4

Energy Ranges For Correlations

Particle	Energy (MeV)
p	12- 80
d	16- 80
^{4}He	47-135

MeV/nucleon than at 40 MeV/nucleon. For negative angles the correlations are almost flat as a function of the angle of the second particle. The p-p and d-^{4}He correlations are exceptions to this trend because they show peaks at θ=-55°. These peaks come from the decay of particle unstable states in ^{2}He and ^{6}Li. The C+Ag and C+Au systems have different systematic behavior. The correlation function is in general almost symmetric about θ=0° with the same side being only slightly preferred. The p-p peak coming from ^{2}He break up in the light C+C systems is considerably weaker in the heavier systems. Both the d-^{4}He and ^{4}He-^{4}He correlations show strong peaks coming from the decay of particle unstable states of ^{6}Li and ^{8}Be. The ^{4}He-^{4}He peak was not observed in the lighter systems because it is difficult to form a ^{8}Be given that the average intermediate velocity source contains only 12 nucleons. The particle pairs that are not shown all exhibit the same characteristics that are seen in Figures IV-7-11. The p-t, p-^{4}He, and t-^{4}He correlations all have peaks at θ=-55° which comes from the decay of particle unstable states.

2. Momentum Conservation Model.

Energy and momentum conservation effects have been used to explain the observed correlations for small systems at lower energies [Ly 82, Ts 84, Ch 86b]. In order to explore the extent to which our data is affected by conservation laws we have carried out calculations incorporating these effects. The calculation [Ly 82, Ha 84] assumes emission of two particles from a source of size A. After the first particle is emitted the source recoils, re-equilibrates, and then emits the second particle. The calculation is repeated with the second particle being emitted first. The two cases are then averaged to produce

the final coincidence cross section. The entire calculation is integrated over impact parameter with each impact parameter having a weight $dW=2\pi b \cdot db \cdot A$ where b is the impact parameter and A is the source size which comes from a fireball model [We 76, Go 77] calculation. The calculation is normalized by the total reaction cross section. The parameters listed in Table IV-2 for the intermediate source were used to describe the emitting source. For greater detail on the momentum conservation calculation see the Appendix.

The results of the momentum conservation calculations are shown in Figures IV-7-11 as solid lines. The calculations have been renormalized to the data at $\theta=+45°$ and $+55°$. The calculations do a good job of reproducing the general trends in the data but miss some of the details. In the lighter systems the same side correlations are basically flat, except for those cases that have contributions from the decay of resonances, while the calculation predicts a broad minimum at about $\theta=-80°$. The heavier systems have a "V" shaped dip around $\theta=0°$, but the calculations show no such dip.

Until now we have assumed that the observed two-particle correlations are coming only from the intermediate source although from the inclusive spectra shown in Figures IV-1-4 it is evident that a substantial fraction of the observed particles come from sources other than the intermediate source. In Figure IV-12a the contribution to the deuteron singles cross section from each of the three observed sources is shown for C+Au system. For small angles the projectile source contributes heavily to the singles cross section while for large angles the target like source dominates the cross section. Even for small angles for which one would expect the projectile-like source to dominate, the target-like source contributes about ten percent of the total cross section. Figure IV-12b shows the

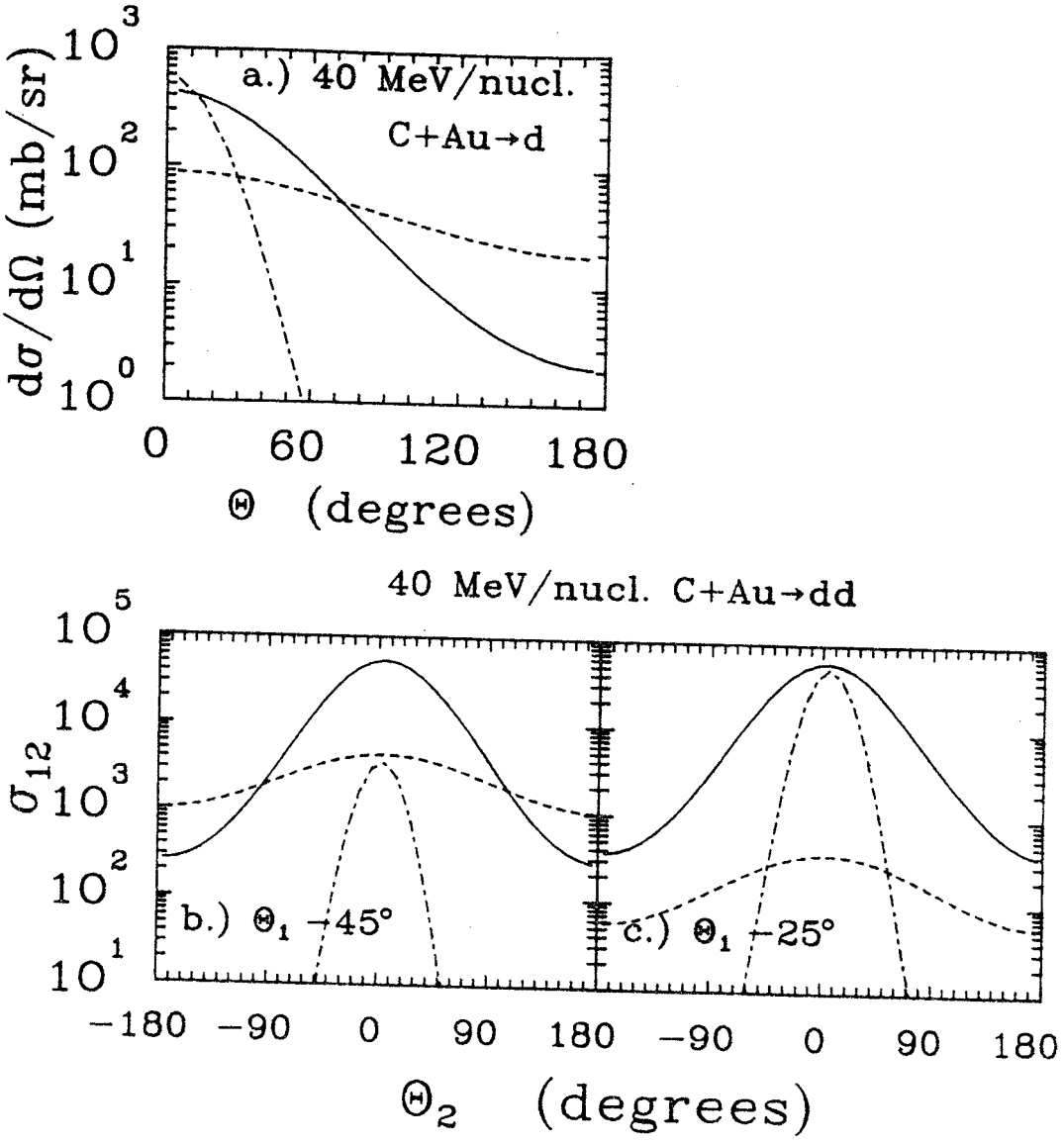

Figure IV-12 Contribution from the three sources to the deuteron singles cross section (a) and to the two deuteron coincidence cross section for Θ_{tag}=-45° (b) and for Θ_{tag}=-25° for 40 MeV/nuc. C+Au.

contribution to the two-deuteron coincidence cross section from each of the three sources according to momentum conservation calculations using the parameters for each of the sources given in Table IV-2. From Figure IV-12b we can see that adding the contributions of the three sources together will increase the coincidence cross section around $\Theta=0°$ by less than 10% while in Figure IV-12a we see that the addition of the projectile and target-like sources more than doubles the singles cross sections near $\Theta=0°$. This summation will lead to the dip around 0° which is observed in the data.

For the lighter systems the effect of the other two sources is somewhat different than for the heavier systems. Figure IV-13a shows the contribution to the deuteron singles cross section for each of the three sources for 40 MeV/nucleon C+C. At forward angles the projectile-like source is far more dominant than it is for C+Au. The projectile-like source is also the leading contributor to the two-deuteron coincidence cross section at the most forward angles as seen in Figure IV-13b for correlations with $\Theta_1=-45°$. The target-like source contribution to the two-deuteron cross section is peaked at about $\Theta_2=+50°$.

The dashed lines in Figures IV-7-11 are the results of three-source momentum conservation calculations. These calculations take into account only correlations between two particles coming from the same source. Unlike the single source calculation discussed earlier no normalization has been applied to the three source calculation. The calculation now produces a "V" shape for small Θ for the heavier systems. Also where the single source calculation had a broad minimum for same side correlations, the three source calculation shows a maximum at about $\Theta=-55°$. This maximum is almost as large as the opposite side maximum for the heavier systems. The most notable disagreement between the data and the three

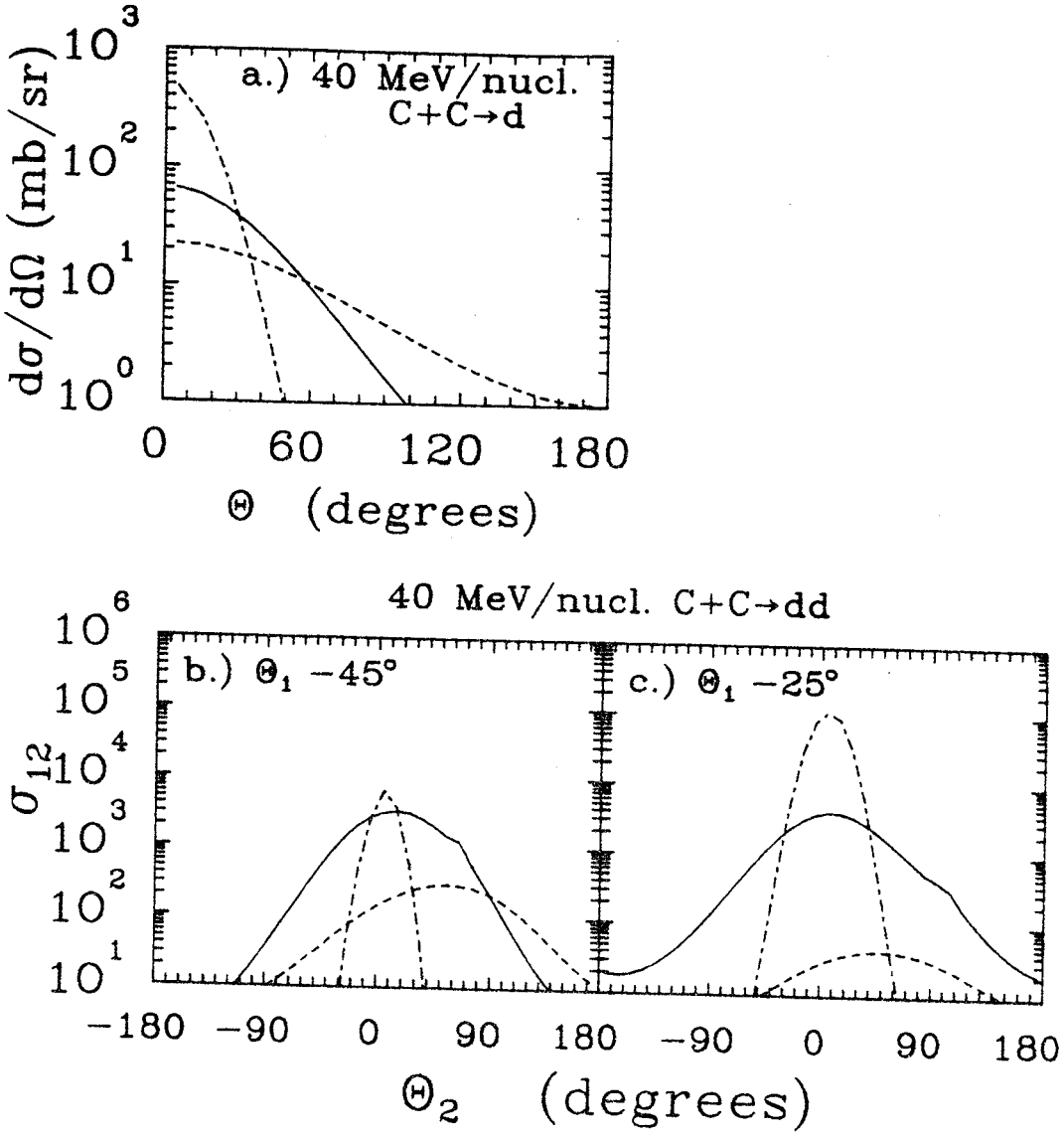

Figure IV-13 Contribution from the three sources to the deuteron singles cross section (a) and to the two deuteron coincidence cross section for Θ_{tag}=-45° (b) and for Θ_{tag}=-25° for 40 MeV/nuc. C+C.

source calculation is the under prediction of the coincident cross section for large θ. This disagreement is probably due to correlations between in which one particle comes from the intermediate velocity source and the other particle comes from the target-like source. Correlations involving particles from different sources are not included in the three-source momentum conservation calculation.

3. Two-Particle Correlations, 25° Tag

The two-particle correlations triggered on a light particle at θ=25° are shown in Figures IV-14-18 for p-p, p-d, d-d, d-^{4}He and ^{4}He-^{4}He. The correlations have the same general features as the correlations triggered on the 45° tag telescopes. The light C+C systems show a strong enhancement of the opposite side, while the heavier C+Ag and C+Au systems are symmetric about θ=0°. Strong peaks are seen in the heavy systems on the same side of the beam for the d-^{4}He and ^{4}He-^{4}He correlations coming from the decay of particle unstable states in ^{6}Li and ^{8}Be. There is also some evidence in all four systems of a enhancement at θ=-15° in the p-p correlations and in the C+C systems for the d-^{4}He correlations.

The lines in Figures IV-14-18 are the results of three source momentum conservation calculations. The calculations do not reproduce the data for θ_1=-25° as well as they do for θ_1=-45°. Most noticeably the calculations predict a strong peak at small positive angles for p-p correlations and for d-d correlations in the C+C systems and for p-p correlations in the heavy systems. The general trends are, however, reproduced in most cases with the best agreement is for d-d correlations in the heavy systems and for ^{4}He-^{4}He correlations in the C+C systems.

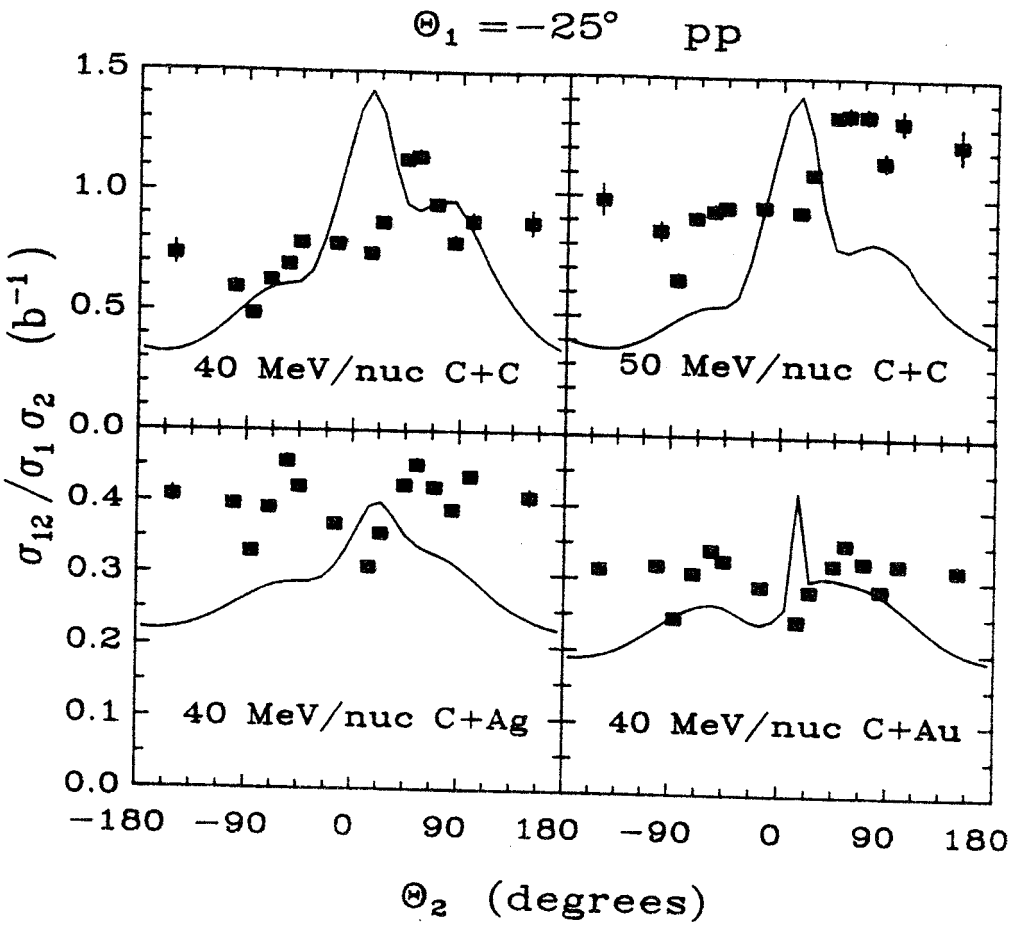

Figure IV-14 Two-proton correlation function for which one proton is detected at Θ=-25°. The lines are described in the text.

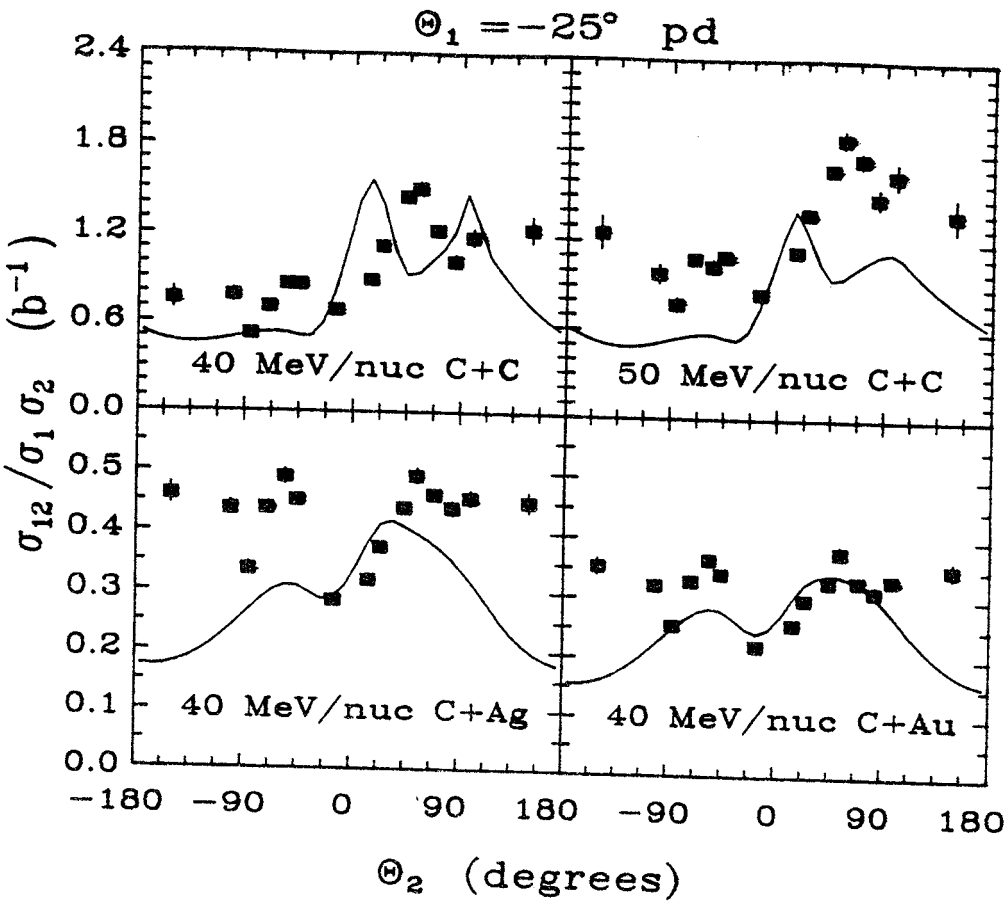

Figure IV-15 Proton-deuteron correlation function for which the deuteron is detected at θ=-25°. The lines are described in the text.

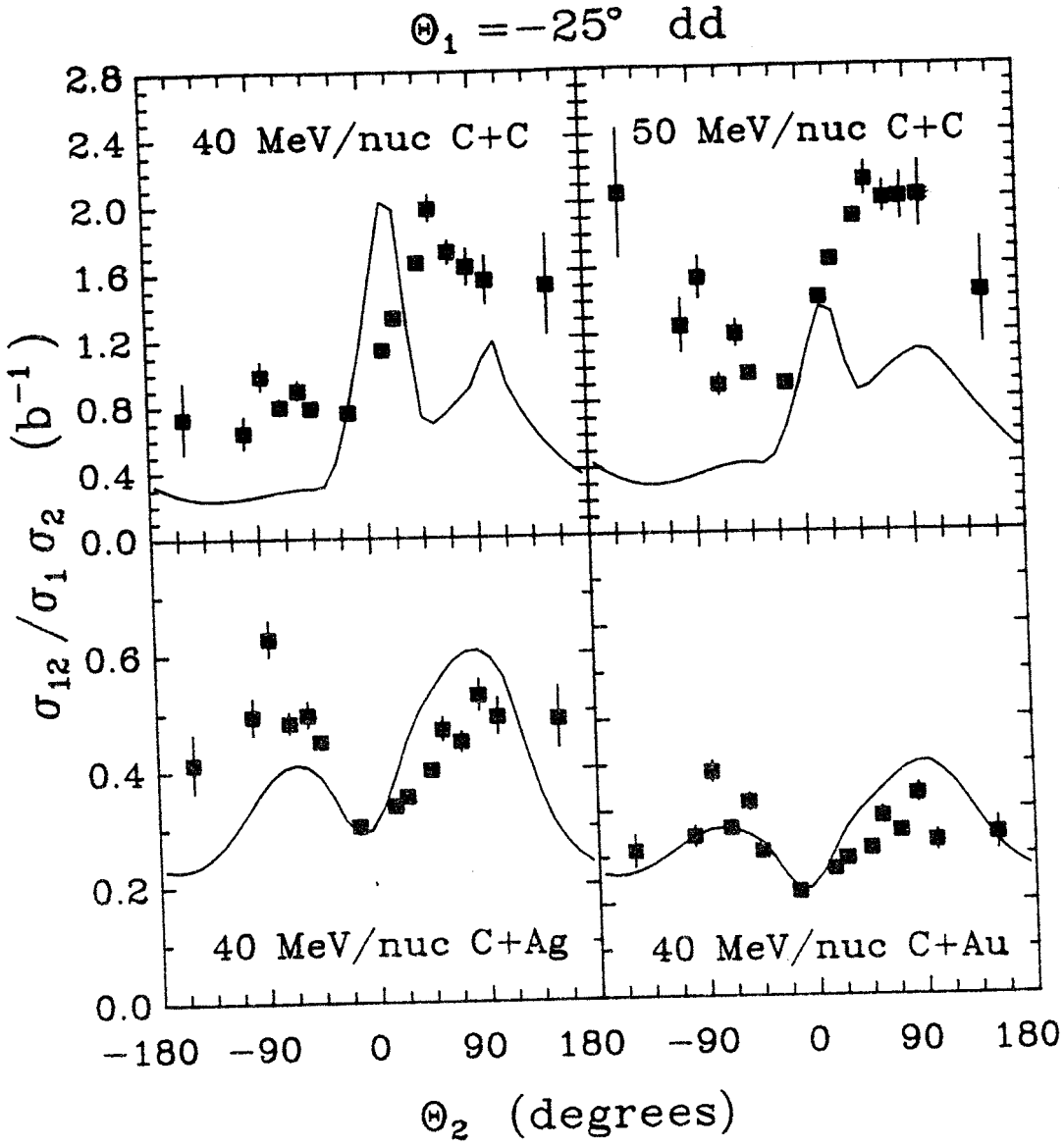

Figure IV-16 Two-deuteron correlation function for which one deuteron is detected at Θ=-25°. The lines are described in the text.

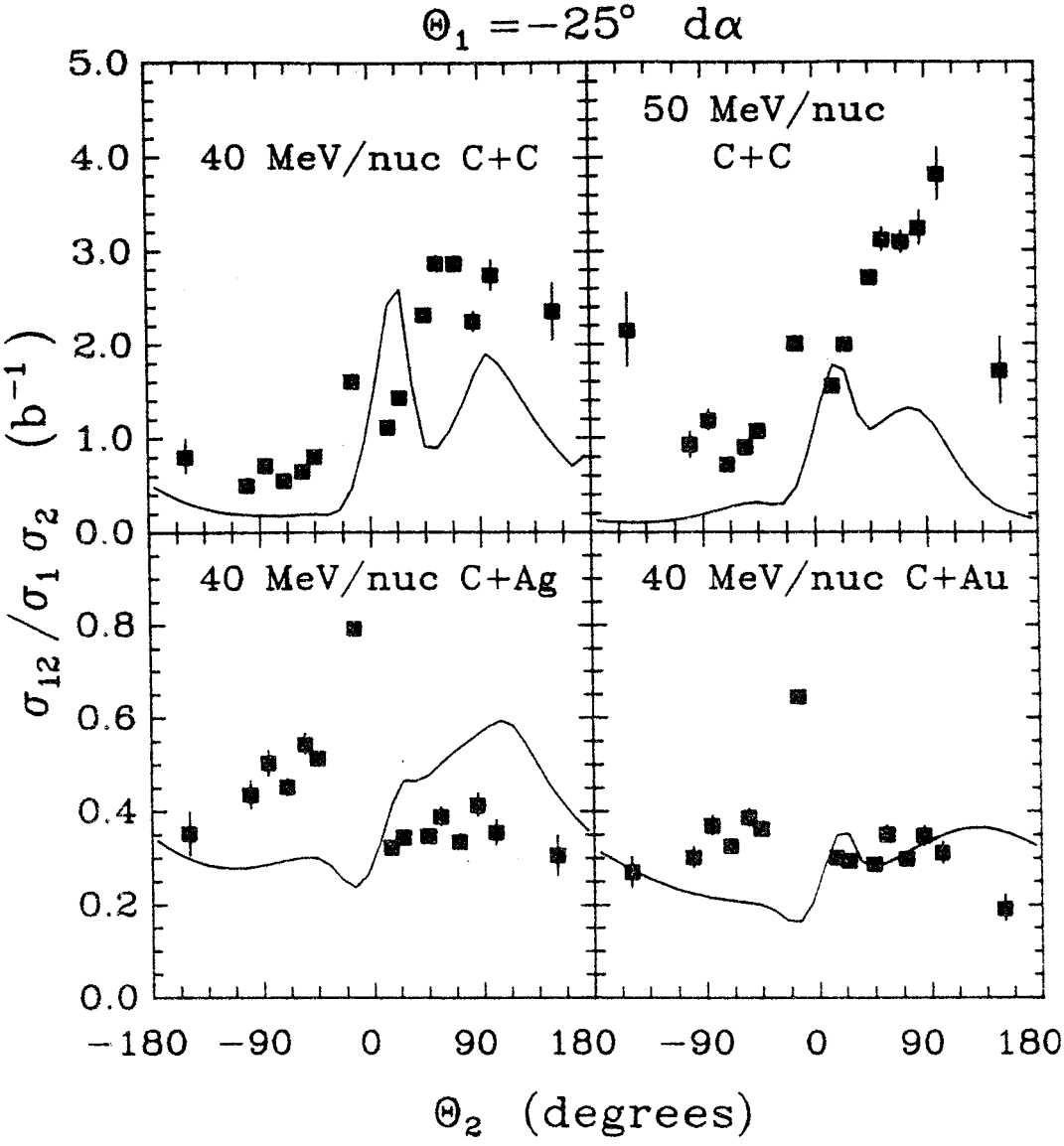

igure IV-17 Deuteron-alpha correlation function for which the alpha is detected at Θ=-25°. The lines are described in the text.

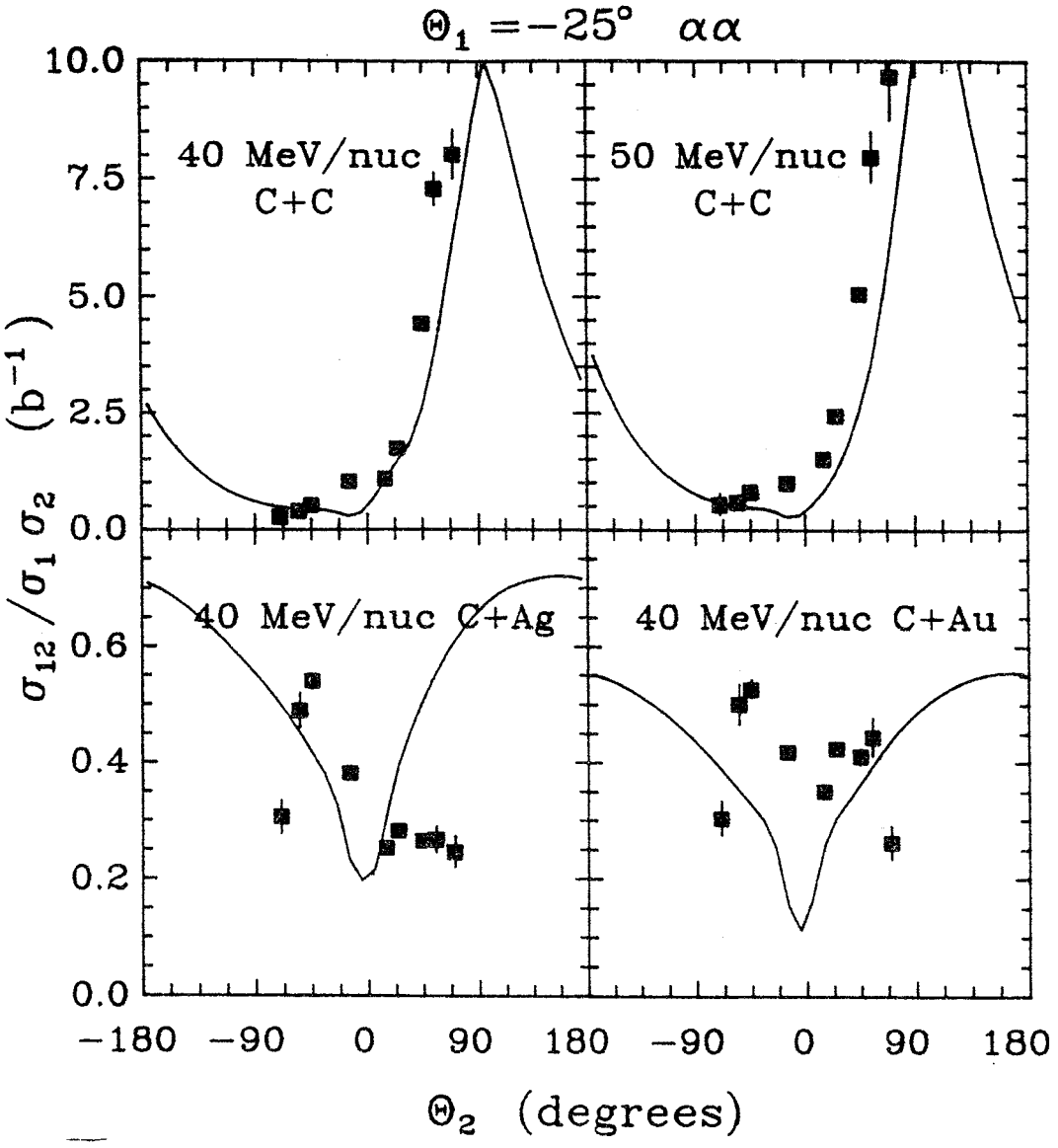

gure IV-18 Alpha-alpha correlation function for which one alpha is detected at Θ=-25°. The lines are described in the text.

The peak at small positive angles for C+C systems comes from the very large contribution to the two-particle correlation function coming form the projectile-like source. This contribution is shown for the two-deuteron correlations in Figure IV-13c. For the C+Au system the projectile-like source contribution at the most forward angles is still less than that of the intermediate source as shown in Figure IV-12c. For both the C+C and C+Au systems the importance of the target-like source is considerably less for θ_1=-25° than it is for θ_2=-45°. The contribution to the two-deuteron coincidence cross section coming from the intermediate source is very similar for the two tag angles.

In addition to light particle-light particle correlations, correlations between light particles and Li and ^{7}Be were measured using the 25° tag telescopes. In these correlations the heavy fragment, Li or ^{7}Be, is detected at θ=25°.

Figures IV-19,20 show the p-Li and p-^{7}Be correlation functions. Once again the light systems show a very strong preference for emission to opposite sides of the beam. It should be noted however, that the peak for positive angles is considerably smaller than the peak in the ^{4}He-^{4}He correlations. This is an exception to the general trend of the peak increasing with increasing mass of the detected particle pair and is probably due to it being more likely that the proton and the Li or ^{7}Be come from different sources. For the C+Ag system there is a large peak in the p-Li correlation function between θ=-15° and -55°, this peak comes from the decay of particle unstable states in ^{7}Be and ^{8}Be that decay by proton emission. For p-^{7}Be the C+Ag system looks very much like the C+C systems in that it shows a strong preference for emission to opposite sides of the beam. The C+Au system is basically flat as a function of angle for both p-Li and p-^{7}Be.

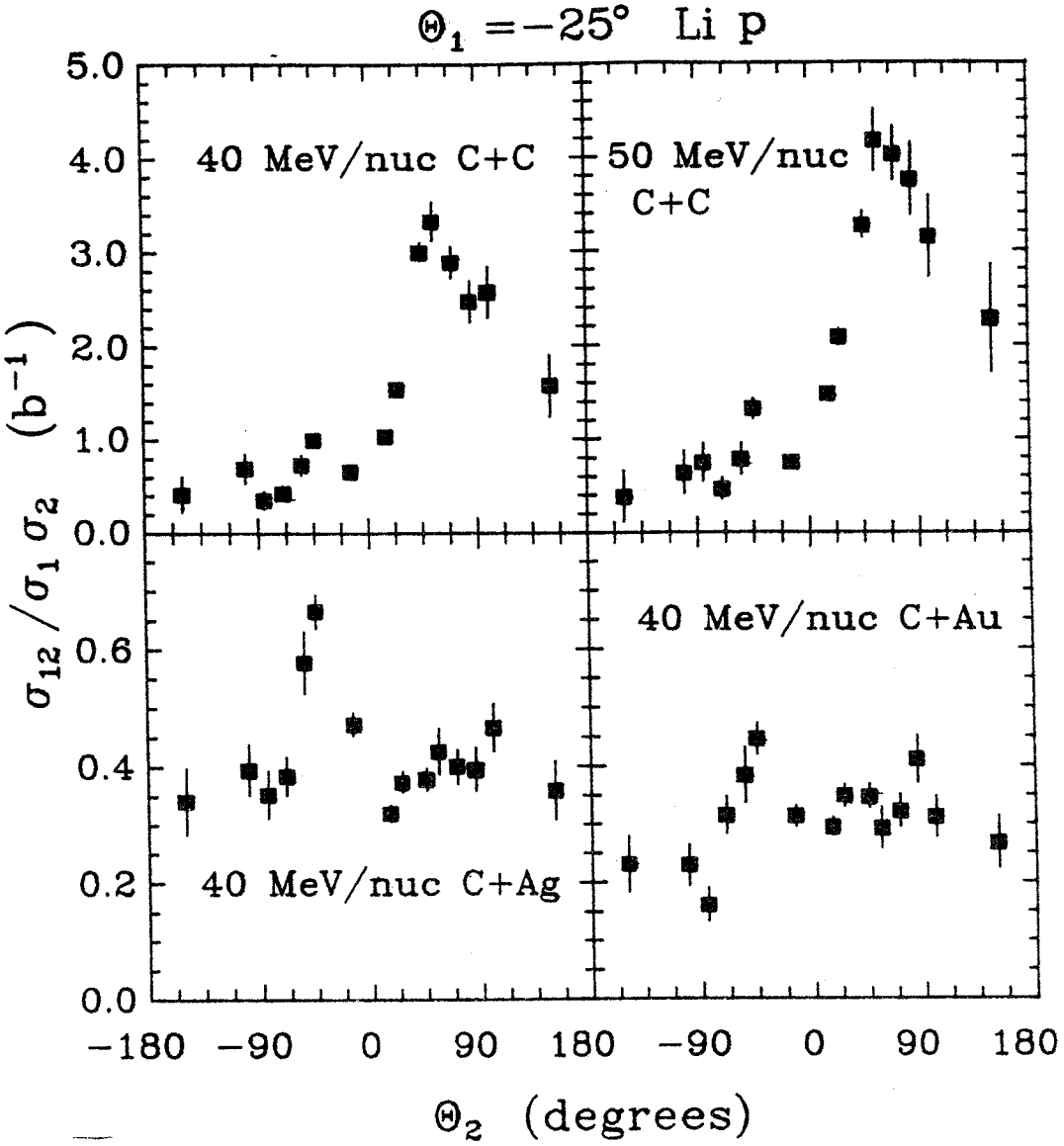

ure IV-19 Lithium-proton correlations for which the lithium is detected at Θ=-25°.

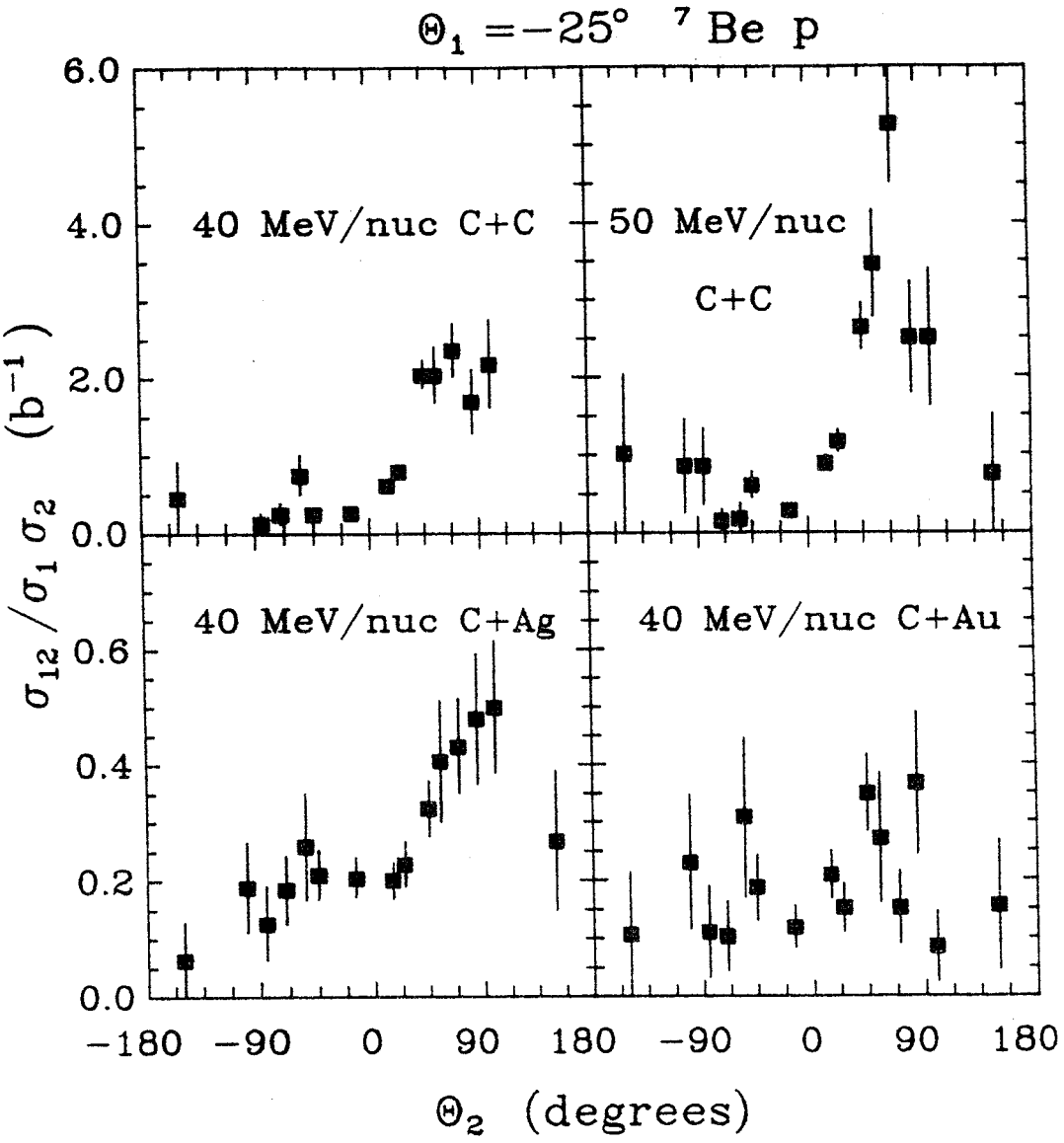

Figure IV-20 ^{7}Be-proton correlations for which the ^{7}Be is detected at θ=-25°.

C. Out-of-plane Correlations

In addition to the in-plane correlations described in the previous section, two-particle out-of-plane correlations were also measured. Correlations were measured between the out-of-plane tag telescopes (Φ=90°) and the nine in-plane detectors with Φ=0°. The correlations will first be presented in terms of the two-particle correlation function used in the previous section. Then the ratio of in-plane to out-of-plane correlations will be discussed.

1. Out-of-plane Correlation Functions

The two-particle out-of-plane correlation functions for p-p, d-d and ^{4}He-^{4}He are shown Figures IV-21-23. The lines are the results of three source momentum conservation calculations. One particle is detected at Φ=90° with Θ=25° (triangles and dashed lines) or 45° (squares and solid lines). The second particle is detected at Φ=0° with 15°$\leq\Theta\leq$150°. The correlations are integrated over the same energy ranges as the in-plane correlations. The correlation functions show very little difference between the different systems. The p-p and d-d correlations rise slowly from Θ_2=15° to 45° and then level off. The ^{4}He-^{4}He correlation functions show a slight decrease with increasing angle.

For the p-p correlations the momentum conservation calculations do an excellent job of reproducing the general trend and magnitude of the data for the heavy systems. In the C+C system, the trend but not the magnitude of the correlations in reproduced for Θ_1=-45°. For Θ_1=-25° the calculation has a large maximum at forward angles where the data has a minimum.

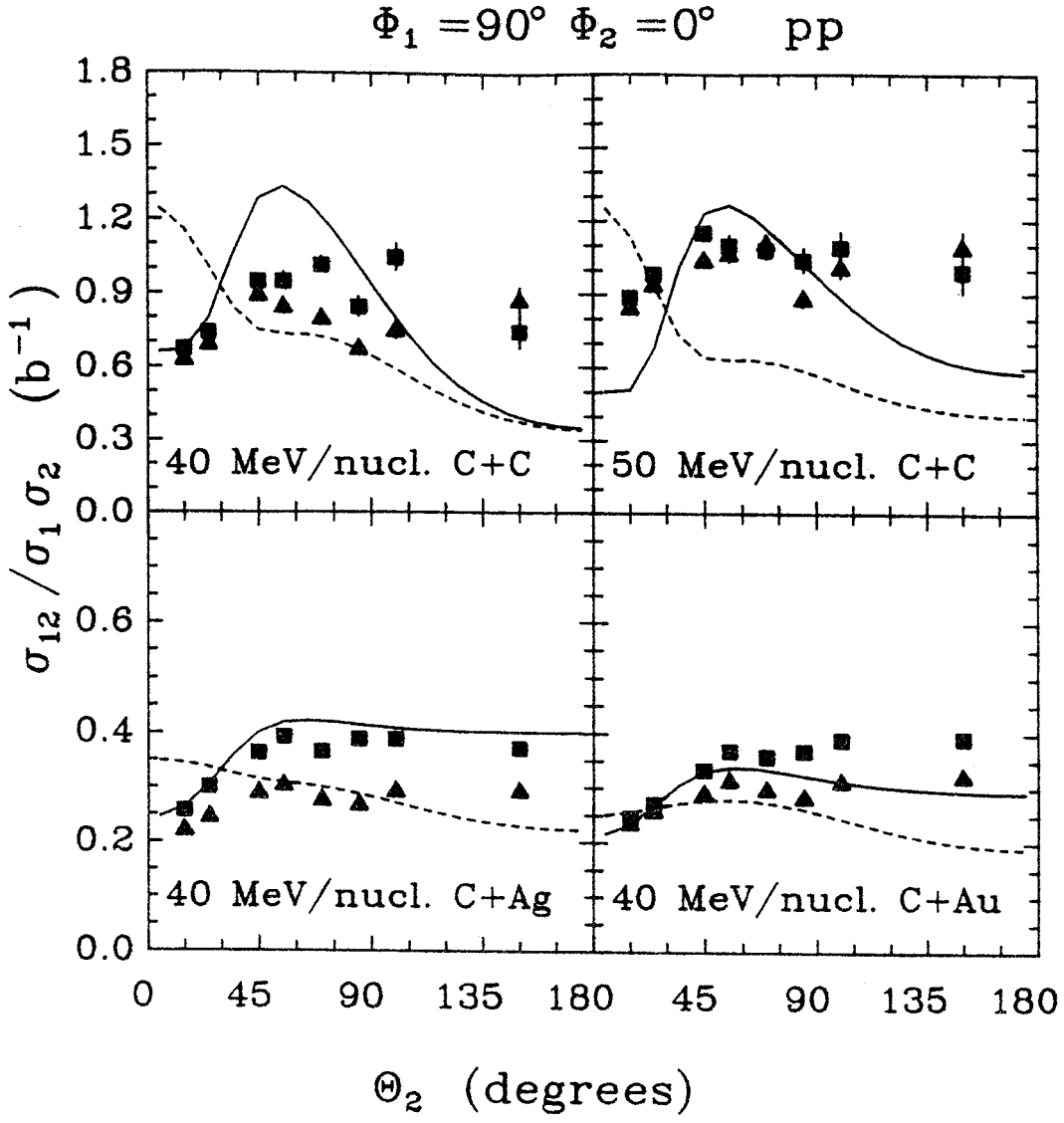

Figure IV-21 Two-proton out-of-plane correlation function for Θ_1=25° (triangles and dashed lines) and Θ_1=45° (squares and solid lines).

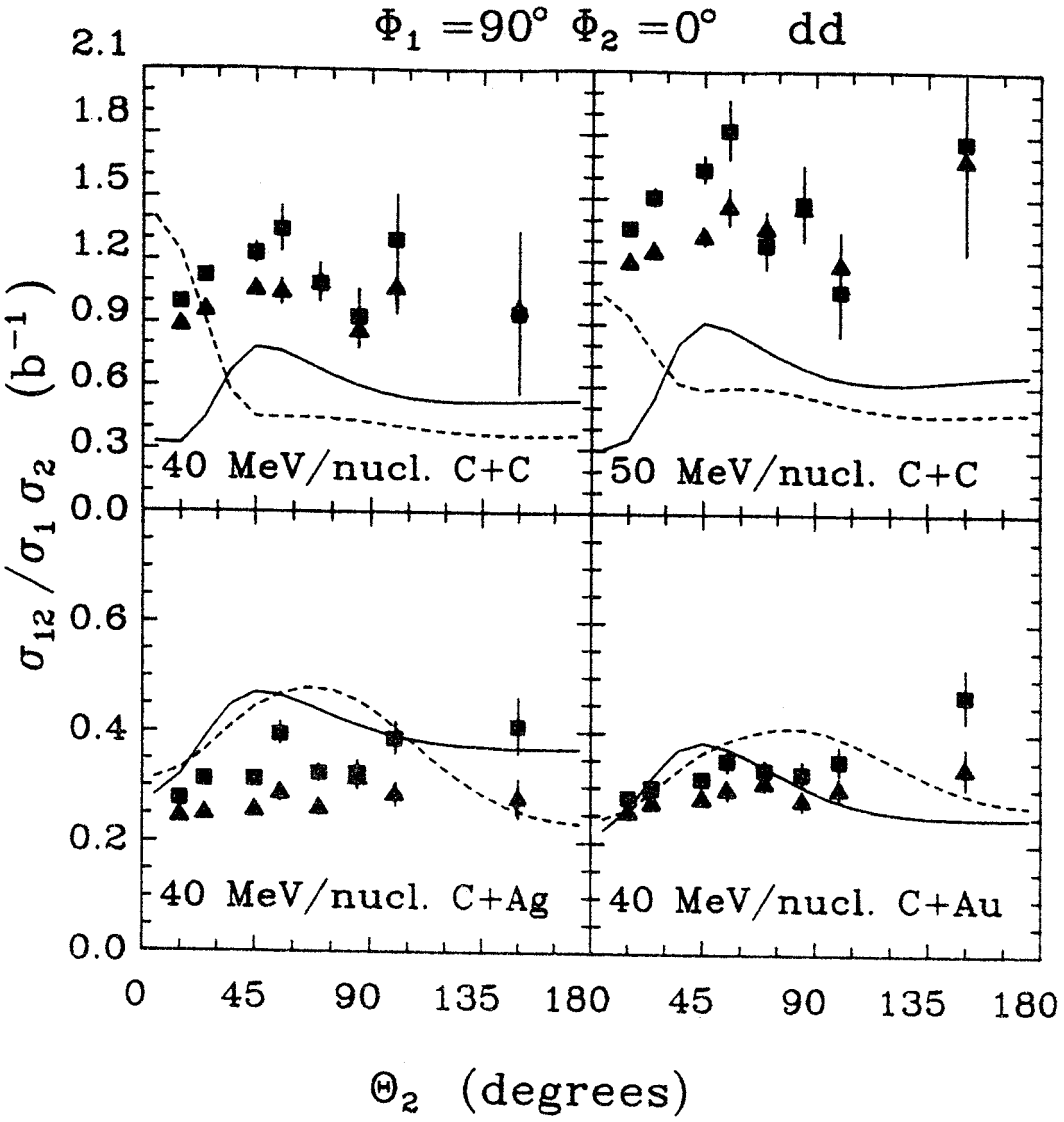

Figure IV-22 Two-deuteron out-of-plane correlation function for θ_1=25° (triangles and dashed lines) and θ_1=45° (squares and solid lines).

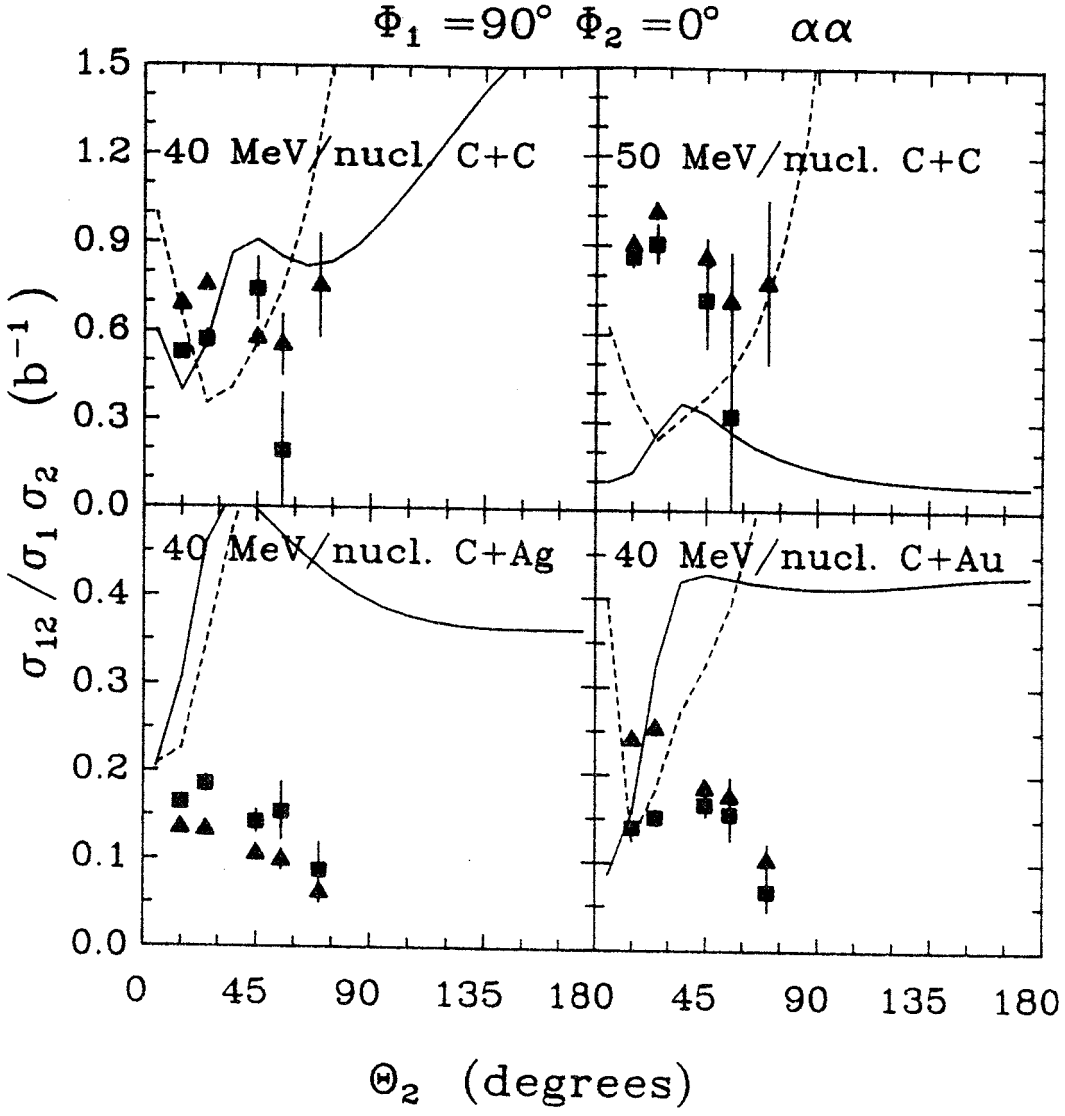

Figure IV-23 Two-alpha out-of-plane correlation function for θ_1=25° (triangles and dashed lines) and θ_1=45° (squares and solid lines).

For the d-d correlations the calculation once again gets the trend but not the magnitude of the C+C systems for Θ_1=-45° and has a maximum at forward angles for Θ_2=-25°. In the heavier systems the general trend is reproduced by the calculations for both angles when one remembers that for large angles correlations between deuterons emitted from the target source and those emitted from either the projectile or intermediate sources are not included in the calculation. These correlations between deuterons from different sources will raise the calculation at backward angels where the singles cross sections are dominated by the target like-source.

For the ^{4}He-^{4}He correlations the calculations do a very poor job of explaining the data. For the heavy systems the magnitude of the correlation function is greatly over estimated although the shape is reasonably similar to the data. For the C+C systems the the calculations do a very poor job of explaining the data.

2. In-plane To Out-of-plane Ratios

The ratio of in-plane to out-of-plane correlations for the tag detectors at Θ_1 is defined as

$$R(\Theta_2) = \frac{\sigma_{12}(\Theta_1,\Phi_1=180°,\Theta_2,\Phi_2=0°)/\sigma_1(\Theta_1,\Phi_1=180°)}{\sigma_{12}(\Theta_1,\Phi_1=90°,\Theta_2,\Phi_2=0°)/\sigma_1(\Theta_1,\Phi_1=90°)} , \qquad (IV--)$$

where σ_{12} is the two-particle coincidence cross section for in-plane (Φ_1=180°) or out-of-plane (Φ_1=90°) and σ_1 is the singles cross section for the in-plane tag (Φ_1=180°) or the out-of-plane tag (Φ_1=90°). The

For the d-d correlations the calculation once again gets the trend but not the magnitude of the C+C systems for θ_1=-45° and has a maximum at forward angles for θ_2=-25°. In the heavier systems the general trend is reproduced by the calculations for both angles when one remembers that for large angles correlations between deuterons emitted from the target source and those emitted from either the projectile or intermediate sources are not included in the calculation. These correlations between deuterons from different sources will raise the calculation at backward angels where the singles cross sections are dominated by the target like-source.

For the ^{4}He-^{4}He correlations the calculations do a very poor job of explaining the data. For the heavy systems the magnitude of the correlation function is greatly over estimated although the shape is reasonably similar to the data. For the C+C systems the the calculations do a very poor job of explaining the data.

2. In-plane To Out-of-plane Ratios

The ratio of in-plane to out-of-plane correlations for the tag detectors at θ_1 is defined as

$$R(\theta_2) = \frac{\sigma_{12}(\theta_1,\Phi_1=180°,\theta_2,\Phi_2=0°)/\sigma_1(\theta_1,\Phi_1=180°)}{\sigma_{12}(\theta_1,\Phi_1=90°,\theta_2,\Phi_2=0°)/\sigma_1(\theta_1,\Phi_1=90°)} , \qquad (IV--)$$

where σ_{12} is the two-particle coincidence cross section for in-plane (Φ_1=180°) or out-of-plane (Φ_1=90°) and σ_1 is the singles cross section for the in-plane tag (Φ_1=180°) or the out-of-plane tag (Φ_1=90°). The

ratio of in-plane to out-of-plane correlations are shown in Figures IV-24-26 for the 45° tag telescopes and Figures IV-27-29 for the 25° telescopes. The lines are the results of three source momentum conservation calculations. The data show very little difference between the two C+C systems and between the two heavier systems (C+Ag and C+Au). The ratio of in-plane to out-of-plane correlations triggered on the 25° tag telescopes is generally slightly lower than the ratio triggered on the 45° tag telescopes for the same particle pair and system.

For the 45° tag telescopes the momentum conservation calculations do an excellent job of reproducing both the shape and magnitude for the heavy systems. For the C+C systems the momentum conservation calculations over predict the in-plane out-of-plane ratio. The over prediction of the ratio for the C+C systems is probably due to the greater importance of correlations between particles from different sources in the light systems than in the heavy systems. Correlations between particles coming from different sources would lower the ratio of in-plane to out-of-plane correlations.

The momentum conservation calculation does not do as good of a job explaining the in-plane to out-of-plane ratio triggered on the 25° tag telescopes. Most of the calculations show two peaks in them, one at very forward angles and the second near 90°. While the structure is not well reproduced the magnitude of the in-plane to out-of-plane ratio is well reproduced by the momentum conservation calculation for the heavy systems. Only for the p-p correlations is the magnitude of the in-plane to out-of-plane ratio well reproduced for the C+C systems. For both the d-d and ^{4}He-^{4}He correlations the data is much lower than the momentum conservation calculation.

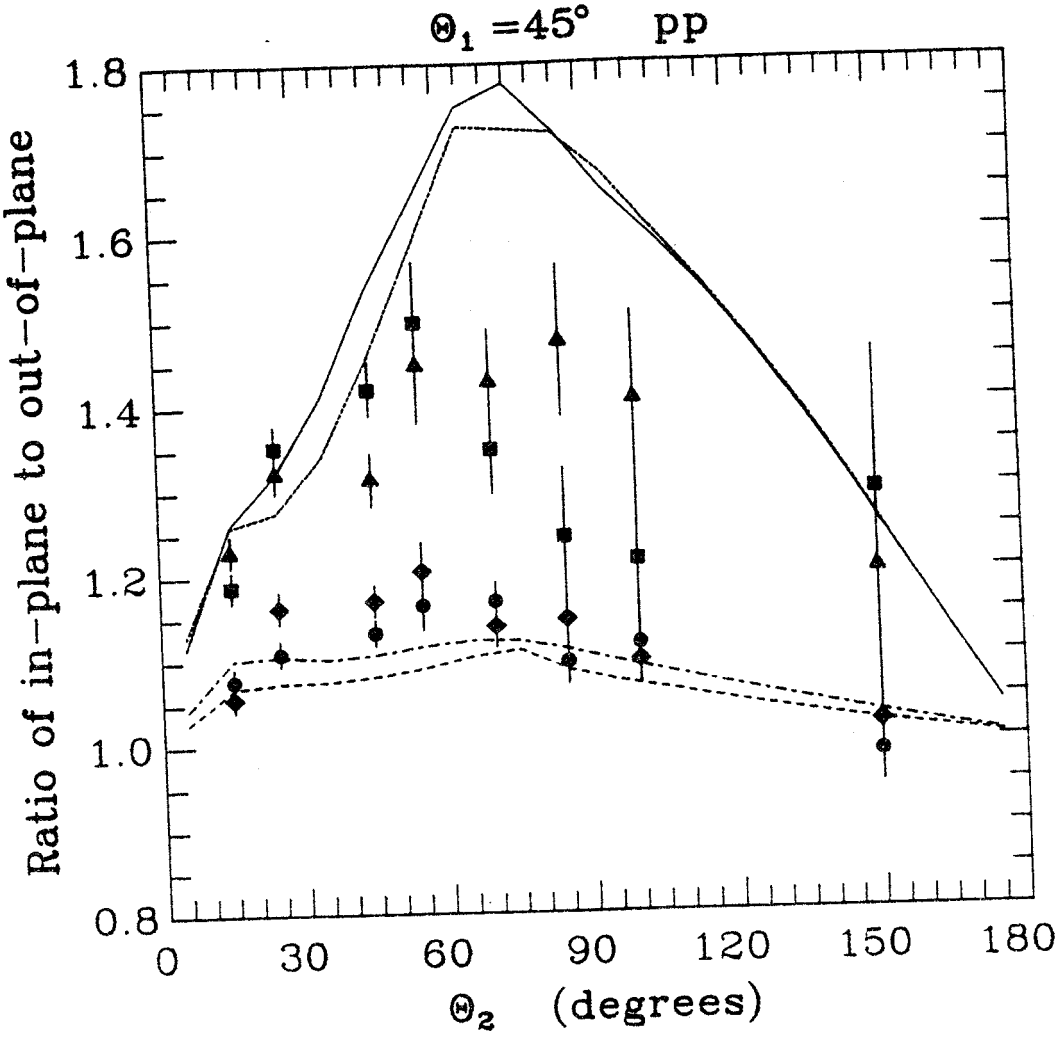

Figure IV-24 Ratio of in-plane to out-of-plane correlations for two-protons for 40 MeV/nucleon C+C (squares and solid lines), C+Ag (circles and dash dot lines), C+Au (diamonds and dashed lines) and 50 MeV/nucleon C+C (triangles and dotted lines). One proton is detected at Θ_1=45°.

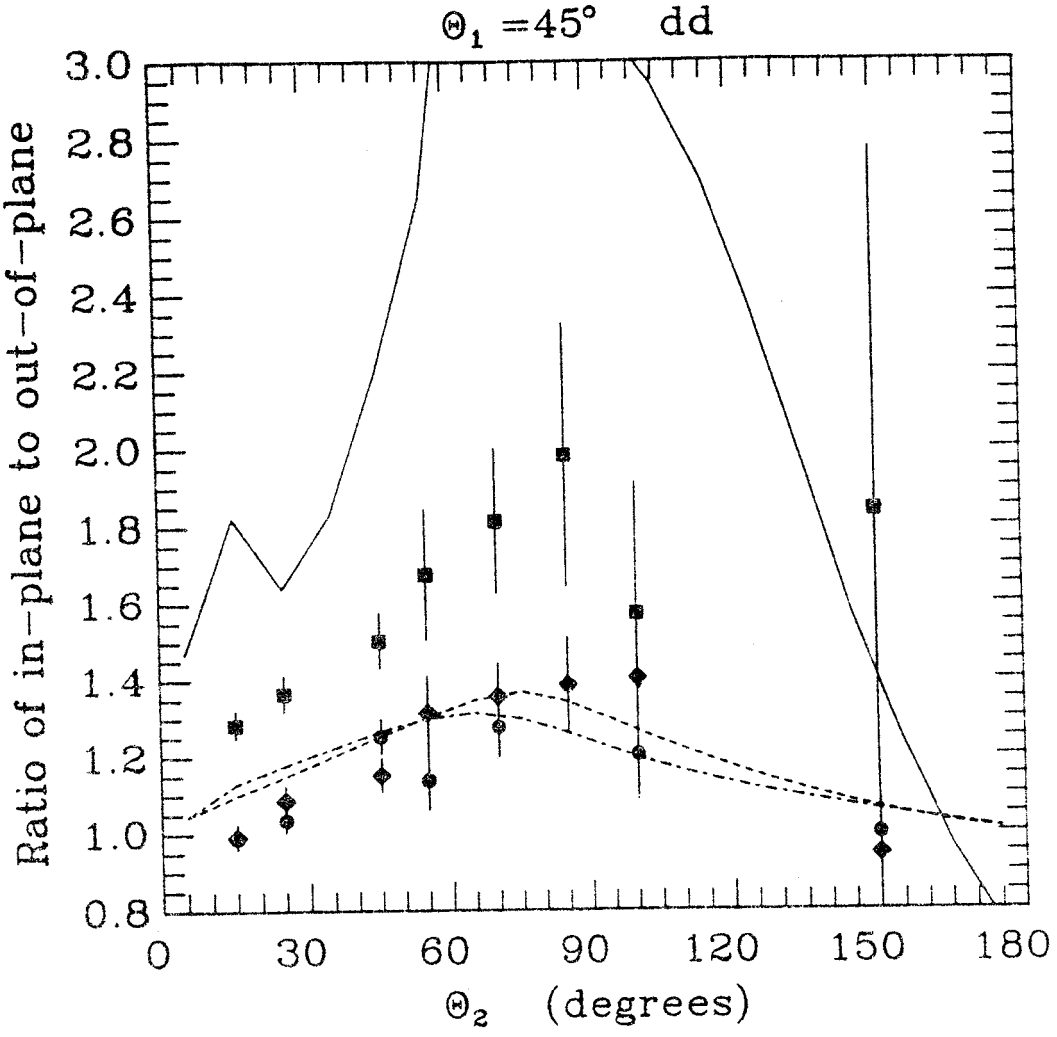

Figure IV-25 Ratio of in-plane to out-of-plane correlations for two-deuterons for 40 MeV/nucleon C+C (squares and solid lines), C+Ag (circles and dash dot lines), C+Au (diamonds and dashed lines) and 50 MeV/nucleon C+C (triangles and dotted lines). One deuteron is detected at θ_1=45°.

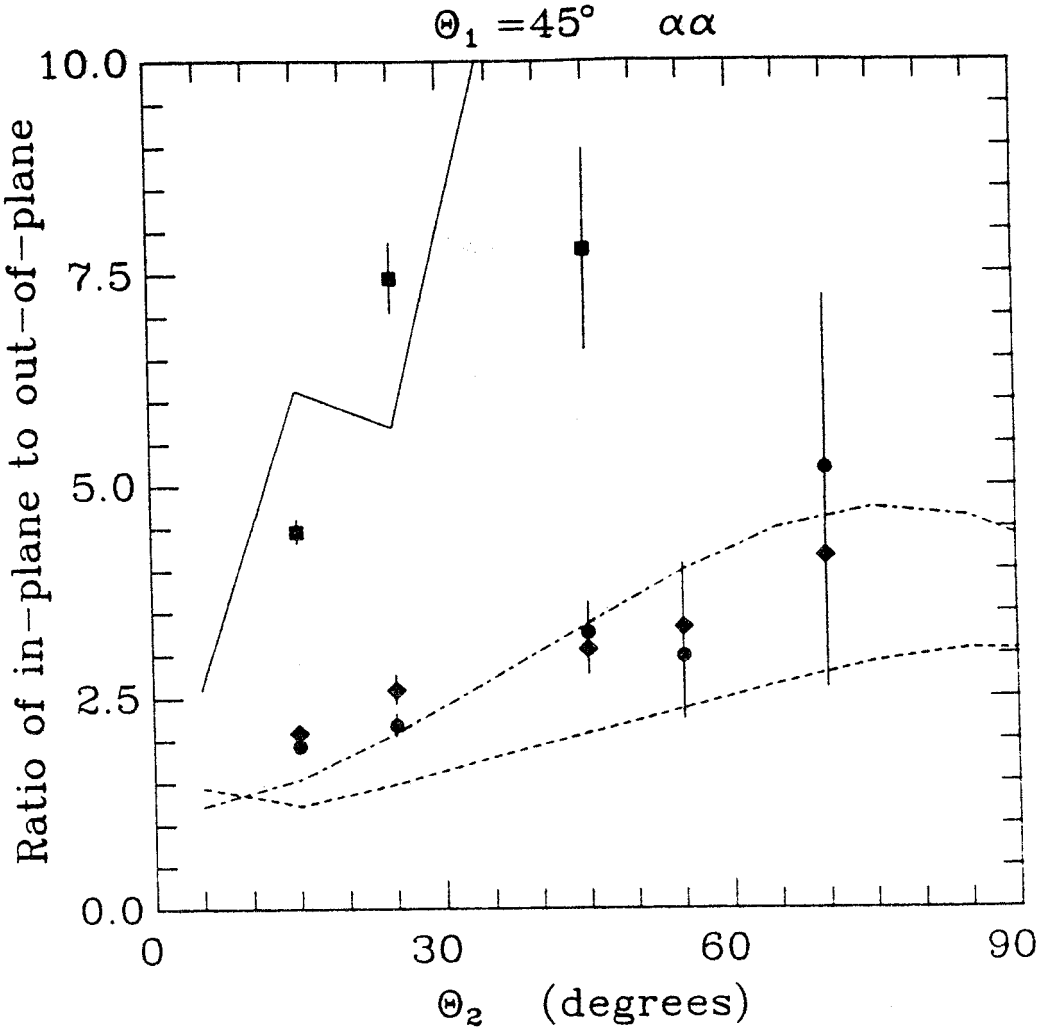

Figure IV-26 Ratio of in-plane to out-of-plane correlations for two-alphas for 40 MeV/nucleon C+C (squares and solid lines), C+Ag (circles and dash dot lines), C+Au (diamonds and dashed lines) and 50 MeV/nucleon C+C (triangles and dotted lines). One alpha is detected at Θ_1=45°.

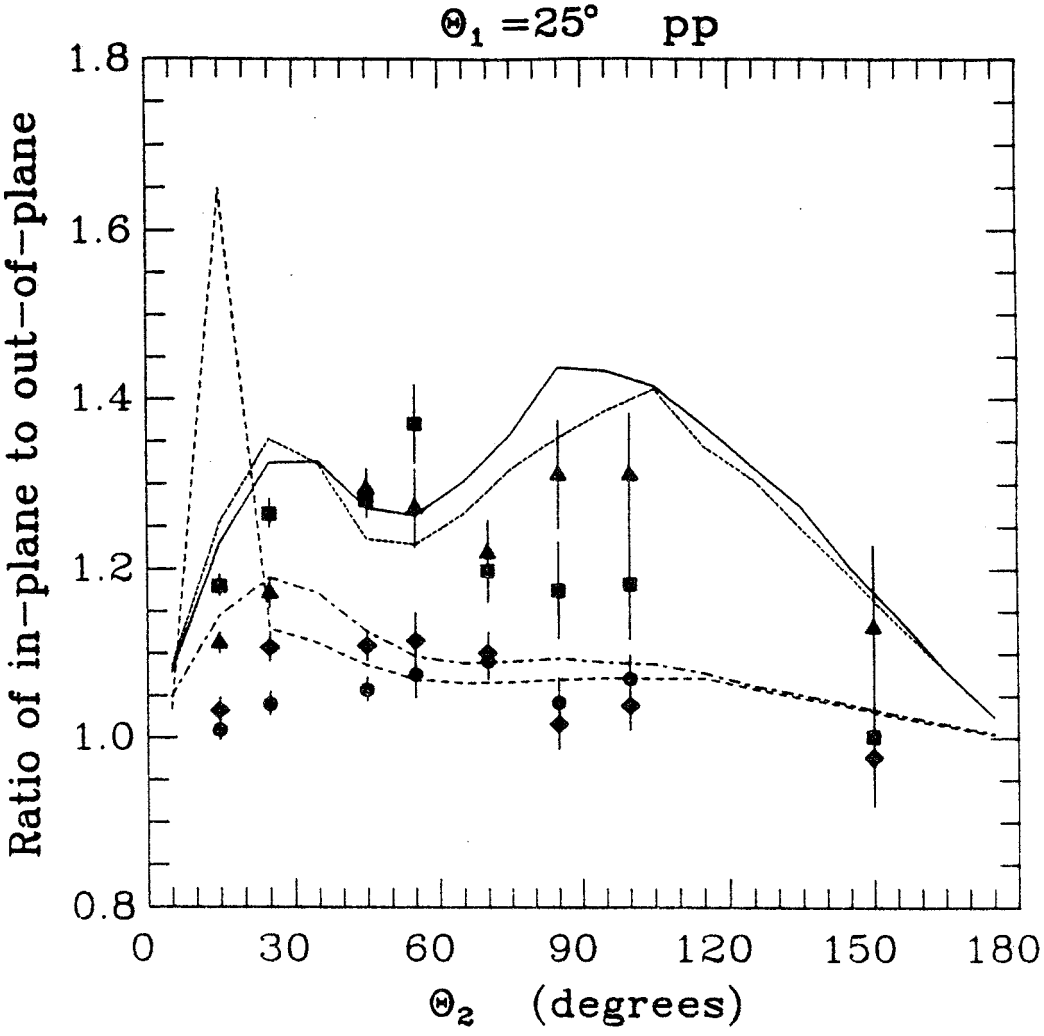

Figure IV-27 Ratio of in-plane to out-of-plane correlations for two-protons for 40 MeV/nucleon C+C (squares and solid lines), C+Ag (circles and dash dot lines), C+Au (diamonds and dashed lines) and 50 MeV/nucleon C+C (triangles and dotted lines). One proton is detected at Θ_1=25°.

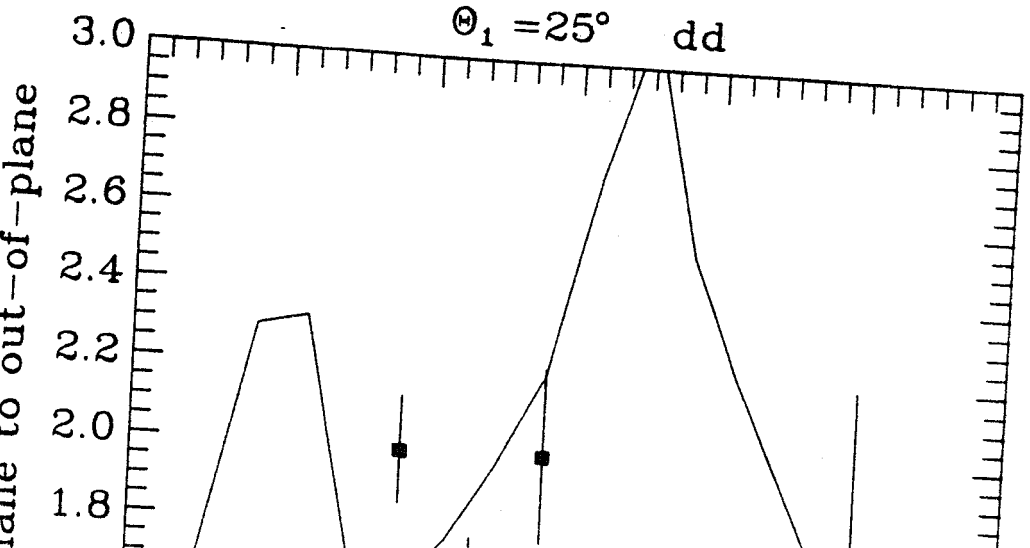
Θ_i =25° dd
3.0
2.8
2.6
2.4
2.2
2.0
1.8
lane to out-of-plane

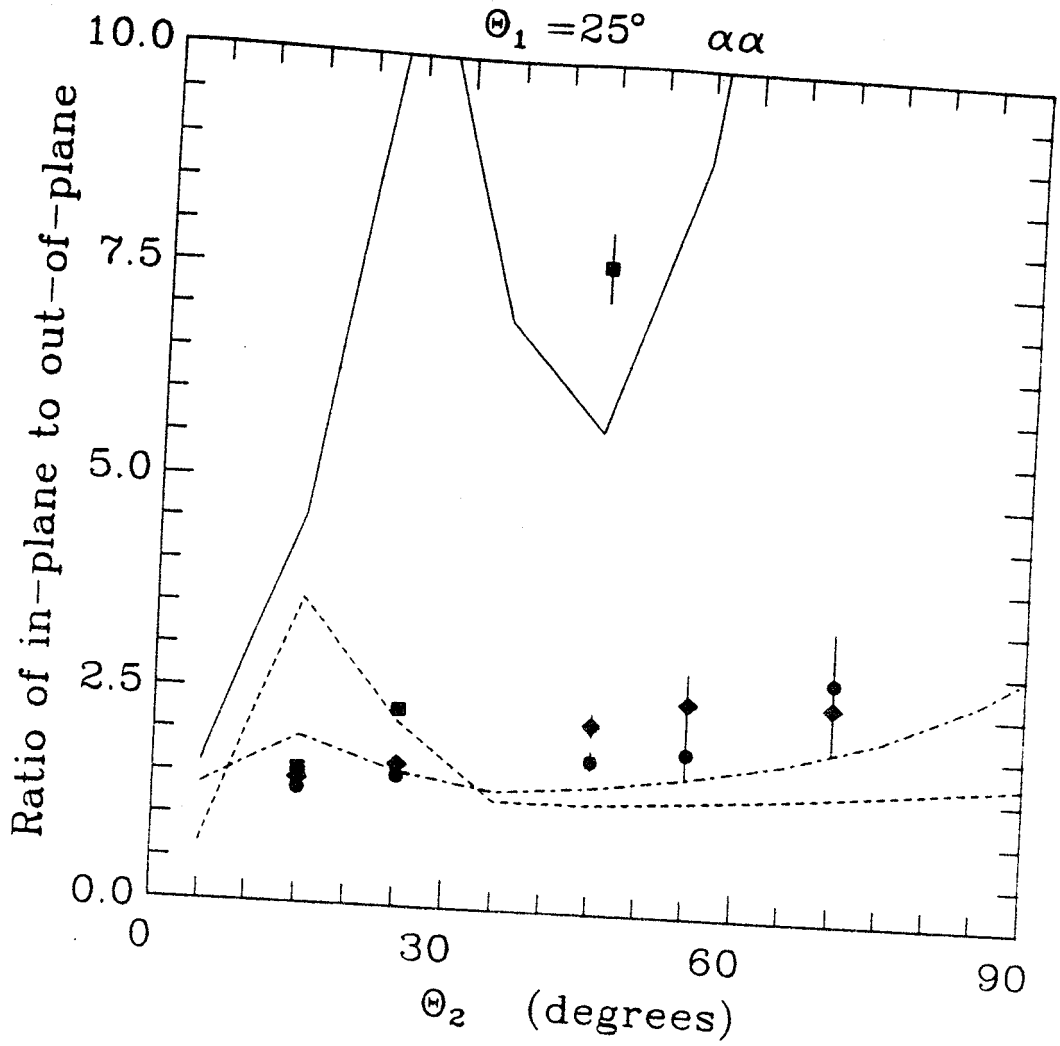

Figure IV-29 Ratio of in-plane to out-of-plane correlations for two-alphas for 40 MeV/nucleon C+C (squares and solid lines), C+Ag (circles and dash dot lines), C+Au (diamonds and dashed lines) and 50 MeV/nucleon C+C (triangles and dotted lines). One alpha is detected at θ_1=25°.

Recently Bauer [Ba 87] has studied two-proton correlations using the Boltzmann-Uehling-Uhlenbeck (BUU) equation modified to conserve momentum. In the BUU approach the reaction being studied is simulated using 100 parallel ensembles of test particles. The test particles move in a mean field with collisions treated using a cascade approach with Pauli blocking. The results, shown in Figure IV-30 for 40 MeV/nucleon C+C→pp, reproduce the overall trend of the data. Bauer's BUU calculations have also reasonably reproduced the in-plane to out-of-plane ratio for 85 MeV/nucleon C+C [Kr 85] and the azimuthal correlations for 25 MeV/nucleon O+C [Ch 86b].

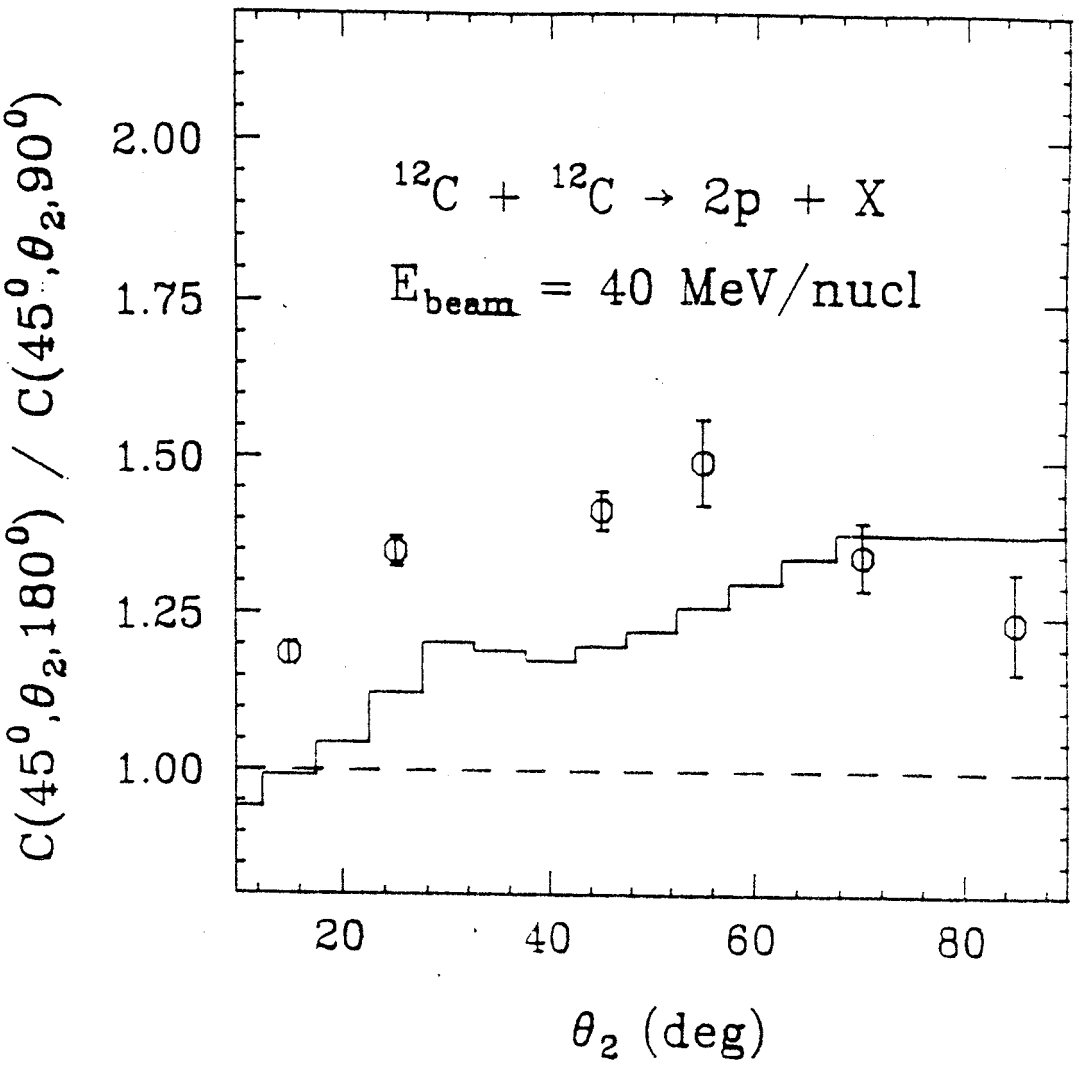

Figure IV-30 Ratio of in-plane to out-of-plane correlations for two-protons using the BUU model (histogram) [Ba 87] compared to the data (circles).

Chapter V

Unstable Resonance Experiment Results And Discussion

In this chapter the results of the unstable resonance experiment will be presented and discussed. First the two-particle correlation functions will be shown. Next the source sizes which were extracted from the correlations will be presented. The populations of the bound and unbound states will then be extracted, and the temperature of the source will be determined from the quantum statistical model.

A. Two-Particle Correlation Functions

In this section the two-particle correlation functions at small relative momentum will be presented. The correlation function, $R(\Delta p)+1$, is defined as

$$R(\Delta p)+1 = N\sigma_{12}(\Delta p)/\sigma'_{12}(\Delta p), \qquad (V-1)$$

where σ_{12} is the number of particle pairs with relative momentum Δp, σ'_{12} is the number of randomized particle pairs with relative momentum Δp and N is a normalization constant picked such that the correlation function for large Δp is one. The random particle pairs are created by keeping the last five of each particle type and calculating their momentum relative to the current particle pair. Thus for each actual correlation ten random correlations are generated.

1. 35 MeV/nucleon N+Ag

The two-particle correlations are shown in Figures V-1-10. The lines in each figure are the results of calculations by Boal and Shillcock [Bo 86] for final state interactions between the emitted particles for various source radii coming from Coulomb and nuclear interactions between the two-particles. For some of the particle pairs (p-t and d-t) the calculation has been carried out using the Coulomb interaction only. The calculations have been smeared to account for the experimental resolution of the MWPC and telescope array. Both the calculations and the smearing will be discussed in the next section.

The two-proton correlation function at small relative momentum is shown in Figure V-1. The correlation function has a broad maximum at Δp=20 MeV/c. The peak height decreases with increasing angle. This peak has been described previously in terms of both emission of ^{2}He [Be 85] and in-flight final state interactions between two randomly emitted protons [Ko 77]. In Koonin's [Ko 77] description the correlation function depends on the space-time extent of the emitting system and is often used to extract the source size of the emitting system. The extraction of source sizes from the correlation functions will be discussed later in greater detail. The correlation function also shows an anti-correlation for small Δp caused by Coulomb repulsion between the two protons. Calculations of the correlation function as a function of the size of the emitting source are shown in Figure V-1 for r=4.0 (solid line), 4.5 (dotted line), 5.0 (dot-dashed line) and 7.0 fm (dashed line).

The proton-deuteron correlation function is shown in Figure V-2. The correlation function rises smoothly until it reaches one and then stays flat at one. The calculated correlation function for source radii

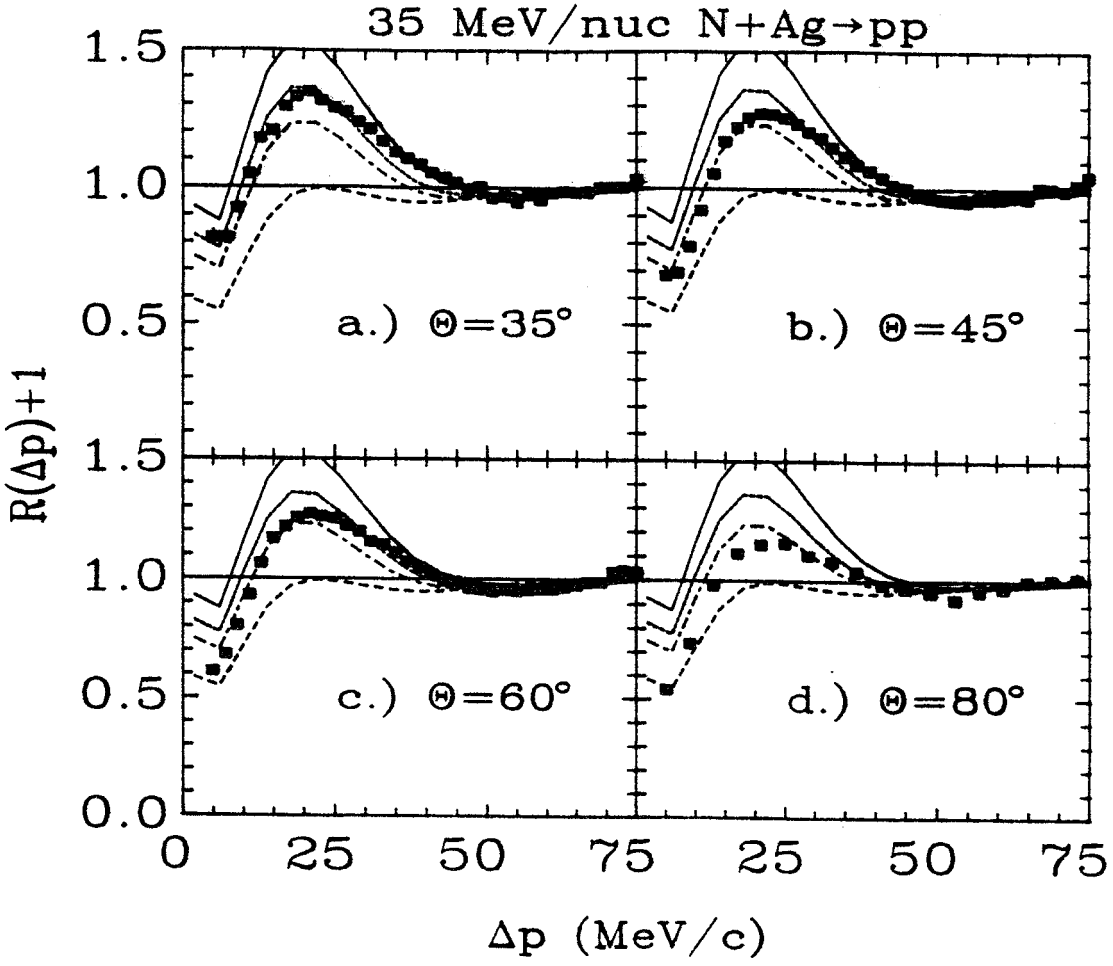

Figure V-1 Two-proton correlation function for 35 MeV/nuc. N+Ag. The lines are described in the text.

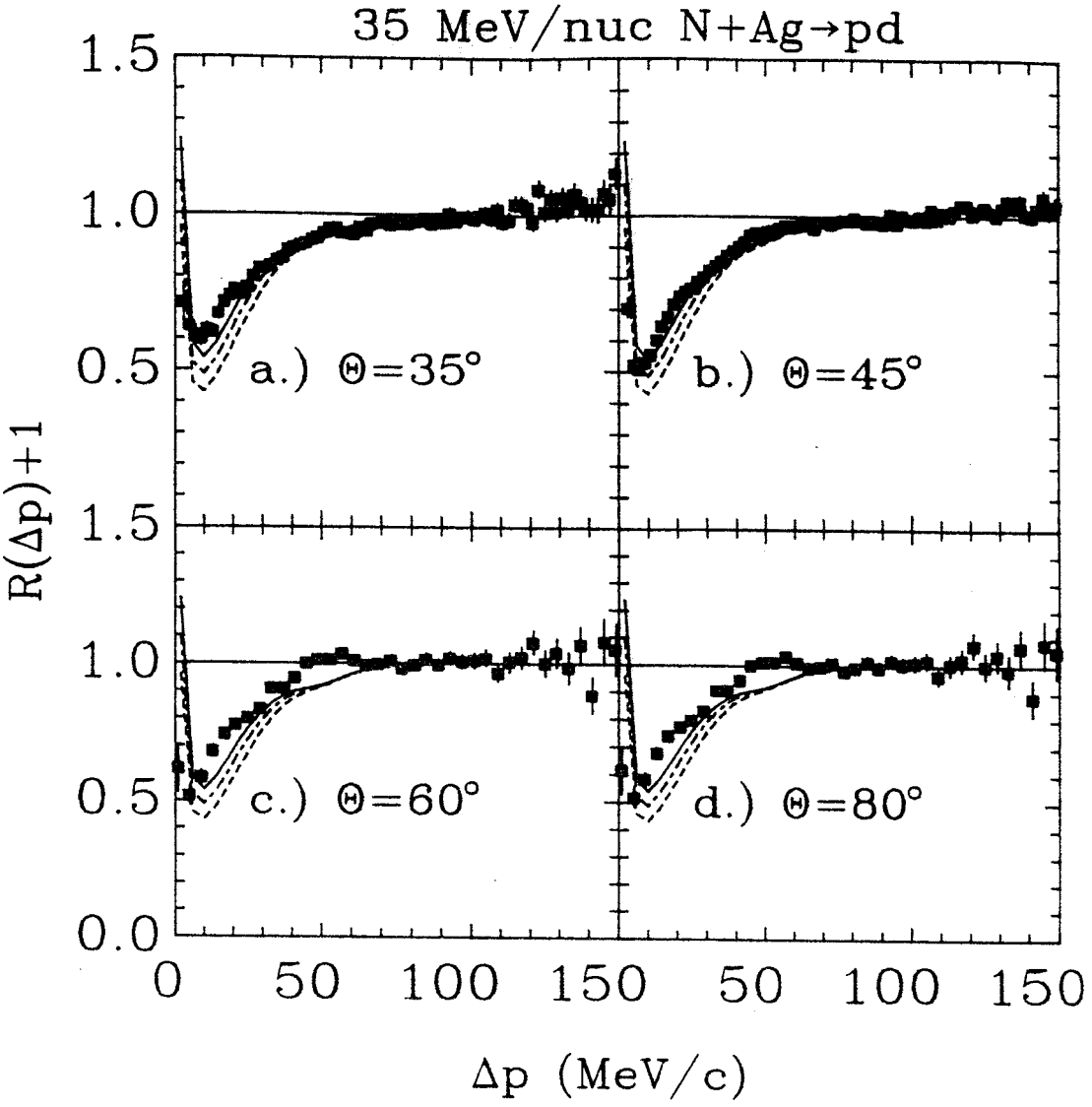

Figure V-2 Proton-deuteron correlation function for 35 MeV/nuc. N+Ag. The lines are described in the text.

of r=7.0 (dashed line), 8.0 (dot-dashed line) and 9.0 fm (solid line) are shown in Figure V-2.

The proton-triton correlation function is shown in Figure V-3. The correlation function has a series of three unresolved peaks corresponding to the first three excited states (E_{ex}=20.1, 21.1 and 22.1 MeV) in ^{4}He which decay via proton or neutron emission. The solid line is the calculated correlation function for a source of radius 7.0 fm.

The proton-alpha correlation function is shown in Figure V-4. The correlation function has a broad maximum at Δp=70 MeV/c which corresponds to the particle unstable ^{5}Li ground state. The ^{5}Li ground state is not resolved from the first excited state ($E_{ex}\approx$7.5 MeV, Γ=5 MeV). The calculated correlation function for source radii of r=4.0 (dashed line), 5.0 (dot-dashed line) and 7.0 fm (solid line) including both nuclear and Coulomb interactions are shown in Figure V-4. The shift in the location of the peak in the correlation function is at least in part due to the effects of the Coulomb force of the emitting source [Po 85b]. The proton and alpha coming from the decay of the ground state of ^{5}Li are accelerated differently by the Coulomb field of the emitting source due to their different charge to mass ratios. In this experiment the protons had a higher low energy cut in MeV/nucleon than the alphas, it has been previously shown [Po 85b] that for correlations for which the proton has a higher velocity than the alpha that the peak in the correlation function is shifted towards larger Δp. The peak location could also be shifted some due to experimental resolutions and calibrations. The dotted line is the calculated correlation for a Coulomb only interaction with a source radius of r=7.0 fm.

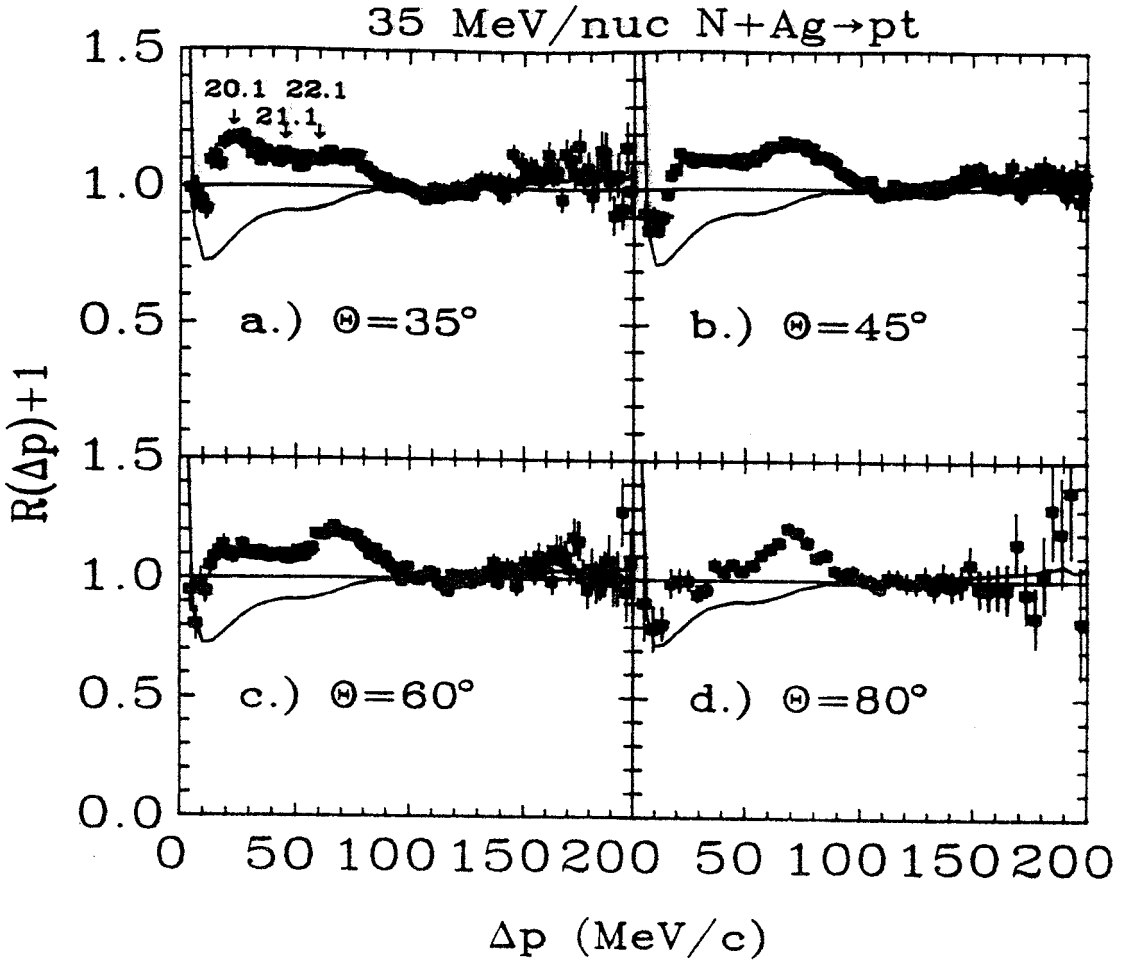

Figure V-3 Proton-triton correlation function for 35 MeV/nuc. N+Ag. The lines are described in the text.

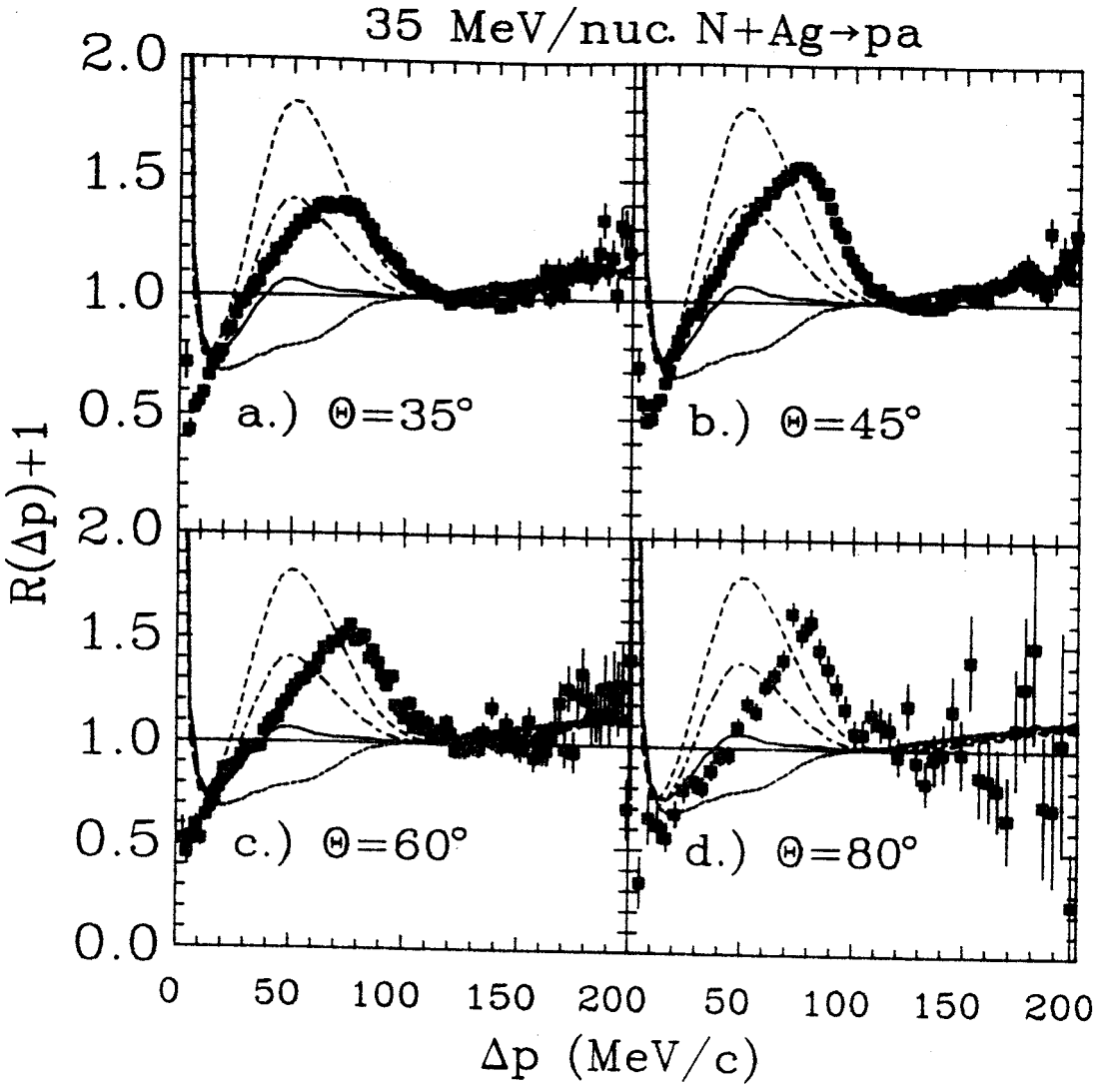

Figure V-4 Proton-alpha correlation function for 35 MeV/nuc. N+Ag. The lines are described in the text.

The two-deuteron correlation function is shown in Figure V-5. Like the proton-deuteron correlation function the two-deuteron correlation function rises smoothly to one. The calculated correlation function is shown for sources of radius 7.0 (solid line) and 8.0 (dashed line).

The deuteron-triton correlation function is shown in Figure V-6. The correlation function has two peaks corresponding to the second and third excited states (E_{ex}=16.76 and 19.8) in ^{5}He.

The deuteron-alpha correlation function is shown in Figure V-7. The large peak at Δp=40 MeV/c comes from the decay of the first excited state of ^{6}Li (E_{ex}=2.186 MeV). Two other states are observed around Δp=90-100 MeV/c, these are the third and fifth excited states (E_{ex}=4.31 and 5.65 MeV) of ^{6}Li. The calculated correlation function for a source of radius 7.0 fm is shown in Figure V-7 with the nuclear interaction included (solid line) and with only the Coulomb interaction (dashed line).

The two-triton correlation function is shown in Figure V-8. Like the proton-deuteron and two-deuteron correlation functions the two-triton correlation function rises smoothly to one. The calculated correlation function is shown in Figure V-8 for sources of radius 6.0 (dot-dashed line), 7.0 (solid line) and 8.0 fm (dashed line).

The triton-alpha correlation function is shown in Figure V-9. The large peak at Δp=70 MeV/c comes from the decay of the second excited state (E_{ex}=4.630 MeV) of ^{7}Li. Lying at higher Δp are the next two states of ^{7}Li (E_{ex}=6.68 and 7.4597 MeV). The bump at Δp=30 MeV/c has been attributed by Pochadzalla et. al [Po 86b] to the 2-step decays such as $^{8}Li^{*} \rightarrow t + {}^{5}Li \rightarrow t + \alpha + n$.

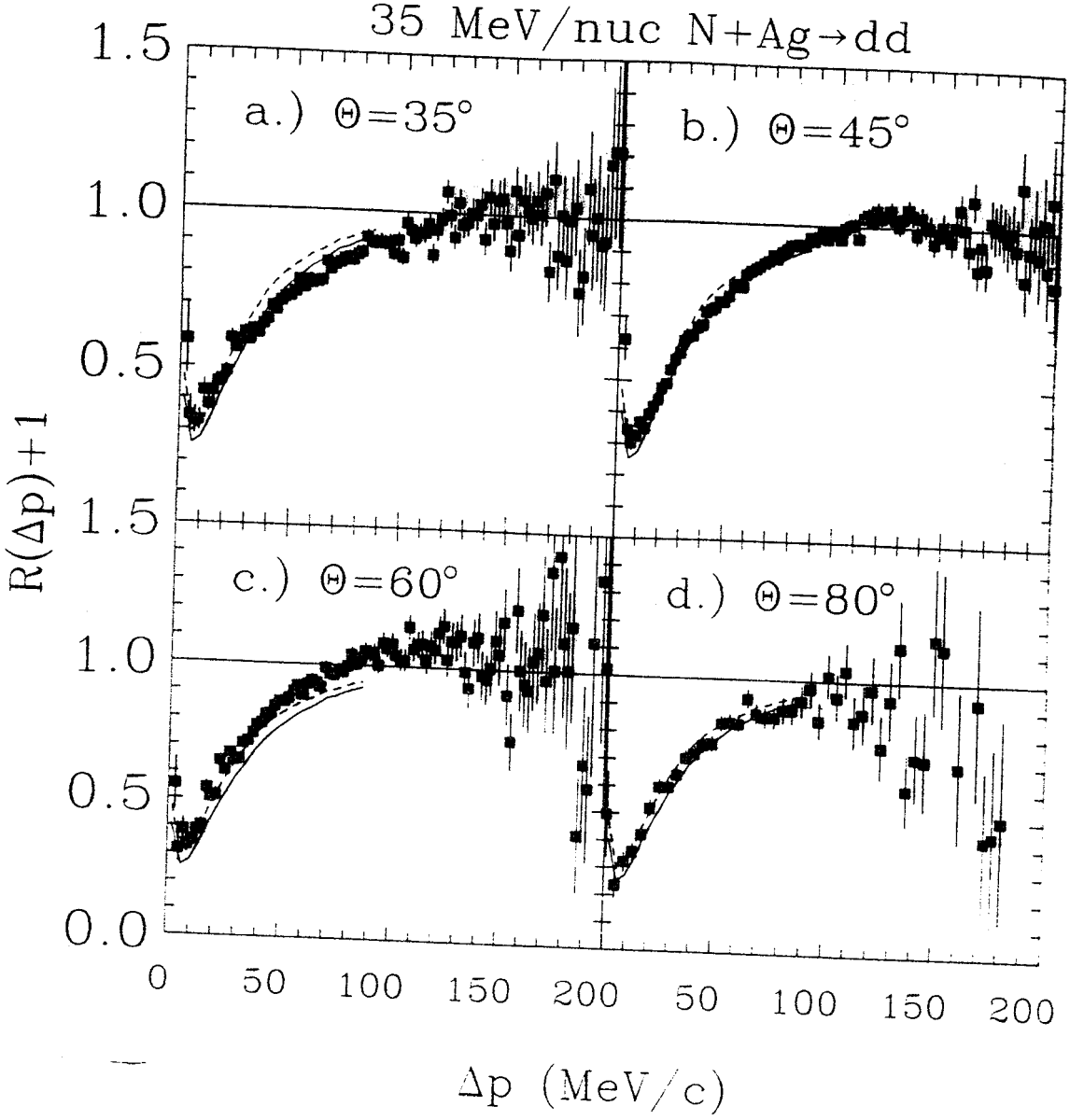

Figure V-5 Two deuteron correlation function for 35 MeV/nuc. N+Ag. The lines are described in the text.

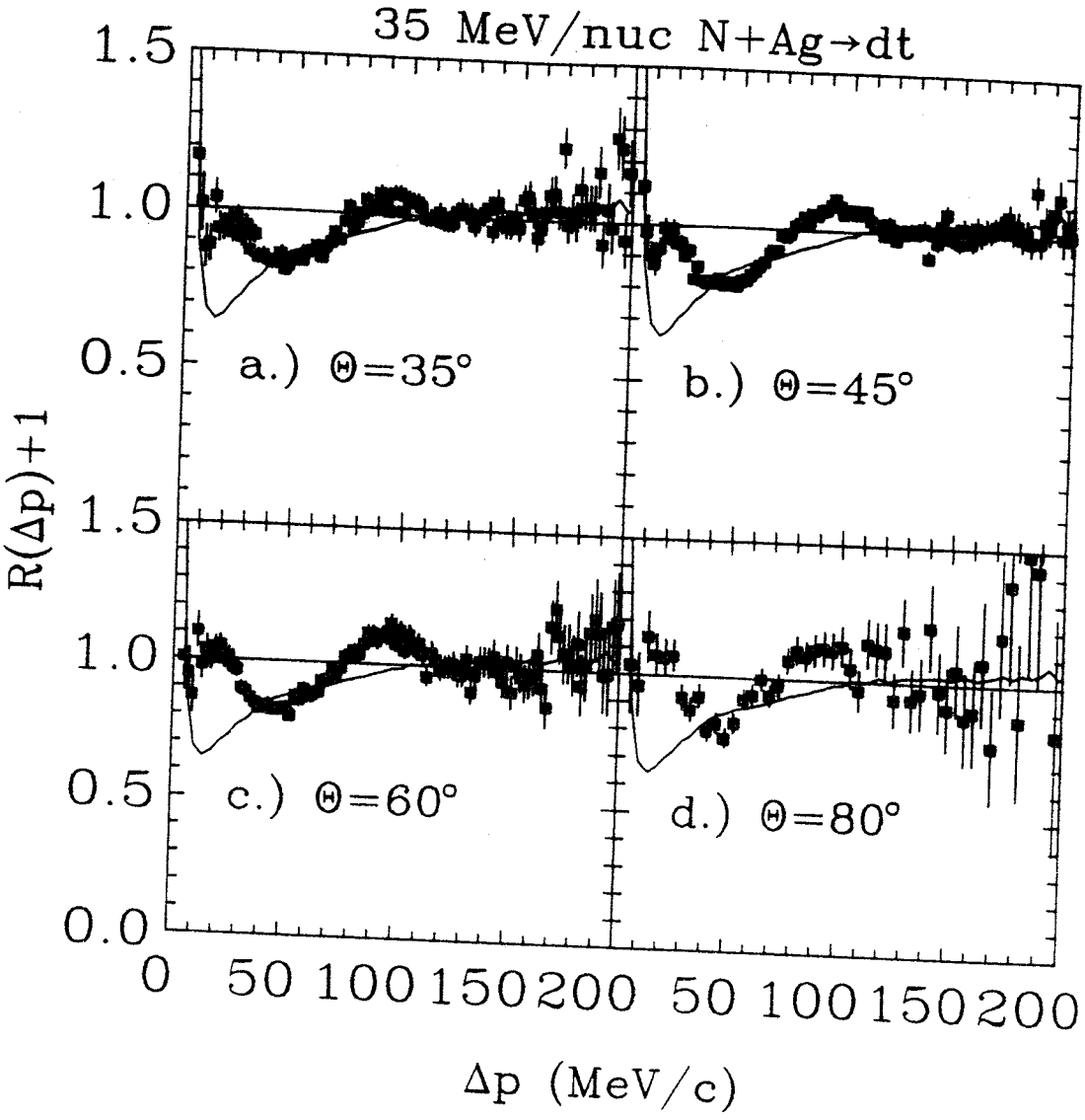

Figure V-6 Deuteron-triton correlation function for 35 MeV/nuc. N+Ag. The lines are described in the text.

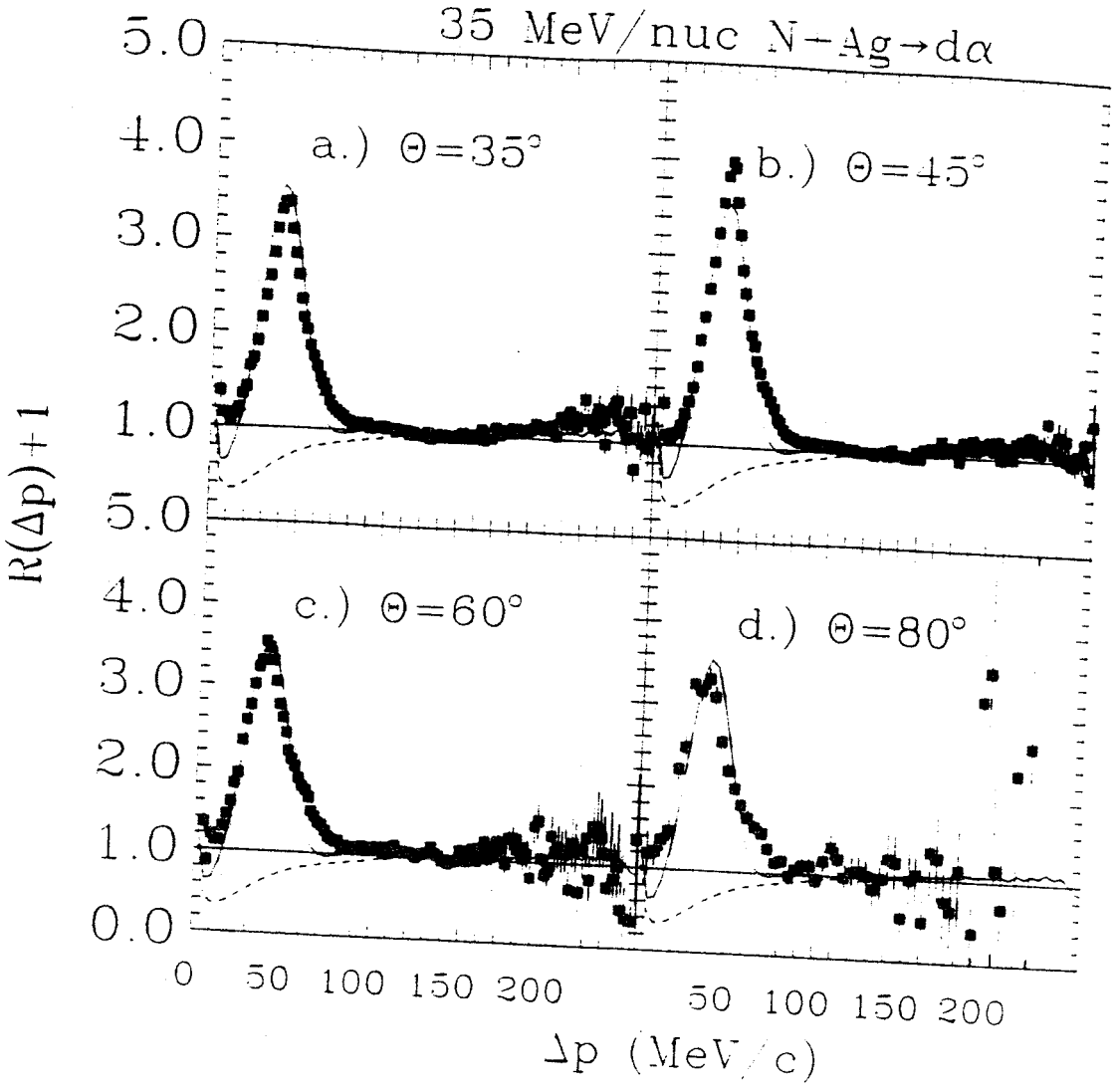

Figure V-7 Deuteron-alpha correlation function for 35 MeV/nuc. N+Ag. The lines are described in the text.

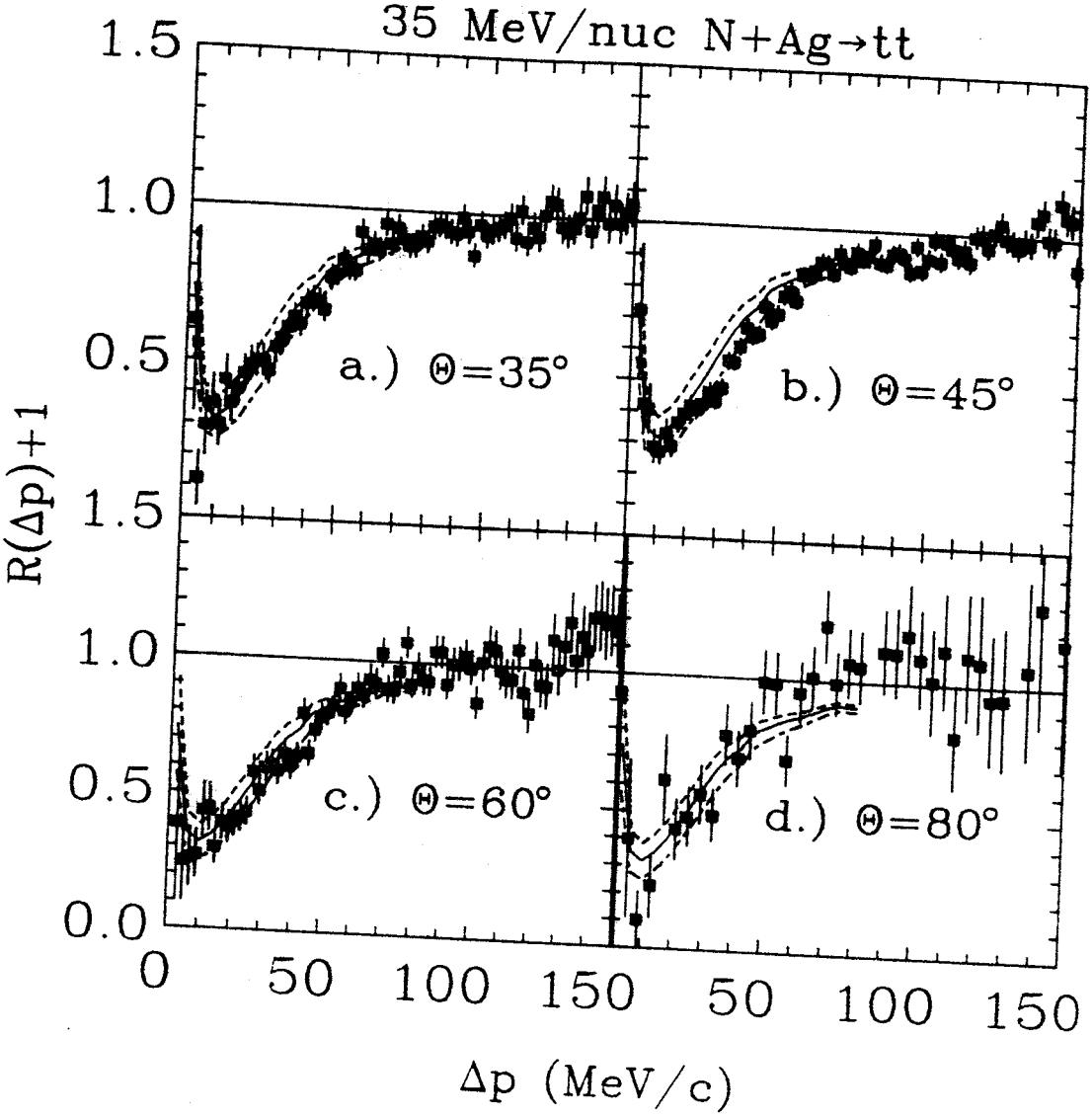

Figure V-8 Two-triton correlation function for 35 MeV/nuc. N+Ag. The lines are described in the text.

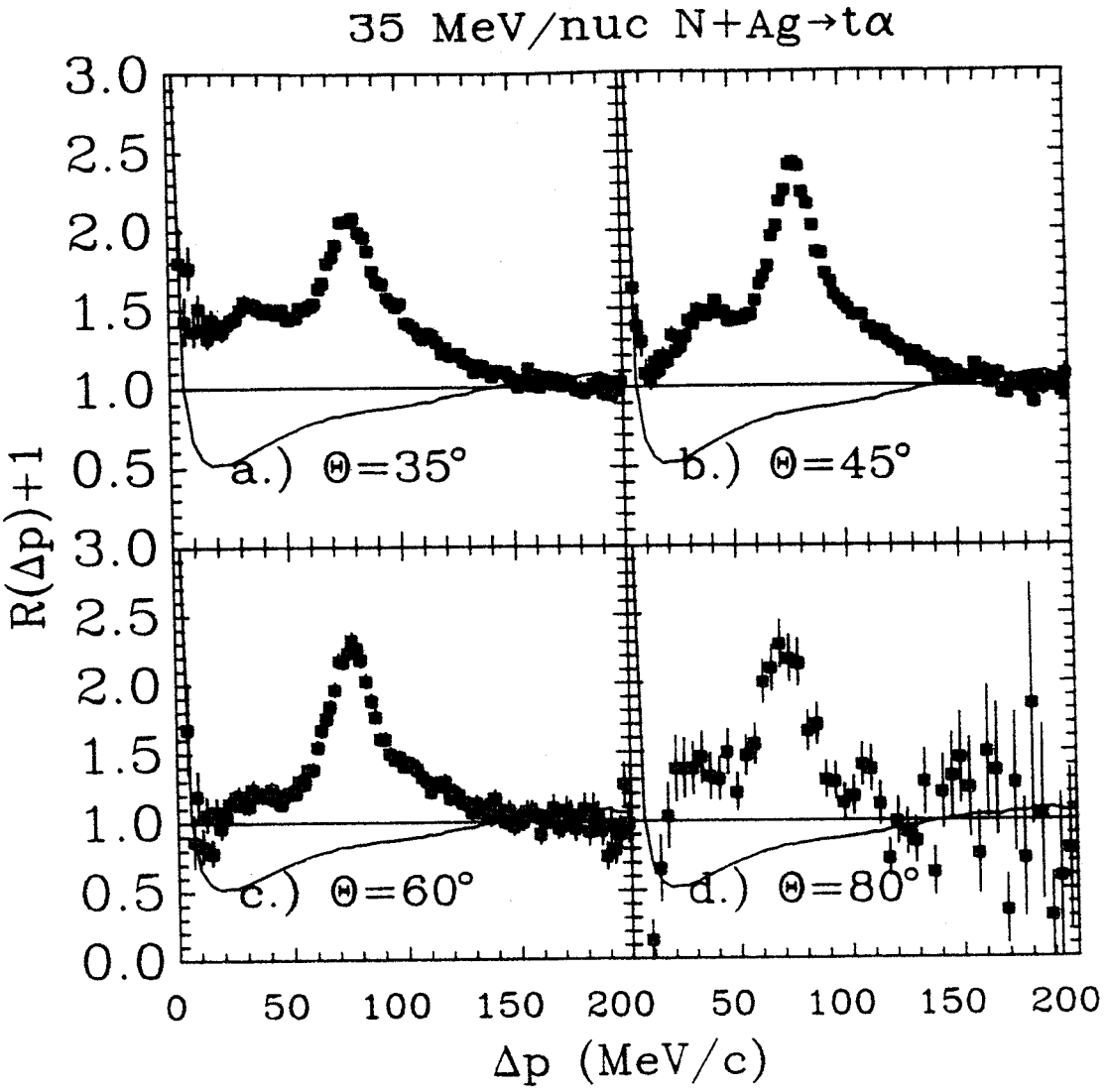

Figure V-9 Triton-alpha correlation function for 35 MeV/nuc. N+Ag. The lines are described in the text.

The two-alpha correlation function is shown in Figure V-10. The peak at Δp=18 MeV/c comes from the decay of the particle unstable ground state of ^{8}Be. The broad peak at Δp=110 MeV/c corresponds to the first excited state (E_{ex}=3.04) of ^{8}Be. The peak at Δp=40 MeV/c is the combination of the decay of the $^{9}Be^{*}_{2.43}$ state which decays by emitting an alpha leaving a ^{5}Li which in turn decays to a proton and an alpha [Po 86b], and the ghost state of the ^{8}Be ground state [Ba 62, Be 71, Be 81]. The calculated correlation function is shown if Figure V-10 for a source of radius 7.0 fm including the nuclear interaction (solid line) and for a Coulomb only interaction (dashed line).

2. 25 MeV/nucleon N+Ag

The two-particle correlation functions for 25 MeV/nucleon N+Ag are shown in Figures V-11-13. The gross features of the correlations are the same as the 35 MeV data.

B. Source Sizes

Two-particle correlations have been used for some time to determine the size of the emitting source. In astronomy the Hanbury-Brown Twist interferometer is used to measure the size of stars by looking at two-photon correlations [Ha 56]. Two-pion correlations have been used in high energy [Ez 77] and nuclear physics [Be 83, Za 84] to measure the space-time extent of the interaction region. In nuclear physics two-proton correlations have been used to extract information about the

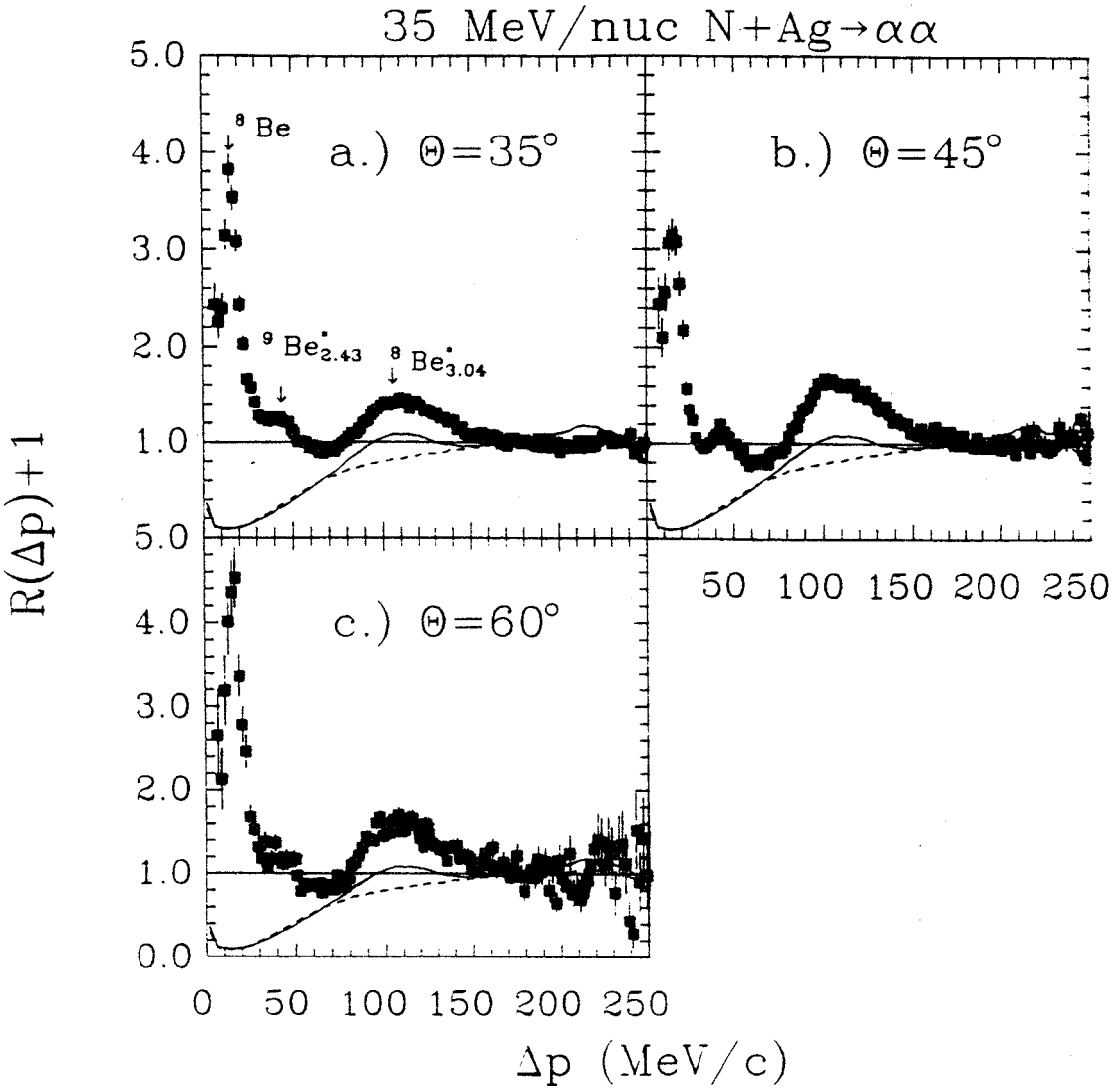

Figure V-10 Two-alpha correlation function for 35 MeV/nuc. N+Ag. The lines are described in the text.

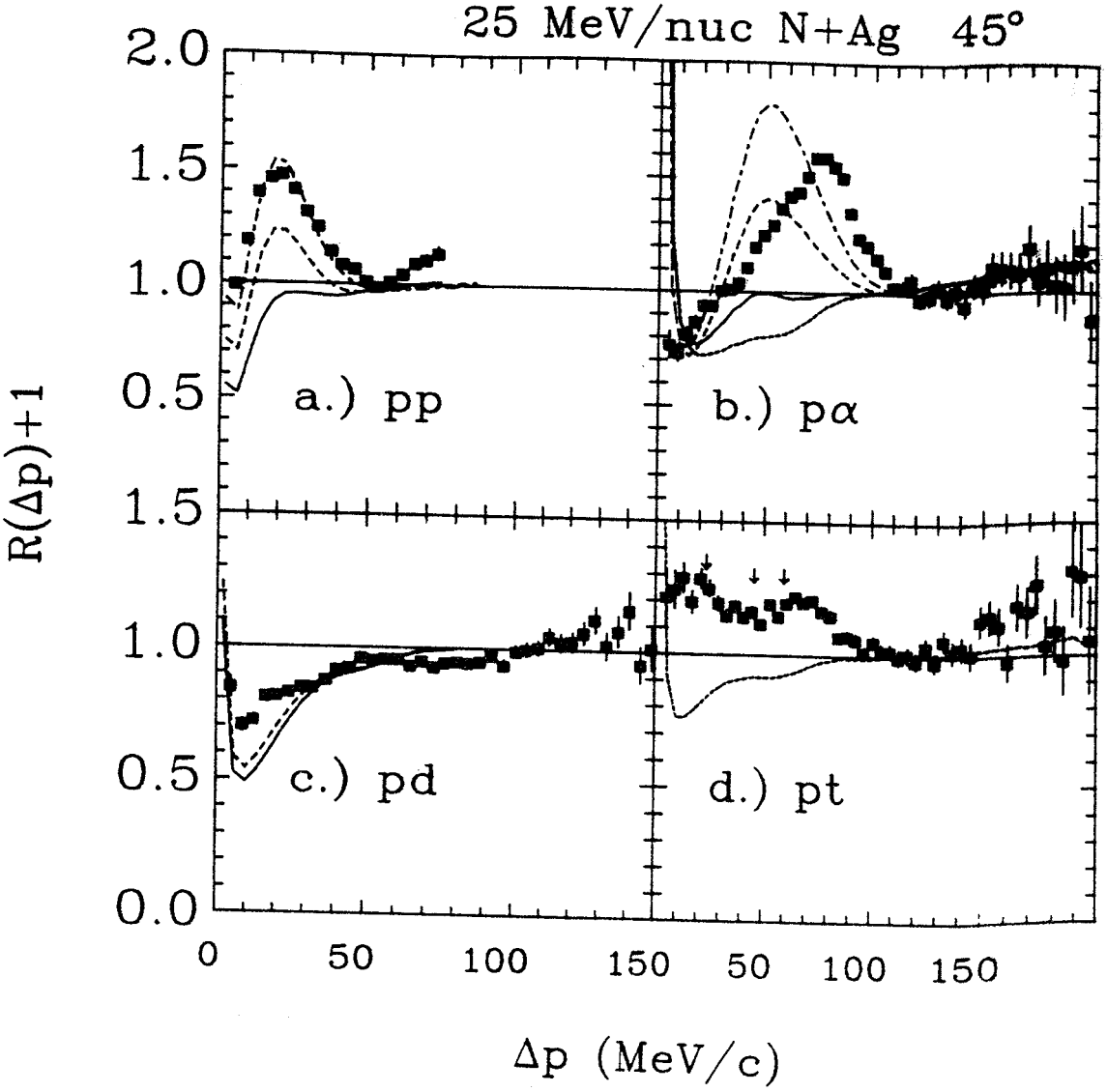

Figure V-11 Two-proton, proton-deuteron, proton-triton and proton-alpha correlation functions for 25 MeV/nuc. N+Ag at θ=45°. The lines are calculations for final state interactions for sources of radius r=4 (dashed dot), 5 (dashed) and 8 fm (solid) for nuclear and coulomb interactions and r=8 fm (dotted line) for coulomb only interactions. The dashed line in c.) if for 9 fm.

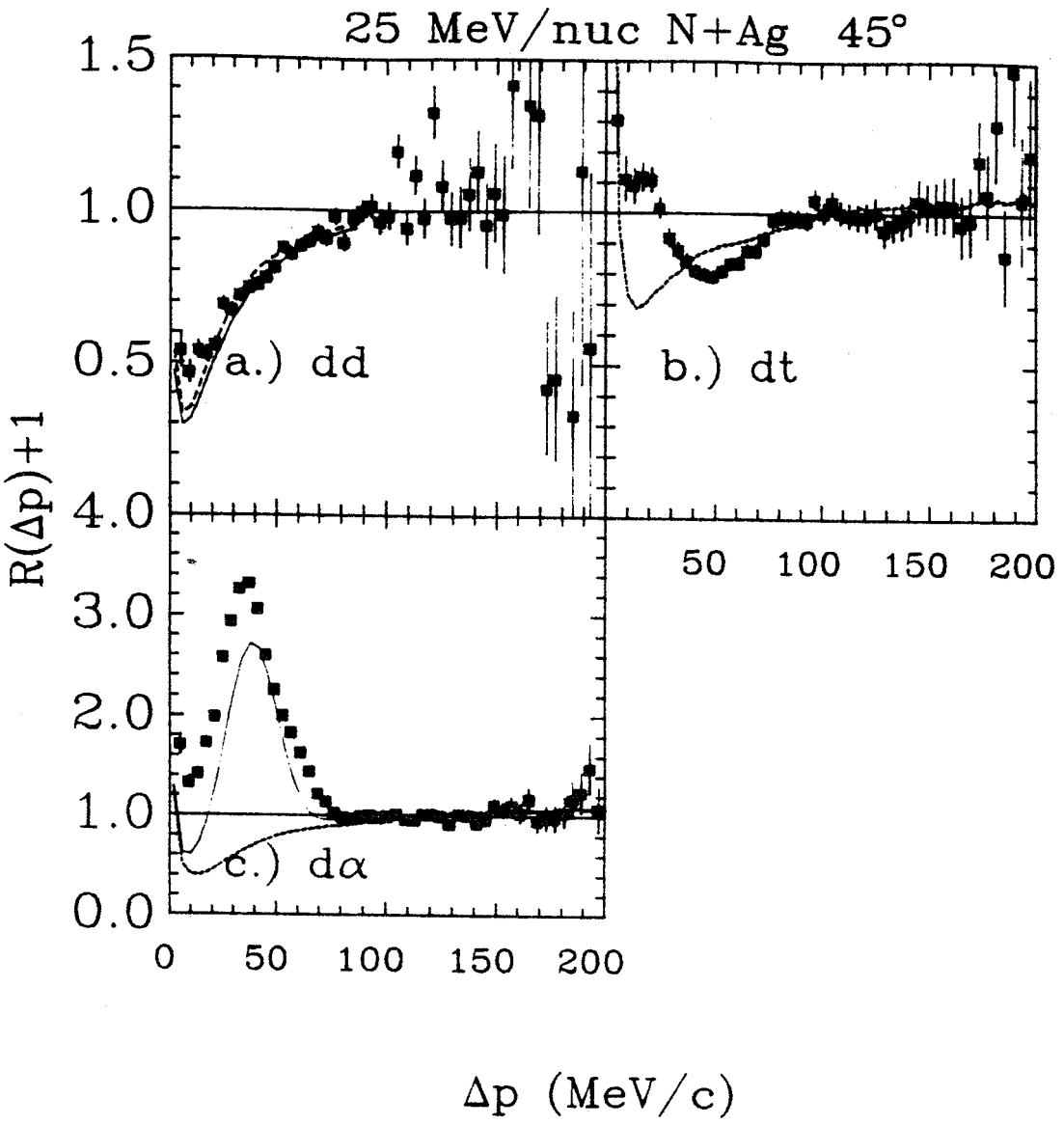

Figure V-12 Two-deuteron, deuteron-triton and deuteron-alpha correlation functions for 25 MeV/nuc. N+Ag at θ=45°. The lines are calculations for final state interactions for sources of radius r=8 (solid) and 9 fm (dashed) for nuclear and coulomb interactions and r=8 fm (dotted line) for coulomb only interactions.

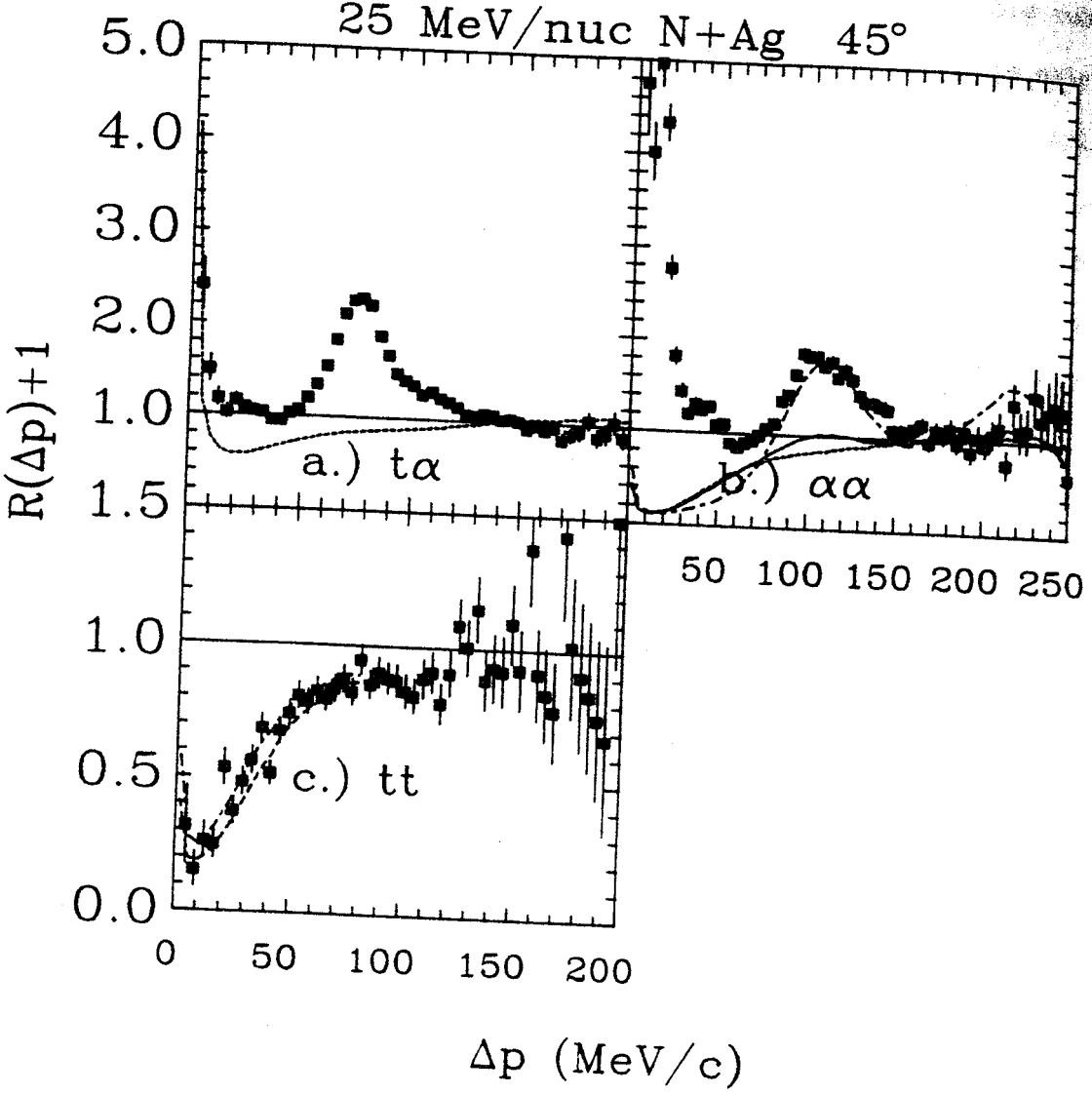

Figure V-13 Two-triton, triton-alpha and two-alpha correlation functions for 25 MeV/nuc. N+Ag at Θ=45°. The lines are calculations for final state interactions for sources of radius r=4 (dashed dot), 5 (dashed) and 8 fm (solid) for nuclear and coulomb interactions and r=8 fm (dotted line) for coulomb only interactions. The dashed dot line in c.) if for r=6fm.

space-time extent of the interaction region by many authors [Za 81, Ly 83, Gu 84, Ba 86] using the description of Koonin [Ko 77]. Recently two-particle nuclear interferometry has been extended to other particle pairs by Boal and Shillcock [Bo 86]. Chitwood et al. [Ch 86a] and Pochodazalla et al. [Po 86a, Po 86b] have used the calculations of Boal and Shillcock to extract source sizes from several particle pairs. In most cases the finite lifetime of the emitting source is neglected. The effect of neglecting the finite lifetime of the emitting source is to increase the extracted source radius.

The source sizes have been extracted for p-p, p-d, p-α, d-d, d-α, t-t and α-α correlations by using the calculations of Boal and Shillcock smeared for the experimental resolution. The smearing was done by taking the calculated correlation function and multiplying by the random correlations, $o'_{12}(\Delta p)$, to produce o_{12}. o_{12} was then smeared assuming a Gaussian shaped distribution of width δp. For the correlations with resonances the width, δp, was adjusted so that the FWHM of the smeared correlation function was the same as the FWHM of the peak in the data. For the correlations without resonances the width was adjusted to give a shape that looked as similar to the data as possible. The smeared calculations are shown in Figures V-1-13 as lines.

The source radii were determined by chi square minimization at each angle for each particle pair. The extracted radii, given in Table V-1, are in general agreement with previous results [Ch 86a, Po 86a, Po 86b]. The extracted radii show little variation with angle or beam energy. For the p-α correlations the source radius was extracted by looking at the peak height only due to the large shift in the location of the peak. Due to the poor resolution for the d-α correlations the source radius was

Table V-1

Extracted Source Radii From Two-Particle Correlations

	35 MeV/nuc. N+Ag					25 MeV/nuc. N+Ag
Correlation	35°	45°	60°	80°	Average	45°
pp	4.3±0.3	4.5±0.3	4.5±0.3	4.8±0.3	4.5±0.2	4.0±0.3
pd	9.3±0.8	9.1±0.7	9.6±0.8	10.2±0.9	9.5±0.4	10.2±0.9
pα	5.0±0.3	4.6±0.3	4.6±0.3	4.4±0.4	4.7±0.2	4.5±0.3
dd	6.7±0.8	7.3±0.7	8.8±0.9	7.6±1.0	7.5±0.4	8.8±0.9
dα	5.2±0.5	4.9±0.4	5.0±0.5	4.9±0.5	5.0±0.2	5.0±0.5
tt	6.6±1.1	5.9±0.8	6.4±1.2	7.1±2.1	6.3±0.5	5.6±1.0
αα	4.7±0.3	4.2±0.3	4.3±0.5		4.4±0.2	3.7±0.4

extracted by integrating both the calculated correlation function and the data over the range of Δp dominated by the first peak. The radius extracted from the d-α correlations are larger by about 2 fm than those obtained previously [Ch 86a, Po 86b]. This difference is probably due to the resolution in the present experiment.

One interesting feature of the extracted radii is that for those correlations involving particle pairs that do not have resonances, (p-d, d-d and t-t), the size of the emitting source is larger than for those pairs that have resonances. This pattern has been seen before [Ch 86a, Po 86a, Po 86b]. Chitwood et al. [Ch 86a] also found that the source radii extracted from the first peak in the d-α correlations was smaller by about 0.5 fm from the radii extracted from the second peak. The calculations by Boal [Bo 86] assume that all the two-particle correlations come from particles that are randomly emitted and then have in-flight final state interactions. For randomly emitted particles experiencing in-flight final state interactions one would expect that a single source size would describe all the states. If, however, some of the observed correlations come instead from the decay of emitted particle unstable nuclei, then the extracted source radius would be smaller than the true radius and since the different states are populated according to the temperature of the system, it is possible that different states will yield different apparent source radii.

It has been suggested that the different extracted source radii may result from a sequential freeze-out [Na 82, Bo 86]. In the case of sequential freeze-out different particles may be used to probe different stages of the interaction.

The source radii extracted using two-particle correlations at small relative momentum can also be compared to the radius extracted using the

coalescence model [Le 79, Sa 81, Ja 85]. For 92 and 137 MeV/nucleon Ar+Ca, Au reactions [Ja 85] the source radius extracted using the coalescence model for particles of mass 2-14 was r = 3.7 fm. This radius is slightly smaller than the radius extracted from pp and αα correlations and much smaller than the radius extracted from pd, dd and tt correlations (6-10 fm). It should be remembered that the extraction of the source radius from the two-particle correlations was done neglecting the lifetime of the emitting system. If one includes the finite lifetime of the emitting system then the measured source radius will decrease.

C. Bound State Spectra

The single particle inclusive energy spectra for He, Li, Be and B are shown in Figure V-14. The lines are the result of single moving source fits to θ=45°, 60° and 80°. The extracted source parameters are listed in Table V-2 along with the Coulomb shifts used in the fits. The fits indicate that the intermediate velocity source dominates the cross sections for θ=45°-80°. The 35° spectra show signs of enhancement due to contributions from the projectile-like source. The extent of contamination of the ^{7}Li spectra by the decay of ^{8}Be, discussed in Chapter II, is estimated to be 4.3 mb of ^{8}Be identified as ^{7}Li per 50 mb of ^{8}Be. Based on the cross sections for the stable Be isotopes this means that about 2-4 mb of the ^{7}Li cross section comes from the decay of ^{8}Be.

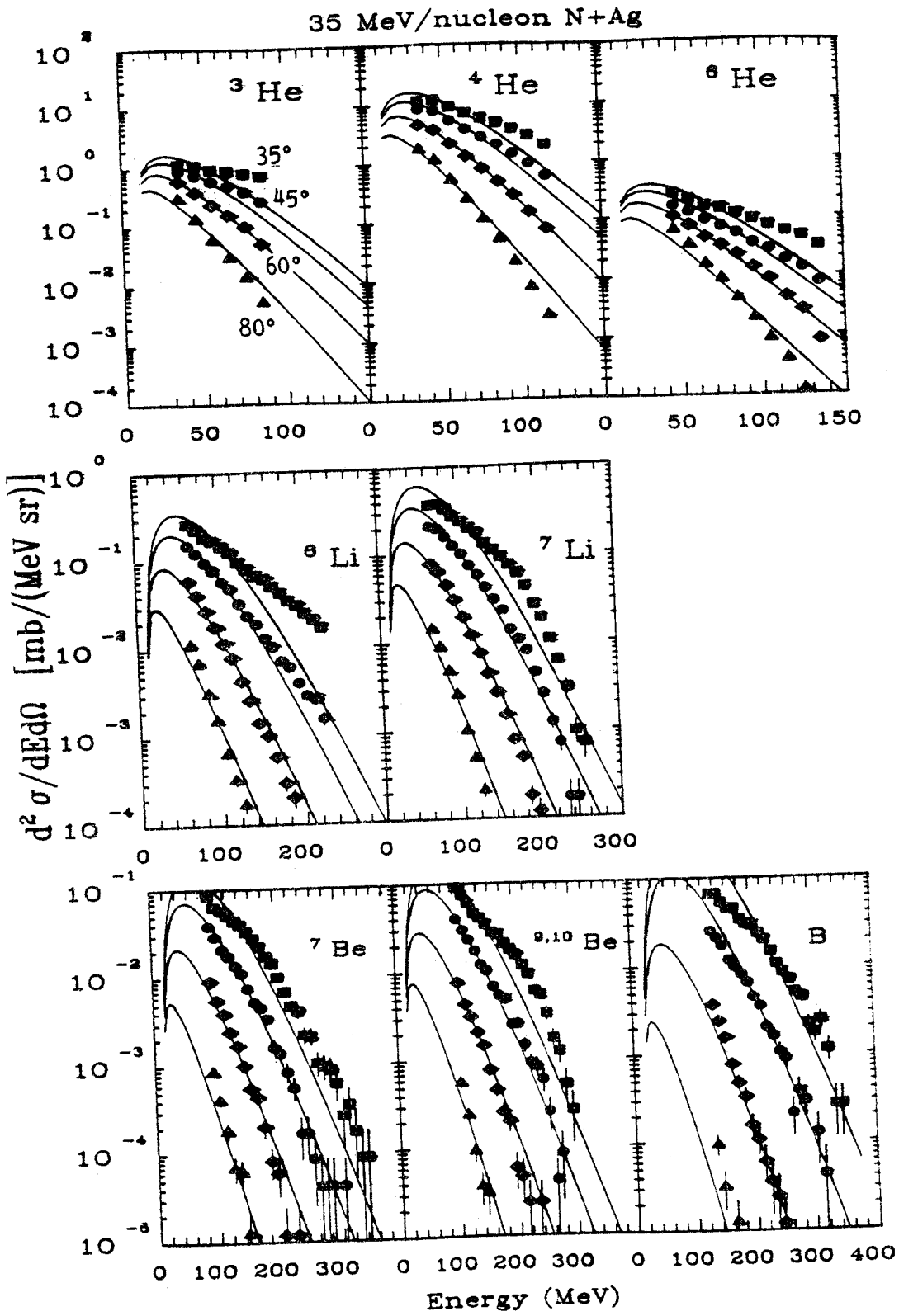

Figure V-14 He, Li, Be and B energy spectra for 35 MeV/nuc. N+Ag. The lines are moving source fits discribed in the text.

Table V-2

Moving Source Parameters For 35 MeV/nucleon N+Ag

Particle	V_c (MeV)	Cross Section (mb)	Velocity	Temperature (MeV)
^{3}He	8	223± 15	0.162±0.011	12.4±0.5
^{4}He	8	2090±100	0.095±0.003	12.1±0.4
^{6}He	8	55± 5	0.072±0.004	14.2±0.5
^{6}Li	12	66± 4	0.116±0.003	15.1±0.3
^{7}Li	12	119± 7	0.108±0.004	14.6±0.3
^{7}Be	16	35± 3	0.128±0.003	14.6±0.3
$^{9,10}Be$	16	40± 3	0.115±0.002	15.2±0.3
B	20	140± 50	0.122±0.004	13.4±0.6

D. Populations Of Particle Unstable States

In order to extract the populations of particle unstable states the contribution to the two-particle correlation functions coming from randomly emitted particles must be subtracted. The populations of particle unstable states were found by integrating the two-particle coincidence cross section $\sigma_{12}(\Delta p)$ over those values of Δp that correspond to the state of interest. For each Δp step the cross section is given by

$$\sigma=(\sigma_{12}(\Delta p)-\sigma'_{12}(\Delta p)[R(\Delta p)+1]/N)/\varepsilon(\Delta p), \qquad (V-2)$$

where $\sigma_{12}(\Delta p)$, $\sigma'_{12}(\Delta p)$, and N are the same as before (sect. A). $R(\Delta p)+1$ is the theoretical correlation function for Coulomb only final state interactions for a source radius R, and $\varepsilon(\Delta p)$ is the efficiency of the MWPC-phoswich array calculated by the procedure outlined in Chapter III, section D. The cross sections were extracted using source radii of R=7 and 8 fm for the theoretical correlation function, $R(\Delta p)+1$. The extracted cross sections are given in Table V-3 are for a source size of R=7 fm with errors including the uncertainty arising from the use of a different source size, a 10% uncertainty for the efficiency calculation, and statistics.

The extraction of the populations of the particle unstable states was done assuming that randomly emitted particles have Coulomb only final state interactions. Two-particle correlations coming from randomly emitted particles which interact through nuclear forces to produce resonant states are indistiguishable from emitted particle unstable states. Possible corrections for these random correlations will be discussed in section F.

Table V-3

Extracted Cross Sections of Particle Unstable States (mb/sr)

	35 MeV/nucleon				25 MeV/nuc.
State(s)	35°	45°	60°	80°	45°
$^{4}He^{*}_{20,21,22}$	3.5±0.6	1.11±0.16	0.24±0.04	0.043±0.007	0.55±0.08
$^{5}He^{*}_{16.76}$	0.39±0.18	0.14±0.08	0.042±0.015	0.008±0.003	0.021±0.010
$^{5}He^{*}_{19.8}$	0.75±0.24	0.44±0.08	0.081±0.018	0.010±0.003	0.006±0.008
$^{5}Li_{gs,7.5}$	11.5±10.6	2.7±0.3	0.42±0.05	0.031±0.005	1.42±0.19
$^{6}Li^{*}_{2.186}$	11.3±10.4	2.7±0.3	0.46±0.06	0.031±0.004	1.65±0.21
$^{6}Li^{*}_{4.31,5.65}$	1.56±0.29	0.34±0.06	0.058±0.010	0.0027±0.0008	0.08±0.03
$^{7}Li^{*}_{4.63}$	7.2±0.9	1.05±0.13	0.151±0.019	0.0074±0.0012	0.66±0.08
$^{7}Li^{*}_{6.68,7.46}$	3.2±0.5	0.44±0.06	0.043±0.008	0.0011±0.0005	0.20±0.04
$^{8}Be^{*}_{3.04}$	3.77±0.03	0.399±0.004	0.0503±0.0011		0.43±0.06

E. Quantum Statistical Model And Extraction Of Nuclear Temperature

Previous work has established the importance of feeding of light nuclei by the decay of heavier particle unbound states [Xu 86, Po 86b, Ha 87]. In order to extract information such as temperature from the relative populations of states, the amount of feeding to each individual state needs to be measured or calculated. Using the quantum statistical model of Hahn and Stöcker [Ha 86] the extent of feeding to each of the observed states may be estimated. In the quantum statistical model the initial population of a state is determined from its chemical potential, statistical weight and the temperature. Approximately 40 stable and 500 unstable nuclear levels up to mass 20 are included in the calculation. After the initial populations are determined the excited states are allowed to decay using the known branching ratios.

We have extracted the nuclear temperature for the 35 MeV/nucleon system by χ^2 minimization using the quantum statistical model. The neutron to proton ratio calculated using the fireball model [We 76, Go 77] was found to be 19/17 for the most probable impact parameter. The break-up density was fixed at $\rho=0.18\rho_0$ which is the density obtained from a break-up radius of 7 fm and a source of 36 nucleons. The temperature was extracted using the populations of the particle bound states measured in the singles run and the particle unstable states extracted from the two-particle correlations. In addition the data of Morrissey [Mo 84, Mo 85] and Bloch [Bl 86, Bl 87] for Y and neutron emitting states for the same system were also included. For the particle bound states the ratio of the cross section each for isotope extracted from the moving source fit to the ^{6}Li ground state cross section was compared to the ratio calculated by the quantum statistical model. For the particle unstable

states the cross sections given in Table V-3 were integrated from θ=45° to 80°, which corresponds to θ=35° to 90° due to the 20° opening angle of the MWPC-phoswich array. The 35° data have been excluded because they contain a component coming from the projectile like source. The ratio of these integrated cross sections were then taken to the cross section of either the ground state of the appropriate isotope or to ^{6}Li ground state integrated over the same angles and energies using the moving source parameters. These ratios are given in Table V-4, the quoted errors include a 10% uncertainty in the absolute normalizations for the particle unstable states and the particle bound states. Using these parameters the temperature was determined to be $4.8^{+2.8}_{-2.4}$ MeV. In Figure V-15 the calculated ratios for temperatures of T=4.8 and 14 MeV are compared to the data. The moving source fits to the bound state kinetic energy spectra indicate a source temperature of about 14 MeV. The 14 MeV calculation shown in Figure V-15 clearly does a very poor job of fitting the data. The extracted temperature of 4.8 MeV agrees with the temperature extracted at higher energies [Po 86b] using the quantum statistical model.

Because the particle bound states were not measured at 25 MeV/nucleon, it was not possible to extract the temperature in the same way as for the 35 MeV/nucleon data. Instead the ratio of each state to the $^{6}Li^{*}_{2.186}$ state was taken. These ratios were found to be similar to the same ratios for the 35 MeV/nucleon data, hence it can be assumed that the temperature is the same at 25 and 35 MeV/nucleon.

To illustrate the importance of feeding Figure V-16 shows the calculated feeding for several states. In general over half the observed bound state spectra come from the decay of heavier states. Two of the particle unstable states ($^{7}Li^{*}_{0.476}$ and $^{8}Be^{*}_{3.04}$) are heavily fed, but most

Table V-4

Excited State Ratios For 35 MeV/nuc0. N+Ag

State	Ratio To	Ratio
$^{4}He^{*}_{20.1,21.1,22.1}$	$^{4}He_{gs}$	$0.013^{+0.006}_{-0.005}$
$^{5}He^{*}_{16.76}$	$^{6}Li_{gs}$	$0.015^{+0.015}_{-0.009}$
$^{5}He^{*}_{19.8}$	$^{6}Li_{gs}$	$0.048^{+0.024}_{-0.018}$
$^{5}Li_{gs,5}$	$^{6}Li_{gs}$	$0.77^{+0.35}_{-0.25}$
$^{6}Li^{*}_{2.186}$	$^{6}Li_{gs}$	$0.60^{+0.27}_{-0.20}$
$^{6}Li^{*}_{4.31,5.65}$	$^{6}Li_{gs}$	$0.074^{+0.038}_{-0.027}$
$^{7}Li^{*}_{4.65}$	$^{7}Li_{gs}$	$0.20^{+0.09}_{-0.06}$
$^{7}Li^{*}_{6.68,7.456}$	$^{7}Li_{gs}$	$0.078^{+0.037}_{-0.027}$
$^{8}Be^{*}_{3.04}$	$^{6}Li_{gs}$	$0.17^{+0.08}_{-0.06}$

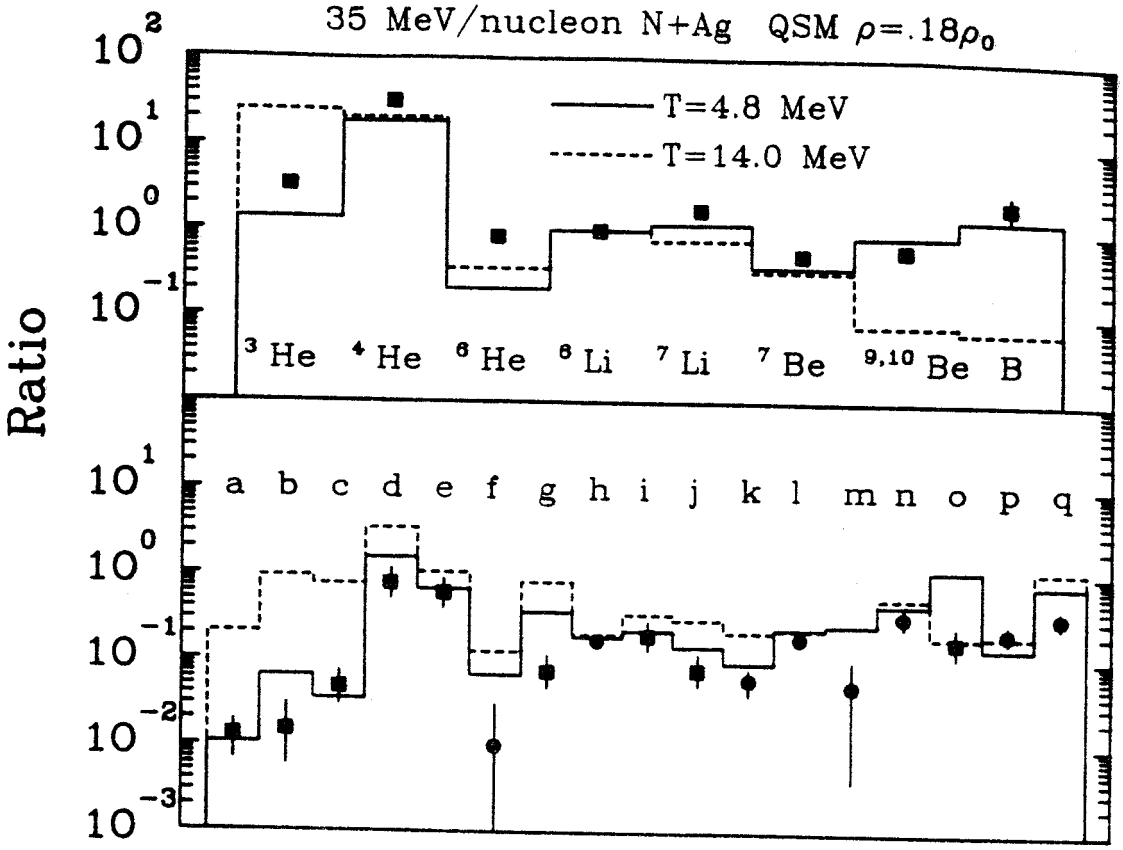

Figure V-15 Quantum statistical model calculation of the production of the measured states for T=4.8 and 14.0 MeV and $\rho=0.18\rho_0$. The excited states and particle unbound ground states shown in the bottom half of the figure are identified in table V-5.

Table V-5

Key To Particle Unstable And Gamma States In Figure V-15

Letter	State	Decay	Reference
a	$^{4}He^{*}_{20.1,21.1,22.1}$	p-t	
b	$^{5}He^{*}_{16.7}$	d-t	
c	$^{5}He^{*}_{19.7}$	d-t	
d	$^{5}Li_{gs,7.5}$	p-α	
e	$^{6}Li^{*}_{2.186}$	d-α	
f	$^{6}Li^{*}_{3.6}$	γ	[Mo 84]
g	$^{6}Li^{*}_{4.35,5.65}$	d-α	
h	$^{7}Li^{*}_{.476}$	γ	[Bl 86]
i	$^{7}Li^{*}_{4.65}$	t-α	
j	$^{7}Li^{*}_{6.68,7.456}$	t-α	
k	$^{7}Li^{*}_{7.456}$	n-^{6}Li	[Bl 87a]
l	$^{7}Be^{*}_{.430}$	γ	[Bl 86]
m	$^{8}Li^{*}_{.98}$	γ	[Mo 85]
n	$^{8}Li^{*}_{2.255}$	n-^{7}Li	[Bl 87a]
o	$^{8}Be^{*}_{3.04}$	α-α	
p	$^{10}Be^{*}_{7.371}$	n-^{9}Be	[Bl 87b]
q	$^{12}B^{*}_{3.388}$	n-^{11}B	[Bl 87b]

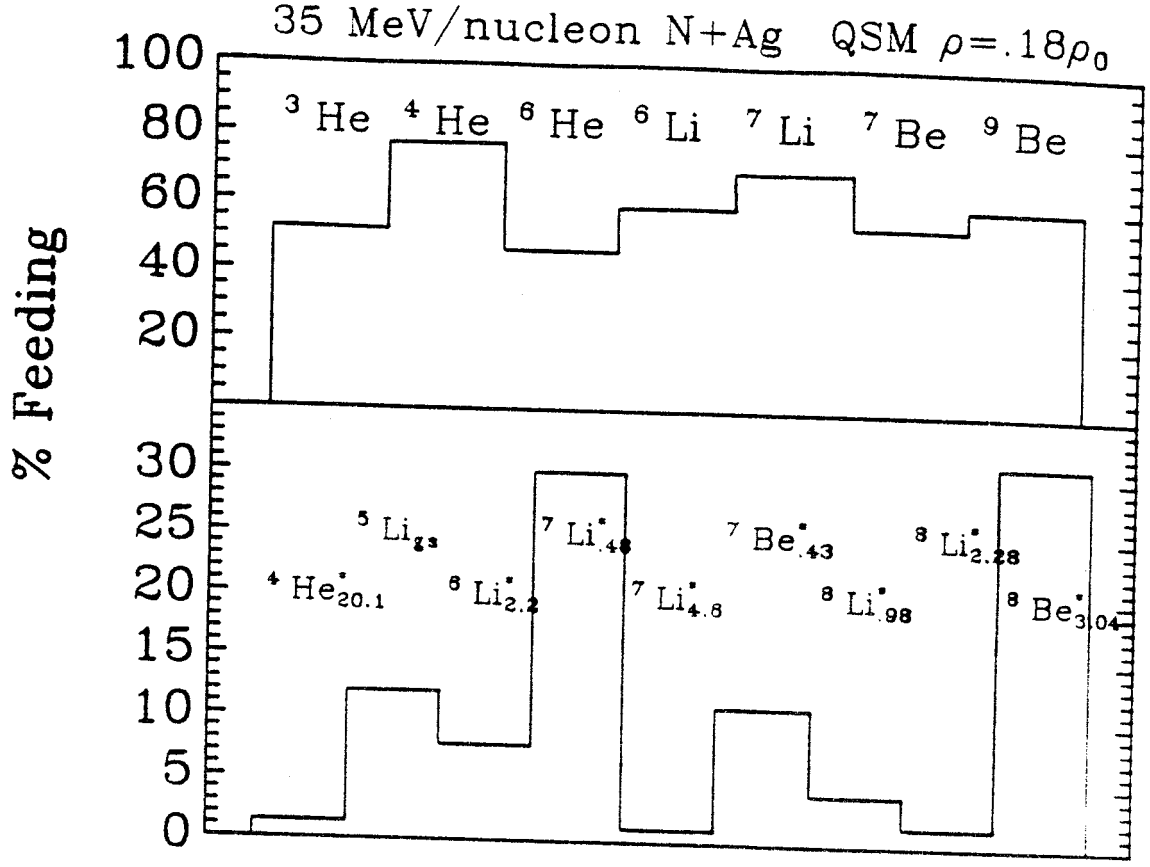

Figure V-16 Quantum statistical calculation of the feeding to the observed states for a source temperature of T=4.8 MeV and freeze-out density of $\rho=0.18\rho_0$.

of the particle unstable states are affected very little by feeding from higher states.

The difference between the temperature extracted from the kinetic energy spectra and the population of the states may be related to time of formation of the complex fragments. The kinetic energy spectra of the protons and neutrons in the intermediate source are fixed in the early hot stage of the interaction. If complex fragments are formed later as the source is cooling, then the distributions of the states will reflect the later cooler temperature. The kinetic energy spectra of the complex fragments reflect are determined by the spectra of the protons and neutrons that coalesced to form the fragment.

Similarly it has been pointed out that while the average energy per particle stays constant during the expansion of the source, the relative abundances of the states change as the source expands and cools [Bo 86]. Thus the kinetic energy spectra will reflect the temperature of the early hot stage of the interaction, while the populations of different states will reflect the temperature at the time of freeze-out. If this is the case, then freeze-out appears to occur at a temperature of around 5 MeV for interactions in the 35-60 MeV/nucleon range.

F. Final State Interactions Vs. Emission Of Particle Unstable Nuclei

One of the most important questions that arises in the measurement of the nuclear temperature through the measurement of particle unstable states is the question of at what point does one consider a particle to have been formed and emitted. In particular, is the emission of particle unstable nuclei the same as in-flight final state interactions or is it a totaly different process? If the latter is the case, then one is only interested in those two-particle correlations that come from the decay of

emitted unstable nuclei when extracting the temperature dependence of the source. The problem then arises of how to eliminate the final state interactions from the observed two-particle correlations. This could be accomplished if one could determine a unique source function for the particles. One would then be able to use the calculated correlation function for the nuclear and Coulomb final state interactions in the extraction of the populations of the particle unstable states.

The problem of determining whether final state interactions and emission of particle unstable nuclei can be examined by looking at the trends shown in the two-particle correlations. As mentioned earlier correlations involving two particles that exhibit resonances in their final state interaction have a consistently smaller extracted source radii then those particles with no resonances. It has been suggested that differences in the time of freeze-out for different particles may be responsible for the observed different radii [Bo 86]. On the other hand if all particles come from a source that is the same size and if the emission of particle unstable nuclei and final state interactions are different processes, then correlations involving particles with resonances will be enhanced and a smaller source radii will be extracted for these correlations. In addition the difference between the extracted source radii for the two peaks in the d-α correlations [Ch 86a] could then be understood in terms of a greater enhancement of the lower lying state leading to a smaller apparent radius for it.

It is also interesting to look at the behavior of two-proton correlations as a function of the size of the target. Two-proton correlations at small relative momentum have been studied for 25 MeV/nucleon ^{16}O + ^{12}C, ^{27}Al [Be 85] and ^{197}Au [Ly 83]. The peak of the correlation function increases with increasing target size. Using

Koonin's model [Ko 77] this leads to a smaller extracted source radii as one increases the target size. If, on the other hand, one interprets the data in terms of the decay of ^{2}He then the data may be explained in terms of the ^{2}He cross section increasing with increasing source size.

The two-particle correlations have been observed to be stronger for higher two-particle total energy [Ch 86a, Po 86a, Po 86b], leading to a smaller extracted source radius. It has been suggested that this may mean that higher energy particles tend to come from smaller sources [Po 86b]. On the other hand, in the case of correlations with resonances this might be due to there being a greater cross section for the emission of the article unstable nuclei at a high energy than the emission of two lighter nuclei of equal energy.

It is known from the large angle correlation presented in Chapter IV that the decay of particle unstable nuclei contribute heavily to the two-particle correlation function at relatively large angles (10°-25°). For the system nearest 35 MeV/nucleon N+Ag, 40 MeV/nucleon C+Ag, the large angle correlations shown in figure IV-11 indicate that there are about twice as many p-α coincidences on the same side of the beam as on opposite sides of the beam. In p-d and d-d correlations it was shown that there is a slight favoring of the opposite side over the same side for this system. The excess clearly must come from the emission of ^{8}Be and not from two alphas that have final state interactions.

Using Boal's [Bo 86] calculations of the final state interaction including both the nuclear and Coulomb potentials for a radius of 7.0 fm the cross section for the first excited state of ^{8}Be was extracted in the same fashion as described in section D. The cross section was found to be 0.507±0.093 mb compared to 0.690±0.097 mb obtained from the Coulomb only calculation. In addition to being smaller by about 25% the cross

section is now much more sensitive to the source radius that is used. Unfortunately the full nuclear and Coulomb calculation exists for only a limited number of the two-particle correlations that have resonances in them. In addition in the present experiment the experimental resolution was good enough to perform the nuclear plus Coulomb background subtraction for the p-p and α-α cases only. The effect of subtracting a background that assumes a component coming from in-flight final state interactions would be to lower the extracted cross sections of particle unstable states and hence reduce the extracted temperatures.

Chapter VI

Summary and Conclusions

Single particle inclusive kinetic energy spectra and two-particle large-angle correlation functions have been measured for 40 and 50 MeV/nucleon C induced reactions. The light particle energy spectra have been well fit with a triple moving source parameterization assuming the emission of particles from three distinct moving sources all moving in the beam direction. One source, the projectile-like source, has a velocity of about 85% of the incident beam velocity and a temperature of about 4-5 MeV. The second source, the target-like source, has a velocity of about 5-10% of the incident beam velocity with a temperature of 3.5-4.5 MeV. The spectra are dominated by the third source, the intermediate velocity source, which has a velocity intermediate between the projectile and target velocities and a temperature of 10-15 MeV. Heavier fragments (Li-C) were measured at forward angles, Θ=5°-45°. These particles were found to come primarily from the projectile-like source.

Two-particle in-plane correlations were measured with tag detectors at Θ=-25° and 45°. For both tag angles the C+C systems showed a very strong preference for emission of two particles to opposite sides of the beam. The enhancement in opposite side emission increases as the total mass of the observed particles increases. Very little difference was observed between the two beam energies, 40 and 50 MeV/nucleon. For the heavier systems, C+Ag and C+Au, the correlations were more symmetric about the beam axis with opposite side correlations only slightly enhanced over same side correlations. For all four systems the decay of particle unstable light nuclei contributed heavily to the two-particle large-angle correlations. For an opening angle of 10°, enhancements in

the correlation function are observed for p+p, p-t, p-^{4}He, ^{4}He-^{4}He and ^{4}He-^{6}He. The contribution to the correlation function from unstable resonances can be as high as 80% (d-^{4}He for 40 MeV). Out of plane correlations were also measured with tag telescopes at 25° and 45° at Φ=90°. The correlations were found to be nearly flat with a slight decrease at more forward angles. The ratio of in-plane to out-of-plane correlations shows an enhancement in the emission of particles in the same plane. As in the in-plane correlations, the enhancement is largest for the light systems and for higher total mass of the emitted particles.

In order to determine the extent to which conservation of momentum effects the measured correlations, momentum conservation calculations were carried out. Using a momentum conservation calculation incorporating emission from all three sources the general trends of the in-plane 45° tag correlations were reproduced. The overall agreement was not as good for the correlations with the 25° tag, perhaps due to the increased importance of correlations involving particles from different sources. For the out-of-plane correlations the agreement between the momentum conservation calculations and the data was good only for the heavier systems. The momentum conservation calculation did a reasonably good job of explaining the ratio of in-plane to out-of-plane correlations for the heavy systems. For the light systems the calculation consistently over predicted the ratio of in-plane to out-of-plane correlations, this may in part be due to correlations between two particles from different sources.

A close packed array of sixteen phoswich telescopes positioned behind a multi-wire proportional counter was used to measure two-particle correlations at small relative momentum for the reaction 35 MeV/nucleon

N+Ag. The correlations were measured at central angles of θ=35°, 45°, 60° and 80°. The correlations have been used to extract information about the space-time extent and temperature of the intermediate velocity source. Source radii extracted from two-particle correlations are in good agreement with the radii extracted by previous authors. The radii are smallest for particle pairs with resonances, pp, pα, dα and $\alpha\alpha$ (4.5-5.0 fm), and largest for nonresonant pairs, pd, dd and tt (6.3-9.5 fm). Little difference was found in the extracted source radii as a function of angle and beam energy. The radii are somewhat larger than those extracted using the coalescence model due, in part, to neglecting the lifetime of the emitting source. If a nonzero source lifetime is used then smaller source radii are obtained.

One important question that has come up is when is a particle considered to have been emitted from the source? In particular are particle unstable nuclei emitted from the source or are all observed resonances the results of in-flight final state interactions? If particle unstable nuclei are emitted in addition to other particles experiencing in-flight final state interactions, then the observed two-particle correlations are the results of a combination of the two processes. If this is the case, then radii extracted from particle pairs with resonances will be smaller than radii extracted from nonresonant pairs because the decay of particle unstable light nuclei will enhance the correlation functions which leads to a larger extracted radius. If, on the other hand, all observed resonances are the results of in-flight final state interactions then the differences in the extracted radii may indicate different emission times for different particles or perhaps that different particle pairs come from different types of collisions.

The difference between the source radii extracted using particle pairs with resonances and those without resonances has also been attributed to different freeze-out times for different particles. Those particles that freeze-out earlier will yield a smaller source radius than particles that freeze-out at a later stage of the interaction. In this view information about the source at different times may be obtained by looking at different particles.

Using the populations of bound and unbound states measured in the present experiment and the Y and neutron emitting states measured by Morrissey et al. and Bloch et al. a source temperature of $4.8^{+2.8}_{-2.4}$ MeV has been extracted using the quantum statistical model of Hahn and Stöcker in order to correct for feeding from higher lying states to the observed states. Overall the quantum statistical model does an excellent job of fitting the populations of all the measured states at the same time. The use of the quantum statistical model to take into account feeding from higher lying states has eliminated the previous descrepency in the temperature between measurements using particle bound Y-ray emitting states and measurements using particle unbound states. The temperature was extracted using the quantum statistical model of Hahn and Stöcker in order to correct for feeding from higher lying states to the observed states. The temperature is in good agreement with the temperature extracted from particle unbound states for 35 MeV/nucleon N+Au and 60 MeV/nucleon Ar+Au. The temperature extracted from the population of states is about 10 MeV lower than the temperature extracted from the kinetic energy spectra. The reason for this disagreement may be that the two temperature measurements represent the temperature of the emitting source at different times. The kinetic energy spectra are fixed early in the interaction while the populations of the states change as the source

expands and cools. Thus the temperature measured from the populations of the states represents the temperature at the time of freeze-out. If this is the case, then the freeze-out temperature does not change measurably for beam energies between 35 and 60 MeV/nucleon.

In conclusion it has been shown that two-particle large angle correlations are consistent with emission from a thermally equilibrated system. While the measured two-particle correlations are not isotropic, as emission from a thermally equilibrated source would require, the effects of momentum conservation requirements have been shown to account for most of the deviation from an isotropic distribution. As the number of nucleons in the emitting source increases the correlation functions become more isotropic.

The use of the quantum statistical model has resolved the discrepency between temperature measurements using the populations of γ-ray emitting states and those using particle unstable states. The temperature extracted from the populations of nuclear states is still considerably lower than the temperature extracted from the kinetic energy spectra. Further work is needed to eliminate the contribution of final state interactions to the populations of the particle unstable states. Theoritical calculations are needed for the nuclear final state interactions of several particle pairs and either a theoritical or experimental value for the freeze out radius is needed.

APPENDIX

Appendix

Momentum Conservation Model

The momentum conservation model used in Chapter IV is based treatment of Lynch et al. [Ly 82]. The model assumes that particles are emitted isotropically in the rest frame of a moving source of size A nucleons with a kinetic energy spectra given by Eqs. (IV-1) and (IV-2). The emission of the first particle of mass m_1 with lab momentum $\vec{p}_{1lab}$ at lab angles Θ_1, Φ_1 changes both the temperature and momentum of the emitting source. In the rest frame of the moving source the Lorentz transformations for the first particle give

$$p_{1x}=\gamma(p_{1lab}\cos\Theta_1-\beta E_{1lab}), \tag{A-1}$$

$$p_{1y}=p_{1lab}\sin\Theta_1\cos\Phi_1, \tag{A-2}$$

$$p_{1z}=p_{1lab}\sin\Theta_1\sin\Phi_1, \tag{A-3}$$

where

$$\gamma=(1-\beta^2)^{-1/2} \tag{A-4}$$

and β= the velocity of the moving source in the lab frame. The x-component is parallel to the beam direction. The cross section in the moving source rest frame is given by

$$\frac{d^2\sigma_1}{p_1^2 dp_1 d\Omega_1} = \frac{\sigma_{01}}{4\pi m_1^3}\ \frac{e^{-E_1/\tau}}{\kappa(m_1/\tau)}, \tag{A-5}$$

where

$$\kappa(m_1/\tau)=2(\tau/m_1)^2K_1(m_1/\tau)+(\tau/m_1)K_0(m_1/\tau), \qquad \text{(A-6)}$$

K_0 and K_1 are modified Bessel functions of the second kind, σ_{01} is the cross section for particle 1 from the moving source fits of Chapter IV, and τ is the source temperature from the moving source fit. The cross section in the lab frame is given by

$$\frac{d^2\sigma_{1lab}}{dE_{1lab}d\Omega_{1lab}} = \frac{p_{1lab}E_1\sigma_0}{4\pi m_1^3}\frac{e^{-E_1/\tau}}{\kappa(m_1/\tau)} . \qquad \text{(A-7)}$$

The source velocity in the lab frame is now given by

$$\beta'_x = \frac{\beta-p_{1x}/m'}{1-\beta p_{1x}/m'_s} , \qquad \text{(A-8)}$$

$$\beta'_y = -p_{1y}/m'_s , \qquad \text{(A-9)}$$

$$\beta'_z = -p_{1z}/m'_s , \qquad \text{(A-10)}$$

where $m'_s = Am_0-m_1$ (m_0= 931.5 MeV). The excitation energies before, E_x, and after, E'_x, the emission of the first particle are related by

$$E'_x = E_x-(E_1-m_1)-(\vec{p}_1)^2/2m'_s . \qquad \text{(A-11)}$$

The initial excitation energy is given by the empirical relation

$$E_x = A\tau^2/(8\ \text{MeV}),$$

and the temperature of the recoiling source may be expressed as

$$\tau' = (E_x' \cdot 8\ \text{MeV}/A')^{1/2}. \tag{A-13}$$

The source may now emit particle 2 with mass m_2, lab momentum p_{2lab} at lab angles θ_{2lab}, Φ_{2lab}. The second particle's momentum transformed in to the source rest frame is given by

$$p_{2x} = \gamma'(p_{2lab}\cos\theta_2 - \beta_x' E_{2lab}), \tag{A-14}$$

$$p_{2y} = p_{2lab}\sin\theta_2\cos\Phi_2 - m_2\beta_y, \tag{A-15}$$

$$p_{2z} = p_{2lab}\sin\theta_2\cos\Phi_2 - m_2\beta_z. \tag{A-16}$$

The source rest frame and lab frame cross section for the emission of particle 2 are given by Eqs. (A-5) and (A-7) by changing subscript 1 to 2 and τ to τ'.

The two-particle coincidence cross section for the emission of particle 1 followed by the emission of particle 2 is proportional to the product

$$P(\vec{p}_1,\vec{p}_2) = \frac{d^2\sigma_{1lab}(\vec{p}_1,\beta,\tau,m_1)}{dE_{1lab}d\Omega_{1lab}} \frac{d^2\sigma_{2lab}(\vec{p}_2,\beta',\tau',m_2)}{dE_{2lab}d\Omega_{2lab}}. \tag{A-17}$$

Experimentally it is impossible to tell which particle is emitted first, hence we also define $P(\vec{p}_2,\vec{p}_1)$ in the same manner as $P(\vec{p}_1,\vec{p}_2)$ using Eq. (A-17) by exchanging the subscripts 1 and 2 and by replacing τ' and β' by

τ'' and β''. The new parameters τ'' and β'' are defined in the same manner as τ' and β' using Eqs. (A-8) through (A-13). The two-particle coincidence cross section is now given by

$$\frac{d^4\sigma}{dE_1 d\Omega_1 dE_2 d\Omega_2} = C_0[P(\vec{p}_1,\vec{p}_2)+P(\vec{p}_2,\vec{p}_1)], \tag{A-18}$$

where C_0 is a normalization constant taken to be

$$C_0 = \sigma_R/\sqrt{2}\ , \tag{A-19}$$

with σ_R is the total reaction cross section given by

$$\sigma_R = 10\pi r^2(1-V_C/E_{cm}) \tag{A-20}$$

where

$$r=1.2(A_{proj}^{1/3}+A_{targ}^{1/3}-1), \tag{A-21}$$

$$V_C=1.44\ Z_{targ}Z_{proj}/r, \tag{A-22}$$

$$E_{cm}=T_{beam}A_{proj}A_{targ}/(A_{targ}+A_{proj}), \tag{A-23}$$

where A_{proj} and A_{targ} are the number of nucleons in the projectile and target, respectively, Z_{proj} and Z_{targ} are the number of protons in the projectile and target, respectively, and T_{beam} is the total beam energy in MeV.

To compare the momentum conservation model to the data Eq. (A-18) is integrated over E_1 and E_2 using the energy ranges listed in Table IV-4 in 3 MeV steps. The values of σ_{01}, σ_{02}, τ and β are taken from Table IV-2 for the appropriate source. The calculation is also integrated over the source size A. Each source is given a weight $dW=2\pi b \cdot db \cdot A$, where b is the impact parameter and A is the number of nucleons from a fireball model calculation [We 76, Go 77].

LIST OF REFERENCES

LIST OF REFERENCES

-A-

[Ar 85] D. Ardouin, H. Delagrange, H. Doubre, C. Gregoire, A. Kyanowski, W. Mittig, A. Peghaire, J. Peter, F. Saint-Laurent, Y.P. Viyogi, B. Zwieglinski, J. Pochodzalla, C.K. Gelbke, W. Lynch, M. Maier, G. Bizard, F. Lefebvres, B. Tamain and J. Quebert, Nucl. Phys. A447, 585c (1985).

[Aw 82] T.C. Awes, S. Saini, G. Poggi, C.K. Gelbke, D. Cha, R. Legrain, and G.D. Westfall, Phys. Rev. C25, 2361 (1982).

-B-

[Ba 62] F.C. Barker and P.B. Treacy, Nucl. Phys. 38, 33 (1962).

[Ba 67] G.D. Badhwar, C.L. Deney, B.R. Dennis and M.F. Kaplon, NIM 57, 116 (1967).

[Ba 86] J. Bartke, M. Kowalski, V.G. Grishin, K. Miller, J. Pluta, T. Pawlak, W. Peryt and Z. Strugalski, Z. für Phys. A324, 471 (1986).

[Ba 87] W. Bauer, preprint UGI-87-2 submitted to Nucl. Phys. A.

[Be 71] E.H. Berkowitz, G.L. Marolt, A.A. Rollefson and C.P. Browne, Phys. Rev. C4, 1564 (1971).

[Be 76] F.D. Becchetti, C.E. Thorn and M.J. Levine, NIM 138, 93 (1976).

[Be 81] F.D. Becchetti, C.A. Fields, R.S. Raymond, H.C. Bhang and D. Overway, Phys. Rev. C24, 2401 (1981).

[Be 83] D. Beavis, S.Y. Fung, W. Gorn, A. Huie, D. Keane, J.J. Lu, R.T. Poe, B.C. Shen and G. VanDalen, Phys. Rev. C27, 910 (1983).

[Be 85] M.A. Bernstein, W.A. Friedman, W.G. Lynch, C.B. Chitwood, D.J. Fields, C.K. Gelbke, M.B. Tsang, T.C. Awes, R.L. Ferguson, F.E. Obenshain, F. Plasil, R.L. Robonson and G.R. Yound, Phys. Rev. Lett. 54, 402 (1985).

[Bi 85] Bicron Corporation data sheets.

[Bl 86] C. Bloch, W. Benenson, E. Kashy, D.J. Morrissey, R.A. Blue, R.M. Ronningen and H. Utsunomiya, Phys. Rev. C34, 850 (1986).

[Bl 87a] C. Bloch, W. Benenson, A.I. Galonsky, E. Kashy, J. Heltsley, L. Heilbronn, M. Lowe, B. Remingtion, D.J. Morrissey and J. Kasagi, MSUCL preprint #592.

[Bl 87b] C. Bloch, PhD thesis, Michigan State University (1987).

[Bo 84] D.H. Boal, Phys. Rev. C30, 749 (1984).

[Bo 86] D.H. Boal and J.C. Shillcock, Phys. Rev. C33, 549 (1986).

[Bu 76] M. Buenerd, D.L. Hendrie, U. Jahnke, J. Mahoney, A. Menchaca-Rocha, C. Olmer and D.K. Scott, NIM 136, 173 (1976).

-C-

[Ch 86a] C.B. Chitwood, C.K. Gelbke, J. Pochodzalla, Z. Chen, D.J. Fields, W.G. Lynch, R. Morse, M.B. Tsang, D.H. Boal and J.C. Shillcock, Phys. Lett. B172, 27 (1986).

[Ch 86b] C.B. Chitwood, D.J. Fields, C.K. Gelbke, D.R. Klesch, W.G. Lynch, M.B. Tsang, T.C. Awes, R.L. Ferguson, F.E. Obenshain, F. Plasil, R.L. Robinson and G.R. Young, Phys. Rev. C34, 858 (1986).

[Ch 87] Z. Chen, C.K. Gelbke, J. Pochodzalla, C.B. Chitwood, D.J. Fields, W.G. Gong, W.G. Lynch and M.B. Tsang, NSCL preprint MSUCL-597 (1987).

-E-

[Ez 77] C. Ezell, L.J. Gutay, A.T. Laasanen, F.T. Dao, P Schübelin and F. Turkot, Phys. Rev. Lett. 38, 873 (1977).

-G-

[Go 77] J. Gosset, H.H. Gutbrod, W.G. Meyer, A.M. Poskanzer, A. Sandoval, R. Stock, and G.D. Westfall, Phys. Rev. C16, 629 (1977).

[Gu 76] H.H. Gutbrod, A. Sandoval, P.J. Johansen, A.M. Poskanzer, J. Gosset, W.G. Meyer, G.D. Westfall and R. Stock, Phys. Rev. Lett. 37, 667 (1976).

[Gu 84] H.A. Gustafsson, H.H. Gutbrod, B. Kolb, H. Löhner, B. Ludewigt, A.M. Poskanzer, T. Renner, H. Riedesel, H.G. Ritter, A. Warwick, F. Weik and H. Wieman, Phys. Rev. Lett. 53, 544 (1984).

-H-

[Ha 56] R. Hanbury-Brown and R.Q. Twist, Nature 178, 1046 (1956).

[Ha 84] B. Hasselquist, PhD Dissertation, Michigan State University, 1984.

[Ha 85] B.E. Hasselquist, G.M. Crawley, B.V. Jacak, Z.M. Koenig, G.D. Westfall, J.E. Yurkon, R.S. Tickle, J.P. Dufour and T.J.M. Symons, Phys. Rev. C32, 145 (1985).

[Ha 86] D. Hahn and H. Stöcker, LBL preprint LBL-21386 (1986).

[Ha 87] D. Hahn and H. Stöcker, Phys. Rev. C35, 1311 (1987).

-J-

[Ja 83] B.V. Jacak, G.D. Westfall, C.K. Gelbke, L.H. Harwood, W.G. Lynch, D.K. Scott, H. Stöcker, M.B. Tsang, and T.J.M. Symons, Phys. Rev. Lett. 51, 1846 (1983).

[Ja 85] B.V. Jacak, D. Fox and G.D. Westfall, Phys. Rev. C31, 704 (1985).

-K-

[Ko 77] S.E. Koonon, Phys. Lett. 70B, 43 (1977).

[Kr 85a] P. Kristiansson, L. Carlen, H.-Å. Gustafsson, B. Jakobsson, A. Oskarsson, H. Ryde, J.P. Bondorf, O.-B. Nielsen, G. Lovhoiden, T.-F. Thorsteinsen, D. Heuer and H. Nifenecker, Phys. Lett. 155B, 31 (1985).

[Kr 85b] P. Kristiansson, J.P. Bondorf, L. Carlen, H-Å. Gustafsson, B. Jakobsson, A. Kristiansson, G. Lovhoiden, H. Nifenecker, O-B. Nielson, A. Oskarsson, H. Ryde, T-F. Thorsteinsen and M. Westenius, Nuc. Phys. A447, 557c (1985).

-L-

[Le 79] M.-C. Lemaire, S. Nagamiya, S. Schnetzer, H. Steiner and I. Tanihata, Phys. Lett. 85B, 38 (1979).

[Ly 82] W.G. Lynch, L.W. Richardson, M.B. Tsang, R.E. Ellis, C.K. Gelbke and R.E. Warner, Phys. Lett. 108B, 274 (1982).

[Ly 83] W.G. Lynch, C.B. Chitwood, M.B. Tsang, D.J. Fields, D.R. Klesch, C.K. Gelbke, G.R. Young, T.C. Awes, R.L. Ferguson, F.E. Obenshain, F. Plasil, R.L. Robinson and A.D. Panagiotou, Phys. Rev. Lett. 51, 1850 (1983).

-M-

[Me 69] D.F. Measday and C. Richard-Serre, NIM 76, 45 (1969).

[Me 81] W.G. Meyer 1981.

[Mo 84] D.J. Morrissey, W. Benenson, E. Kashy, B. Sherrill, A.D. Panagiotou, R.A. Blue, R.M. Ronningen, J. van der Plicht and H. Utsunomiya, Phys. Lett. 148B, 423 (1984).

[Mo 85] D.J. Morrissey, W. Benenson, E. Kashy, C. Bloch, M. Lowe, R.A. Blue, R.M. Ronningen, B. Sherrill, H. Utsunomiya and I. Kelson, Phys. Rev. C32, 877 (1985).

[Mo 86] D.J. Morrissey, C. Bloch, W. Benenson, E. Kashy, R.A. Blue, R.M. Ronningen and R. Aryaeinejad, Phys. Rev. C34, 761 (1986).

-N-

[Na 79] S. Nagamiya, L. Anderson, W. Bruckner, O. Chamberlain, M.-C. Lemaire, S. Schnetzer, G. Shapiro, H. Steiner and I. Tanihata, Phys. Lett. 81B, 147 (1979).

[Ne 61] E. Newman, A.M. Smith and F.E. Steigert, Phys Rev 112, 1520 (1961).

-P-

[Pa 84] Particle Data Group, Rev. Mod. Phys. 56, 48 (1984).

[Po 85a] J. Pochodzalla, W.A. Friedman, C.K. Gelbke, W.G. Lynch, M. Maier, D. Ardouin, H. Delagrange, H. Doubre, C. Gregoire, A. Kyanowski, W. Mittig, A. Peghaire, J. Peter, F. Saint-Laurent, Y.P. Viyogi, B. Zwieglinski, G. Bizard, F. Lefebvres, B. Tamain and J. Quebert, Phys. Rev. Lett. 55, 177 (1985).

[Po 85b] J. Pochodzalla, W.A. Friedman, C.K. Gelbke, W.G. Lynch, M. Maier, D. Ardouin, H. Delagrange, H. Doubre, C. Gregoire, A. Kyanowski, W. Mittig, A. Peghaire, J. Peter, F. Saint-Laurent, Y.P. Viyogi, B. Zwieglinski, G. Bizard, F. Lefebvres, B. Tamain and J. Quebert, Phys. Lett. 161B, 256 (1985).

[Po 85c] J. Pochodzalla, W.A. Friedman, C.K. Gelbke, W.G. Lynch, M. Maier, D. Ardouin, H. Delagrange, H. Doubre, C. Gregoire, A. Kyanowski, W. Mittig, A. Peghaire, J. Peter, F. Saint-Laurent, Y.P. Viyogi, B. Zwieglinski, G. Bizard, F. Lefebvres, B. Tamain and J. Quebert, Phys. Lett. 161B, 275 (1985).

[Po 86a] J. Pochodzalla, C.B. Chitwood, D.J. Fields, C.K. Gelbke, W.G. Lynch, M.B. Tsang, D.H. Boal and J.C. Shillcock, Phys. Lett. B174, 36 (1986).

[Po 86b] J. Pochodzalla, C.K. Gelbke, W.G. Lynch, M. Maier, D. Ardouin, H. Delagrange, H. Doubre, C. Gregoire, A. Kyanowski, W. Mittig, A. Peghaire, J. Peter, F. Saint-Laurent, B. Zwieglinski, G. Bizard, F. Lefebvres, B. Tamain, J. Quebert, Y.P. Viyogi, W.A. Friedman and D.H. Boal, MSU NSCL preprint #569 (1986).

[Po 87] J. Pochodzalla, private communication.

-S-

[Sa 81] H. Sato and K. Yazaki, Phys. Lett. 98B, 153 (1981).

[St 83] H. Stöcker, G. Buchwald, G. Graebner, P. Subramanian, B.V. Jacak, G.D. Westfall, Nuc. Phys. A400, 63c (1983).

-T-

[Ta 80] I. Tanihata, M.-C. Lemaire, S. Nagamiya and S. Schnetzer, Phys. Lett. 97B, 363 (1980).

[Ta 81] I. Tanihata, S. Nagamiya, S. Schnetzer and H. Steiner, Phys. Lett. 100B, 121 (1981).

[Ts 84] M.B. Tsang, W.G. Lynch, C.B. Chitwood, D. Fields, D.R. Klesch, C.K. Gelbke, G.R. Young, T.C. Awes, R.L. Ferguson, F.E. Obenshain, F. Plasil and R.L. Robinson, Phys. Lett. 148B, 265 (1984).

-V-

[Va 85] A. Vander Molen, R. Au, R. Fox and T. Glynn, Nucl. Instr. and Meth. A236, 359 (1985).

-W-

[We 76] G.D. Westfall, J. Gosset, P.J. Johansen, A.M. Poskanzer, W.G. Meyer, H.H. Gutbrod, A. Sandoval, and R. Stock, Phys. Rev. Lett. 37, 1202 (1976).

[We 82] G.D. Westfall, B.V. Jacak, N. Anantaraman, M.V. Curtin, G.M. Crawley, C.K. Gelbke, B. Hasselquist, W.G. Lynch, D.K. Scott, M.B. Tsang, M.J. Murphy, T.J.M. Symons, R. Legrain, and T.J. Majors, Phys. Lett. 116B, 118 (1982).

[We 84] G.D. Westfall, Z.M. Koenig, B.V. Jacak, L.H. Harwood, G.M. Crawley, M.W. Curtin, C.K. Gelbke, B. Hasselquist, W.G. Lynch, A.D. Panagiotou, D.K. Scott, H. Stöcker and M.B. Tsang, Phys. Rev. C29, 861 (1084).

-X-

[Xu 86] H.M. Xu, D.J. Fields, W.G. Lynch, M.B. Tsang, C.K. Gelbke, M.R. Maier, D.J. Morrissey, J. Pochodzalla, D.G. Sarantites, L.G. Sobotka, M.L. Halbert, D.C. Hensley, D. Hahn and H. Stöcker, Phys. Lett. B182, 155 (1986).

-Z-

[Za 81] F. Zarbakhsh, A.L. Sagle, F. Brochard, T.A. Mulera, V. Perez-Mendez, R. Talaga, I. Tanihata, J.B. Carroll, K.S. Ganezer, G. Igo, J. Oostens, D. Woodard and R. Sutter, Phys. Rev. Lett. 46, 1268 (1981).

[Za 84] W.A. Zajc, J.A. Bistirlich, R.R. Bossingham, H.R. Bowman, C.W. Clawson, K.M. Crowe, K.A. Frankel, J.G. Ingersoll, J.M. Kurck, C.J. Martoff, D.L. Murphy, J.O. Rasmussen, J.P. Sullivan, E. Yoo, O. Hashimoto, M. Koike, W.J. McDonald, J.P. Miller and P. Truöl, Phys. Rev. C29, 2173 (1984).